KINEMATICS OF FEMOROACETABULAR IMPINGEMENT

by

Ashley Lynn Kapron

A dissertation submitted to the faculty of
The University of Utah
in partial fulfillment of the requirements for the degree of

Doctor of Philosophy

Department of Bioengineering

The University of Utah

December 2013

The University of Utah Graduate School

STATEMENT OF DISSERTATION APPROVAL

The dissertation of **Ashley Lynn Kapron**

has been approved by the following supervisory committee members:

Andrew E. Anderson	, Chair	**10/21/13** Date Approved
Kent N. Bachus	, Member	**10/21/13** Date Approved
Jeffrey A. Weiss	, Member	**10/21/13** Date Approved
Christopher L. Peters	, Member	**10/21/13** Date Approved
Richard D. Rabbitt	, Member	**10/21/13** Date Approved
K. Bo Foreman	, Member	**10/21/13** Date Approved

and by **Patrick A. Tresco** , Chair of

the Department of **Bioengineering**

and by David B. Kieda, Dean of The Graduate School.

ABSTRACT

Femoroacetabular impingement (FAI) describes subtle structural abnormalities, including femoral asphericity and acetabular overcoverage, which reduce clearance in the hip joint. FAI is a common cause of hip pain for young, athletic adults. The first theme of this dissertation investigated if FAI morphology is more prevalent in athletes and if physical exams could be used to identify individuals with underlying FAI morphology. In a cohort of collegiate football players, 95% were found to have radiographic abnormalities consistent with those seen in FAI patients. This finding not only suggests that athletes, such as football players, may have an increased risk for developing symptomatic FAI, but also highlights that FAI morphology may frequently occur in asymptomatic subjects. In the same cohort, radiographic measures of femoral asphericity and femoral head-neck offset were mildly correlated to maximum internal rotation. As such, athletes with diminished internal rotation in whom hip pain develops should be evaluated for FAI.

Altered articulation in FAI hips is believed to cause chondrolabral damage and may lead to osteoarthritis, but FAI kinematics have not been accurately quantified. To this end, the second theme of this dissertation focused on developing, validating, and applying a dual fluoroscopy and model-based tracking protocol to accurately quantify

three-dimensional in vivo hip kinematics. In a cadaver experiment, model-based tracking was compared to the reference standard, dynamic radiostereometric analysis. Model-based tracking was found to have a positional error less than 0.48 mm and rotational error was less than 0.58°. The methodology was then applied to evaluate a cohort of asymptomatic control subjects and three patients with differing FAI morphology. The results, which represent the most accurate data collected on hip kinematics to date, demonstrate that hip articulation is a highly complex process, including translation, pelvic motion, no bone contact, and labrum involvement in large ranges of motion. Collected data provide necessary baseline results for future comparison studies and could be used to validate computer simulations of impingement, guide pre-operative planning, and serve as boundary conditions in finite element models investigating chondrolabral mechanics.

This work is dedicated to my parents who have given me so much
and have always supported me. Thank you.

TABLE OF CONTENTS

LIST OF FIGURES

LIST OF TABLES

ACKNOWLEDGEMENTS

I would like to thank the following individuals for their help, mentorship, and/or support (in no particular order): Andrew Anderson, Kent Bachus, Bo Foreman, Richard Rabbitt, Jeff Weiss, Chris Peters, Steve Aoki, Christine Abraham, Mike Harris, Corinne Henak, Mike Bey, Roger Zauel, Kristen Ciarelli, Steve Mass, Greg Stoddard, David Rawlins, Heath Henninger, Bruce MacWilliams, Dorthyann Isackson, Alex Drew, Andy Guss, Krista Ellis, Heather Greenwall, Blake Zimmerman, Justine Goebel, Mikey Kutschke.

CHAPTER 1

BACKGROUND AND INTRODUCTION

1.1 The Hip Joint

The hip joint, comprised of the pelvis and femur bones, is central to mobility (Figure 1.1). It is functionally and anatomically considered to be a ball and socket joint, with the acetabulum as the socket and the femoral head as the ball. However, both normal hips and hips with structural deformities exhibit some degree of asphericity and possibly, a translating center of rotation.

The hip joint is cushioned by hyaline cartilage, covering both the femoral head and acetabulum (Figure 1.1). Cartilage is comprised of chondrocytes, extracellular matrix, and water. Chondrocytes are responsible for the creation and maintenance of the cartilage matrix, which includes both collagen and proteoglycans.[1] Type II collagen is the primary type of collagen found in the matrix and contributes to the tensile strength of cartilage.[2] Compressive strength is provided by proteoglycans, which are also responsible for balancing fluid and electrolytes within cartilage.[3] Water, which makes up 65-80% of the wet weight of cartilage, is responsible for the viscoelastic properties of cartilage, including time-dependent deformation and load dissipation.[4] Instantaneous compressive loads are supported primarily by the interstitial fluid pressure. When cartilage undergoes

constant loading, fluid exudes from the tissue and the load is transferred to proteoglycans.[5]

The cartilage constituents are arranged in four zones.[2,4] The thin superficial zone has the highest collagen and water content and exhibits high tensile and shear strength due to collagen fibrils arranged parallel to the surface. The superficial zone is covered by synovial fluid which substantially decreases friction between cartilage layers. The transitional zone is the largest zone by volume (40-60%) and contains collagen fibrils scattered obliquely to the surface and has more proteoglycans than the superficial zone. The deep zone has the greatest compressive strength, the highest proteoglycan content, and largest diameter collagen fibrils, arranged perpendicular to the surface. Finally, the calcified cartilage zone contains chondrocytes amidst a calcified matrix that attaches to subchondral bone.

The acetabular labrum, a fibrocartilagenous structure, lines the acetabular rim (Figure 1.1). Its triangular shape is attached to the bone through calcified cartilage.[6] Morphologically, it deepens and stabilizes the hip socket, increasing the acetabular surface area and volume by 60 and 120%, respectively.[7] The labrum may seal the joint, retaining the synovial fluid for lubrication and load distribution.[8] Three layers to the labrum have been identified.[9] The most superficial layer is a thin membrane of woven collagen fibrils. It covers a second stratiform layer, 20-100 μm think. The third layer is the bulk of the labrum, and is comprised of thick Type 1 collagen fiber bundles. The majority of these fibers run parallel to the acetabular rim, but some bundles run obliquely to this principle direction to tie the larger fibers together. This third inner layer facilitates

the physiological function of the tissue, resisting compression and circumferential stretching and compression, but potentially vulnerable to shearing.

The hip joint is enclosed by the joint capsule and capsular ligaments and is surrounded by musculature. The joint capsule is comprised of longitudinal fibers running from the outer edge of the acetabulum to the femoral head, circumferential fibers surrounding the femoral neck known as the zona orbicularis and four ligaments (iliofemoral, ischiofemoral, quadrupedal, and posterior).[10,11] The capsular structures contribute to hip stability and limit hip distraction.[11] Dynamic stability and motion of the hip are enabled by numerous hip muscles.[12] The primary hip flexors are psoas major, illiacus, rectus femoris, and sartorius; the extensors include gluteus maximus and most of the hamstrings. Internal rotation is facilitated by the anterior part of gluteus medius and minimus as well as the tensor fascia lata, while gluteus maximus, sartorius, piriformis, quadratus femoris, and pectineus externally rotate the hip. Abduction in enabled primarily by gluteus medius and minimus while the adductor muscles (longus, brevis, magnus, and minimus) act to adduct the hip.

1.2 Overview of Hip Osteoarthritis

Osteoarthritis (OA) is the painful degradation of the articular cartilage and subchondral bone. One in four adults will develop symptomatic OA of the hip joint before the age of 85.[13] The pain and stiffness resulting from hip OA can substantially limit range of motion, and therefore decrease activity and quality of life. In mild cases, pain is intermittent. Low impact exercise and physical therapy may be recommended to reduce pain and improve function while acetaminophen and nonsteroidal anti-

inflammatory drugs are used for pain management. In cases of advanced OA, chronic pain and severely limited function motivates the need for total hip arthroplasty. Hip OA results in at least 200,000 total hip replacements each year.[14]

Classic radiographic signs of hip osteoarthritis include joint space narrowing, subchondral cysts, and osteophytes.[15] Disease severity on x-ray is often ranked according to the Tonnis grade.[16] Grade 1 hips have slight narrowing of the joint space. Small cysts, increased narrowing, and moderate loss of femoral head sphericity indicate Grade 2. Hips with Grade 3 have severe narrowing or no joint space, large cysts, severe femoral head deformity, and possibly avascular necrosis. Total hip arthroplasty is often required when radiographic degeneration is advanced, but may be indicated in less severe cases, depending on symptoms and quality of life.[17]

There are many known causes and possible risk factors for the development of osteoarthritis. Generally, osteoarthritis occurs in hips with compromised cartilage, which can result from normal stresses on cartilage with abnormal physiology or abnormal stresses on normal cartilage.[18] The normal physiology of cartilage may be altered by aging, genetic predisposition, genetic/metabolic disease, or inflammation.[14,18] Cartilage can experience abnormal stresses as a result of obesity, structural deformities, trauma, joint instability, or intense physical demand from sport or occupation.[14]

In healthy cartilage, the extracellular matrix is maintained through a balance of matrix degredative enzymes, matrix synthetic enzymes and inhibitors.[18] In osteoarthritic cartilage, this balance is lost. The collagen network fractures and proteoglycans unravel as chondrocytes increase synthesis of matrix degredative enzymes. In addition, nitric oxide is released, which inhibits collagen and proteoglycan synthesis.[18] Normal matrix

protein synthesis is further limited as chondrocytes undergo apoptosis or phenotypic modulation such that they express different genes and start producing different types of collagen/proteoglycans.[19] As the proteoglycan and collagen content of cartilage is reduced, the tissue material properties change. The permeability increases, so fluid flows out of the tissue faster under sustained load.[5] The equilibrium and dynamic mechanical stiffness decreases.[5]

1.3 Femoroacetabular Impingement (FAI)

While the possible causes of hip osteoarthritis are numerous, this dissertation focuses on a recently described structural deformity, femoroacetabular impingement. Femoroacetabular impingement, or FAI, is a reduction in clearance in the hip joint as a result of subtle abnormalities of the femur and/or acetabulum.[20] Hips with FAI are categorized into three subtypes, cam, pincer, and mixed. Cam FAI presents as femoral head asphericity or decreased offset between the femoral head and neck (Figure 1.2). Pincer FAI describes hips with excessive acetabular coverage of the femoral head (Figure 1.3). This overcoverage may exist for the entire acetabulum, appearing as a deep socket, or only the anterior rim of the acetabulum may be involved, giving the hip a backward facing, or retroverted, appearance. Finally, hips with mixed FAI exhibit some aspects of both cam and pincer morphology. Approximately 50-75% of patients exhibit evidence of both classifications.[21]

1.3.1 History of FAI

Subtle structural deformities of femur, distinct from Perthe's disease and slipped capital femoral epiphysis, have been linked to OA as early as 1965. Murray hypothesized that slight abnormalities causing incongruity between the femoral head and acetabulum may increase the risk for development of osteoarthritis.[22] He reported a femoral tilt deformity, believed to be the result of mild epiphysiolysis and similar to modern cam FAI, was present in 39.5% of hips with osteoarthritis with no previously attributed cause. He later suggested that this deformity could result from increased athleticism during adolescence.[23] His hypothesis was supported over the next three decades by reports from Solomon, Harris, and colleagues.[24-28] It was not until 2001 that the modern term, definition, and hypothesized damage mechanism of cam FAI was officially described by Ganz and colleagues.[29]

The understanding of acetabular overcoverage as a cause of impingement and osteoarthritis is more recent. Acetabular retroversion was first identified as a subtype of acetabular dysplasia in 1987.[30] As a variant of dysplasia, retroversion was understood to be the result of posterior acetabular wall deficiency. Over a decade later, in 1999, the damage observed in hips with acetabular retroversion was attributed less to posterior deficiency and more to impingement between the femoral neck and anterior acetabular rim.[31] The name pincer FAI, describing both retroverted and generally deep sockets, was coined in 2003 by Ganz and colleagues.[20]

1.3.2 Clinical Presentation of FAI

FAI is a common cause of hip pain in young adults. Cam FAI occurs predominantly in young males, while pincer impingement is more common in middle-aged females.[32] Patients often report groin pain during or after athletic activity or prolonged sitting or walking.[20] Painful locking or catching sensations can occur during motion. Sports requiring extensive hip range of motion or quick pivoting (e.g. hockey, football, golf, soccer, and dance) are known to cause hip pain in the presence of a radiographic diagnosis of FAI.[33]

Clinical exams are commonly used to evaluate hip range of motion and reproduce pain. Symptomatic FAI patients often have limited range of motion, with decreases noted in flexion, abduction, adduction, and internal and external rotation.[34] The impingement test has a high sensitivity for reproducing hip pain in symptomatic FAI patients.[20,35,36] In this exam, the supine subject's hip is flexed to approximately 90 degrees then manipulated through adduction and internal rotation simultaneously (Figure 1.4).[20,37] The presence of pain constitutes a positive exam finding. Another common physical exam used in the diagnosis of FAI is the flexion-abduction-external rotation (FABER) test, in which the hip is positioned in a figure four position with the lateral ankle resting on the contralateral knee (Figure 1.4). The distance between the lateral border of the patella and the exam table is measured and compared between the involved and contralateral hips. A positive exam occurs if the distance is less on the involved hip. In a study of 301 patients with FAI, 99% had positive impingement tests and 97% had positive FABER tests.[36]

1.3.3 Diagnosis of FAI via Imaging

A diagnosis of FAI relies on positive imaging findings in the presence of hip pain and characteristic exam findings. Radiographs are the primary imaging modality in the clinic due to their availability and affordability. However, both computed tomography (CT) and magnetic resonance (MR) scanners, and the three-dimensional (3D) images they provide, are becoming more popular to diagnose the complex 3D deformities of FAI. While the trained clinician can make a diagnosis of FAI with a cursory overview of images, especially in severe cases, numerous 2D and 3D measurements have been proposed to quantify the type, degree, and severity of the deformities.

2D measurements of cam FAI attempt to quantify the degree of femoral head asphericity and offset between the femoral head and neck (Figure 1.5). The alpha angle is drawn on both anteroposterior (AP) and lateral views of the femur as the angle between the longitudinal axis of the femoral neck and a line connecting the femoral head center and the point where the head deviates from a best fit circle.[38] The alpha angle can also often be measured on single CT or MR image slices. Head-neck offset, also drawn on both anteroposterior and lateral views, measures the difference in radius between the femoral head and neck.[39] While the best radiographic projection to complete these measurements has yet to be firmly established, lateral views seem to be more descriptive than anterior views. Most cam lesions are found in the anterior and anterosuperior region of the femoral head-neck junction. Thus, the lateral views capture these regions better than the AP view. In contrast, the AP view better highlights the superior head-neck junction.[34,40]

Measures of pincer FAI are completed on AP radiographs. The lateral center edge angle measures the coverage of the femoral head by the acetabulum and is defined by the angle formed by a vertical line and a line connecting the femoral head center with the lateral edge of the acetabulum.[39] Finally, the acetabular index, which describes the slope of the acetabular roof, is measured as the angle formed by a horizontal line and a line connecting the medial point of the sclerotic zone with the lateral center of the acetabulum.[39] Finally, the crossover sign, an indicator of retroversion, is positive if the posterior wall of the acetabulum crosses the anterior wall, making projected lines of the acetabular walls appear as a figure eight.[39]

There is limited consensus on the cutoff values for the above measurements that should be used to delineate FAI hips from normal hips. For example, the cutoff for a normal alpha angle can range from 42 to 68 degrees and the lateral center edge angle cutoff from 35 to 45 degrees.[39,41-49] One of the more commonly used set of criteria to diagnose FAI is: alpha angle greater than 50 degrees, head-neck offset less than eight millimeters, acetabular index greater than zero degrees, and lateral center edge angle greater than 40 degrees, and presence of the crossover sign.[34,39,43,50] However, numerous studies have reported that asymptomatic hips often meet one or more of these criteria.[41,42,51-53] Thus, a diagnosis of FAI must be made through the combination of clinical exam findings and measurements of images.

While heavily relied upon in the clinic, radiographs and their associated 2D measures do not fully capture the 3D geometry of the pelvis and femur. Further, hips with FAI do not necessarily show the classic signs of OA; radiographs of hips with FAI may show normal joint space. To this end, researchers have developed objective measures

based on 3D reconstructions of the pelvis and femur from CT and MR data. For example, femoral head asphericity can be assessed throughout the head by measuring deviation from a best fit sphere.[54] 3D acetabular coverage of the femoral head can also be quantified by projecting the rim of the acetabulum to the femoral head and analyzing the percent coverage globally, or by regions.[55] The addition of arthrography (i.e. contrast agent) to a MR or CT scan provides the ability to evaluate the labrum and femoral and acetabular cartilage. MR arthrography is commonly used to assess the hip for chondrolabral tears and cartilage delamination.[50,56] Finally, recent developments in biochemical quantitative MR sequences, such as T2* mapping, show promise for assessing the integrity and health of articular cartilage.[57]

1.3.4 Damage Patterns in FAI Hips

Damage observed in hips with FAI and may be considered the start of osteoarthritic degeneration. Common findings include cartilage delamination, labral tears, fibrocystic changes, and labral ossification. The presence of cartilage delamination and labral tears is typically confirmed with CT and MRI. Cartilage damage has been reported in 44% to 79% of hips undergoing surgery for the treatment of FAI.[48,49] In addition, one study identified an odds ratio of 4.0 for delamination in hips with an alpha angle greater than or equal to 65 degrees.[58] FAI is considered the primary cause of labral tears, with 87% of labral tears occurring in hips with bony abnormalities seen on x-ray.[59] Comparing hips undergoing arthroscopic surgery for FAI, hips with labral tears had significantly higher alpha angles than those without labral tears.[49] Labral ossification and fibrocystic changes can be identified on x-ray. Labral ossification can be found in 7.5-56% of

symptomatic FAI patients.[60,61] Fibrocystic changes, rare in dysplastic hips (0/132 dysplastic patients in one study), are often found at the femoral head-neck junction in FAI patients (39/117 FAI patients in same study).[62]

Patterns of damage are different between cam and pincer FAI hips. Chondrolabral damage is most often localized anterosuperiorly in cam hips, while damage is observed more circumferentially in pincer hips.[21] Cartilage lesions are largest in the superior and anterosuperior region in cam hips and largest in the posteroinferior region in pincer hips.[63] Histologically, two distinct types of labral tears are observed.[6,21,58] The first type of tear, which is predominately found in pincer FAI hips, occurs perpendicular to the labrum surface, extending in severe cases to the subchondral bone.[64] The second type of tear, which is predominately associated with cam FAI, occurs at the chondrolabral junction. Here, the structure of the labrum is left generally intact, but separated from its cartilage attachment at the base.[58,64]

The varying damage patterns observed in cam and pincer hips have led some to hypothesize that mechanisms of impingement also differ.[21,58] In pincer FAI, it is believed that the labrum acts as a bumper between the femoral neck and overcovering acetabulum. The labrum is compressed at the limits of femoral head rotation, and compressive forces are transmitted to the cartilage adjacent to the chondrolabral junction. In cam FAI, it is believed that compressive and shear stresses are elevated at the chondrolabral junction as the anterior femoral head rotates into the anterosuperior acetabulum in flexion, internal rotation, and/or adduction. Separation between cartilage and labrum occurs as the femoral head compresses the cartilage medially and stretches the labrum laterally.[21] Chondral lesions and labral ossification at the posteroinferior region of the acetabulum are thought

to occur by the "counter-coup effect." Specifically, for overcovered hips, the femur reaches its range of motion limit anteriorly, rocks on the pivot point, slightly subluxates, and abuts the posterioinferior acetabular wall.[21,65,66] While supported by observed damage patterns, the aforementioned mechanisms have not been directly observed in vivo.

1.3.5 Risk Factors for FAI

Heredity, ethnicity, aging, gender, and deleterious joint mechanics at the development stage have all been proposed as possible risk factors of FAI morphology. Compared to a control population, siblings of patients with symptomatic FAI had a significantly greater prevalence of cam and pincer morphology, supporting a hereditary link.[67] Preliminary investigations have identified a few genes influencing both general hip shape and osteoarthritic changes, but work specific to FAI is needed.[68,69] FAI is more prevalent in individuals of white European descent than Asian descent, demonstrating that ethnicity may influence risk of FAI.[70,71] Finally, FAI abnormalities may become more prevalent with age, as offset between the femoral head and neck has been shown to decrease with age, but only in males.[72]

The prevalence of pincer and cam deformities may vary between gender, with cam deformities anecdotally accepted to be more common in males and pincer deformities in females.[73] Interestingly, a recent multicenter study has of over 1000 symptomatic patients demonstrated that cam FAI was slightly more common in females, while mixed FAI was slightly more common in males.[60] Pincer FAI was very rare in both genders (8% of all patients), but occurred more often in females.[60]

Elevated joint loading may increase the risk of FAI morphology. Athletes who participate in high impact sports during adolescence may be susceptible to insidious development of cam deformities. Specifically, subclinical physeal injury and subsequent femoral remodeling may occur if the epiphyseal plate is overloaded as it is closing during puberty.[74-77] For example, one study of 44 adolescents demonstrated that cam morphology does not occur prior to physeal closure, and that after closure, subjects with cam morphology had higher activity levels than those without.[75] An elevated body mass index, which also increases joint loading, may increase the risk of slipped capital femoral epiphysis, and may similarly increase the risk of cam FAI.[78] Abnormalities to the acetabulum may develop in response to femoral head remodeling, with cam deformities promoting the formation of pincer deformities. Specifically, cam lesions may cause repeated microtrauma to the labrum, which can subsequently ossify, extending the acetabular rim, increasing coverage, and leading to mixed FAI.[67,79]

Despite the evidence linking FAI to OA, there are still many individuals (including those with elevated activity levels) who have morphologic abnormalities consistent with FAI but do not develop symptoms, chondrolabral damage, or early OA.[80-82] For example, in one study of 96 asymptomatic hips with FAI, 79 did not have signs of OA at mean max follow-up 18.5 years.[81] Progression of FAI to a symptomatic and/or degenerative condition may therefore be dependent on additional factors. For example, the ability of cartilage to sustain elevated or abnormal loading without substantial damage may vary between hips. Thus, in the presence of FAI morphology, individuals that do not develop OA may have more resilient cartilage than those that do develop OA.[71] While cartilage resilience may prevent daily, repeated impingement from causing degeneration,

hips with FAI morphology may still be susceptible to acute injuries. For example, the pivoting and twisting motions often required in sports like soccer have been proposed as an mechanism for acute labral tears.[33] Nonetheless, more research is needed to improve the sensitivity and specificity of identifying who is at risk for developing symptomatic FAI and which hips with FAI may progress to OA if left untreated.

1.3.6 Treatment of FAI

Conservative treatments such as anti-inflammatory drugs, physical therapy, and the avoidance of activities that generate impingement may reduce symptoms associated with FAI, but clinical evidence is weak.[83] As such, surgery is the primary approach to treat symptomatic FAI. The goals of surgical treatment of FAI are to alleviate symptoms, restore function, preserve the native hip, and reduce the risk of developing end-stage OA. To address these goals, open and arthroscopic surgical strategies have been designed to correct the bony abnormalities and address chondrolabral damage. Several strategies are available to correct isolated cam and pincer deformities and can be combined to address mixed FAI hips. When multiple options are available, the selected approach ultimately depends on the surgeon.

Cam FAI patients are treated with femoral debridement to increase femoral head sphericity and head-neck offset. This can be completed through open surgical dislocation, a mini-open approach, or arthroscopic surgery.[84,85] Cam deformities located anteriorly are relatively easy to access athroscopically, while superior and posterior lesions are more challenging. As such, superior and posterior deformities are often addressed through open procedures, but they can be successfully corrected by experienced arthroscopists.[86] Mini-

open procedures have been designed to bridge the less invasive nature of arthroscopy and increased visualization of fully open approaches.[84,87] Regardless of approach, the biggest challenge in cam FAI surgery is determining the optimal amount of bone to resect.

Multiple strategies exist to correct pincer FAI hips, due to the range of presentations. For example, the crossover sign indicative of retroversion may be present in hips with normal/increased anterior coverage and deficient posterior coverage, or hips with increased anterior coverage and normal posterior coverage. In the former case, a periacetabular osteotomy (PAO) may be recommended to rotate the acetabulum into a position that simultaneously eliminates anterior impingement and improves posterior coverage.[88,89] In the latter case, an "acetabular rim trim" may be used to eliminate anterior impingement while preserving normal posterior coverage.[89,90] This rim trim may also be employed to treat globally overcovered sockets or posteriorly deficient hips contraindicated for PAO due to cartilage damage.[89,90]

If present, chondrolabral damage is also addressed at the time of surgery. Depending on severity, labral tears can be excised or repaired. Labral repair/preservation is associated with better outcomes.[91,92] Delaminated cartilage is addressed through chondroplasty and/or microfracture.[93] Microfracture, employed after osteochondroplasty of the offending bone or chondroplasty of unstable flaps, facilitates fibrocartilage regrowth, with an average of 93% of the microfracture area filled at short-term follow-up.[94]

Short- to mid-term follow-up data generally demonstrate that surgical treatment of FAI can reduce symptoms, improve range of motion, and return patients to previous activity levels, including professional sports.[84,95] However, long-term outcomes are not

yet available and therefore, it is unknown if joint preserving surgery will reduce the risk for future development of OA. Further, surgeries performed on patients with osteoarthritic changes and/or severe pain commonly result in poor outcomes and/or early conversion to a total hip replacement.[93,96] Therefore, timely diagnosis and treatment is essential to avoid total hip arthroplasty and optimize clinical outcomes. Unfortunately, prior to being diagnosed with FAI, many patients consult multiple healthcare providers and even undergo unnecessary surgical procedures.[20,97-99] Even professional athletes are not treated immediately, with the average time from onset of symptoms to treatment reported to be 29.6 months.[35]

1.4 Methods to Investigate FAI Kinematics

In the context of OA, joint kinematics (i.e. rotations, translations) have been shown to contribute to cartilage maintenance and repair.[100-103] In the context of FAI, abnormal articulation between the femoral head and the acetabulum may play a pivotal role in damage to the cartilage and labrum, thereby initiating OA. Specifically, damage is believed to result from the nonspherical head forcing itself into the acetabulum in cam hips[64,104] and from premature contact between the femoral head-neck junction and the protruding rim of the acetabulum in pincer hips.[20,21,64] However, these hypothesized mechanisms of impingement have not yet been accurately quantified in vivo. An accurate assessment of in vivo hip joint kinematics could confirm or refute the current understanding of FAI damage mechanisms and provide evidence to support or refine current diagnostic and treatment strategies.

Numerous techniques have been employed to quantify FAI kinematics. In the clinic, a goniometer can detect hip range of motion limitations in FAI patients.[49,105] The accuracy of the measurements are limited as goniometer arm alignment is subjective. Also, the measurement is completed in a static position. Further, angular measurements obtained on the surface of the skin cannot provide insight into how motion is restricted within the joint. Skin marker motion analysis enables dynamic assessment of activities. Research has shown that FAI patients have reduced range of motion during walking or squatting when compared to normal subjects.[106-108] Such differences may be due to compensatory changes in muscle recruitment/activation; limits in range of motion quantified dynamically are submaximal compared to those measured passively.[106] Skin marker analysis requires that joint centers and axes of rotation be estimated from anthropometric measurements or calculated as the sphere fit of skin markers during hip circumduction. Soft tissue artifact degrades the accuracy substantially; errors in the estimation of the hip joint center can be greater than 20 mm, or roughly, the radius of the femoral head.[109,110] Therefore, while skin motion analysis can be used to detect gross differences in hip kinematics, it cannot be used to quantify what may be subtle differences in the manner in which the hip articulates.

Numerous studies have attempted to investigate the interaction of the femur and pelvis using computer simulations.[65,111-113] In these studies, 3D surfaces of the bones from MRI or CT are prescribed motions to simulate clinical ROM exams. In a program developed by Tannast *et al.,* ROM limits are calculated based on collision between the bone surfaces.[112] This program has been used to investigate ROM before and after virtual[113] and actual[65] surgery to correct FAI abnormalities. While this software may be

useful to demonstrate that surgical removal of bone increases clearance in the joint, it has substantial limitations. Compared to ROM measured with a navigation system in cadavers, the software overestimates ROM by an average of 5° (range 19° to -7°).[112] Further, the software assumes the joint is concentric and the femur has a fixed center of rotation. In FAI patients, this is likely not the case because the femoral head is not spherical and has a center of rotation that may translate relative to the pelvis following collision and subluxation.

In a similar study, Audenaert *et al.* prescribed clinical ROM measurements to surfaces of cam FAI patients.[111] The software enabled them to identify the location of apparent intrusion of cam lesions to the acetabulum. In flexion, abduction, and internal rotation, cam lesions were found to abut against the anterosuperior quadrant of the acetabular cartilage. The model is limited by prescribed motions captured with a magnetic-based kinematic system, which is subject to the same skin motion error and center of rotation limitations as traditional skin motion capture. Finally, soft-tissue (i.e. cartilage, labrum, musculature, adipose tissue) was not included in both Tannast's and Audenaert's software. Thus, motion predicted in these studies is likely overestimated as soft-tissue (i.e. capsule, labrum) may prevent direct bone-bone contact.

Both single plane fluoroscopy and dynamic CT have been used to visualize hip joint articulation. Single plane fluoroscopy has visualized subluxation of the femur and led to conclusions that bone-to-bone impingement does not occur unless the labrum is fully ossified.[114] The technique only provides a 2D analysis, which severely limits its applicability to understanding FAI as a 3D pathology. Dynamic CT provides a 3D assessment and has been used to classify posterior and anterior impingement and

visualize subluxation, but is subject to substantial motion blur (due to a limited acquisition rate) prohibiting accurate measurements.[115]

In conclusion, the aforementioned techniques and related studies have advanced the understanding of FAI. However, more accurate, 3D methods are needed to better understand and quantify how the hip articulates and how 3D pathology influences bone motion.

1.5 Dual Fluoroscopy and Model-Based Tracking

A technique known as dual x-ray and model-based tracking can quantify in vivo joint kinematics with submillimeter accuracy. This technique is based on image registration, requires no assumptions regarding joint axes or centers of rotations, and is not subject to skin marker error. This technique captures 3D joint kinematics through registration of volumetric CT data with video images acquired in vivo by two fluoroscopes or two pulsed x-rays systems.[116,117] The following subsections outline the components and function of standard fluoroscopes, the modifications required to convert standard fluoroscopes to a high-speed dual fluoroscopy system, the tracking methodology, and the validation and application of the technique.

1.5.1 Standard Fluoroscopes: Components and X-ray Generation

Fluoroscopes have a number of clinical applications. For example, they allow surgeons to visualize their instrumentation relative to patient anatomy during surgical navigation for stent, metalwork, and pacemaker placement. Modern fluoroscopes are user-friendly, allowing operation without an intimate working knowledge of the system.

However, a deeper understanding is necessary to utilize them for nontraditional applications such as the quantification of in vivo joint kinematics.

The main components of the fluoroscopic imaging chain include the generator, x-ray tube, and image intensifier. The generator is a high voltage transformer circuit. It converts the available standard electrical AC voltage, which is limited to 480 V and oscillates at 60 Hz, to the DC voltage required by the x-ray tube, a constant 20-150 kV.[118] The constant power delivered to the x-ray tube enables x-rays of consistent strength, essential for safe operation of the machine.

The x-ray tube converts the electrical energy from the generator into x-ray photons. The tube houses a cathode and anode in a vacuum envelope. At the cathode, a low voltage circuit from the generator provides current to heat the tube filament (a helical tungsten wire).[119] As the filament is heated, it releases electrons via thermionic emission. The generator also establishes a large potential voltage difference between the cathode and anode, which accelerate the electrons towards a tungsten target. X-rays are generated as the electrons hit the target. The number of photons in the resulting x-ray beam is proportional to the tube current (mA), while the beam energy is proportional to the voltage difference (kVp).

The majority of the x-rays are produced via the Bremsstrahlung process and are called “breaking radiation,” while approximately 20% of x-rays originate from characteristic x-ray production.[119] In the Bremsstrahlung process, x-rays are produced when an electron passes close to a nucleus of the target material. The positively charged nucleus decelerates the electron and changes its direction. The lost kinetic energy of the electron is converted into an x-ray. Characteristic x-ray production occurs when the

accelerated electrons interact with inner shell electrons in the target material. Orbital electrons are bound to the nucleus at discrete binding energies. If the energy of the accelerating electron is greater than the binding energy, the inner shell electron is ejected, leaving an empty spot in the shell. An outer shell electron will move to fill this spot and emit an x-ray equivalent to the energy difference in binding energies between its original and new shells.

X-ray production is a very inefficient process. Less than 1% of the accelerated electrons' kinetic energy is converted to radiation, and the rest is lost to heat.[119] While the target material, tungsten, is chosen for its high melting point, there is substantial heat load. To limit damage to the material, the target is designed as a rotating disk.[120] This allows for greater x-ray intensity as the heat load is distributed over a larger surface area. X-rays are also emitted in all directions from the target, so the tube housing contains a lead layer to shield users and patients from this unnecessary radiation. Lead collimators limit the x-rays to a single beam; the size can be adjusted depending on the application. The beam is also filtered to remove low energy rays that would otherwise increase dosage without contributing to image formation.

Incident x-rays are converted into an image in the image intensifier. The x-rays pass a convex input window made of aluminum and hit the input screen made of phosphor crystals, usually cesium iodide. Its convex shape provides better mechanical strength and maximizes the useful entrance field size, but does introduce some distortion.[121] Through fluorescence, the phosphor crystals convert the x-ray photons to light photons. A photocathode layer made of antimony-cesium then absorbs these light photons and emits photoelectrons. The image intensifier anode and focusing electrodes

accelerate and condense the electrons to the output phosphor screen, which is much smaller in diameter than the original input window. The screen fluoresces with a maximum emission of 530 nm, or visible green light.[121] The output from the phosphor screen is coupled to a video camera to record the image.

In a C-arm fluoroscope, the image intensifier is rigidly mounted across from the x-ray emitter on a mobile half-circle ("C") frame. This provides substantial flexibility to alter to the angulation and position of the imaging chain components. C-arms have been designed for use in surgery, where there is need for x-rays in a variety of positions.

1.5.2 Application of Standard Fluoroscopes to Dual Fluoroscopy

There are a number of limitations associated with the use of standard clinical c-arm fluoroscopes for three-dimensional motion tracking. Although correctable, most fluoroscopes come standard with an eight inch diameter image intensifier. This size may be large enough to view a single joint on its own, but when the fluoroscopes must be positioned so that the joint of interest can be viewed throughout a range of motion in both machines, the overlapping field of view is often much smaller. Increasing the diameter to 12 or more inches is common, and will increase the combined FOV.

Another limitation is that a standard clinical fluoroscope will have a video camera coupled to the image intensifier that can only capture images up to 30 frames per second. Most joint motion analysis systems sample at a rate of at least 100 Hz.[122] Thus, for the purpose of dual fluoroscopy, the original camera must be removed and replaced with a high speed camera. These digital cameras also provide the essential synchronization of the video collected by both machines.

Also, if a fixed arm is used to mount both the x-ray source and image intensifier, vibrations caused by the rotating anode can propagate along the metal c-arm. As a result, the image intensifier vibrates, causing motion artifact in the final video. Even minor vibrations can be problematic as they become exacerbated at the end of the cantilevered camera housing. The vibration in the resulting images prohibits accurate measurement of joint kinematics using dual fluoroscopy. To eliminate vibrations, the fluoroscopes can be modified by removing the metal c-arm, and mounting the image intensifier and x-ray emitter on separate bases. An additional benefit of the separation is the increased flexibility to position the system; in the absence of the c-arm, it becomes possible to position the system around objects such as a table or treadmill.

1.5.3 Image Distortion Correction

One of the limitations of x-ray fluoroscopes for motion analysis applications is image distortion, which can originate from four sources (Figure 1.6). Local distortions can occur from poor assembly or small magnetic device interactions. The video camera and its lenses also introduce optical distortion. Pincushion distortion occurs when the x-ray beam is projected on the curved input phosphor, introducing nonlinear magnification of the image (with magnification greatest at the periphery). Finally, sigmoidal distortion occurs when external electromagnetic fields (including the earth's magnetic field) affect the photoelectron path when traveling from the photocathode to the output phosphor, curving the image into an "S" shape.

The distortion is insignificant in the clinical or surgical setting, but distortion reduces the accuracy of direct measurements made from the images. State-of-the-art flat-

panel detectors have begun to replace the image intensifier and are not subject to pincushion distortion as the x-rays are mapped to a flat input screen.[123,124] Unfortunately, these detectors are not widely available and are extremely expensive; standard image intensifiers are often used in dual fluoroscopy and must be corrected after acquisition.

Image distortion correction software employs a variety of global and local mapping techniques.[125-128] Fluoroscopic images of some type of grid, such as a perforated steel sheet or acrylic plate with implanted radiopaque beads, can be used to correct distortion. Software can identify a transformation that maps the distorted pattern to a target configuration (Figure 1.6). Global methods correct the image with a single pair of equations, while local techniques divide the image into small areas and correct each section separately.[125,126,129,130] Global corrections may not detect and correct local distortions, but local techniques can introduce discontinuities in the corrected image as each section is corrected independently. The optimal algorithm may apply a combination of these approaches.[131]

1.5.4 Motion Analysis with Dual Fluoroscopy

Dynamic radiostereometric analysis (DRSA) and model-based tracking are two techniques used to extract bone motion from dual fluoroscopy images. In both approaches, a calibration cube is first placed in the combined field of view to establish the relative configuration of the two focal spots (x-ray emitters) and imaging planes (image intensifiers). DRSA is an extension of direct linear transformation theory to the tracking of small radiopaque spheres implanted into the bone of interest.[132-134] DRSA is the reference standard method and is suitable for cadaveric, animal, and some post-

operative human studies. However, the surgical implantation of radiopaque beads into bone is unethical for research involving normal or pre-operative subjects. To this end, model-based tracking techniques have been developed.

Model-based tracking can be completed via intensity-based registration or shape-based registration. In intensity-based registration, CT images are segmented to delineate the bone of interest. The bone model contains all voxels enclosed within the boundary of the bone and their associated intensities, representing bone density. The registration software generates a digitally reconstructed radiograph (DRR), or fake x-ray, via ray tracing through the bone model (Figure 1.7).[117,135] Two DRRs are created and overlaid on the respective fluoroscopy images. The software then iterates the pose of the bone until the correlation of pixel intensities between the DRRs and the fluoroscopy images is optimized (Figure 1.8).[135] This process is repeated for all frames of the fluoroscopy video.

The process is similar for shape-based registration, except the bone model represents only the surface of the bone.[136,137] As such, CT or MR imaging can be used to obtain the 3D bone geometry. Additionally, the technique can be applied to orthopaedic implants using the computer-aided design (CAD) surfaces from the manufacturer. In shape-based registration, ray casting (not ray tracing) generates a silhouette of the bone which is then matched to corresponding edges in the fluoroscopy video. The optimal pose of the bone is determined by minimizing the distance between the fluoroscopic edges and points on the silhouette edges.

Prior to employing dual fluoroscopy and model-based tracking to answer research questions, the accuracy of the methodology must be determined. The accuracy varies for

each bone, depending on factors including the geometric complexity, soft-tissue x-ray attenuation, and overlap with other bones. Bey *et al.* recommend validation studies should be completed for each joint and motion of interest.[116] The accuracy of model-based tracking is assessed by comparing bone kinematics obtained from model-based methods to those quantified using DRSA. As the more accurate tracking method, DRSA serves as the reference standard to quantify errors in model-based tracking.[117] The validation is completed with cadavers to avoid implantation into human subjects.

Dual fluoroscopy and model-based tracking have been applied to investigate the kinematics of a number of joints, including the ankle, shoulder, spine, and knee.[117,138-148] Joint angles and translations are the most common outcome measure and are calculated directly from the bony landmarks without the interference of soft-tissue.[116,117,134,142,148-151] Some model-tracking studies have extended the quantification of bony movement to the evaluation of joint articulation and soft-tissue behavior. Bone-to-bone distance has been calculated in studies of the knee and hip.[150,152-154] Cartilage deformation has been inferred in both the ankle and knee from the overlap of cartilage in joint models prescribed motion from dual fluoroscopy.[139,147,153-155] While the applications have been numerous, the methodology has not yet been extended to answer clinically relevant questions regarding the hip.

1.6 Overall Motivation and Summary of Chapters

The body of this dissertation is composed of research that can be divided into two themes, both aimed at expanding the understanding of FAI. While the number of research studies on FAI has increased exponentially since its original description in 2001, many

questions surrounding the disease remain. For example, we knew very little about who is at risk for FAI, why damage is seen in some hips with structural deformities but not others, and how chondrolabral damage actually occurs.[29] Research in these areas has the potential to improve the sensitivity and specificity of the diagnosis process and refine treatment strategies.

The first theme of this dissertation investigates athleticism as a risk factor for FAI and explores methods to noninvasively identify athletes who are at risk. While certainly not the only persons affected by FAI, athletes do comprise a predominant portion of the patient population. One possible explanation for this observation is that athletic activity, especially during adolescence, may increase the risk of developing underlying FAI deformities, as described in Section 1.3.5. A second possible explanation is that athletic activity, especially activities that incorporate extreme range of motion or repeated impact loading, forces the abnormalities into repeated impingement and causes otherwise asymptomatic deformities to become symptomatic. In Chapter 2 of this dissertation, the former hypothesis is evaluated. The study is the first to quantify the prevalence of FAI in an asymptomatic athletic population, specifically collegiate football players, following modern radiographic definitions.

As mentioned in Section 1.3.6, timely diagnosis and treatment of FAI may be essential to optimize clinical outcomes, yet misdiagnosis that delays treatment is common, even in professional athletes. Further, many community physicians are unaware of FAI as a cause for hip pain. A screening protocol to identify those persons who are at-risk for the development of symptomatic FAI would likely reduce the time between onset of symptoms and diagnosis/treatment. That is, assuming symptoms

developed, the subject could communicate knowledge of being at risk for FAI to their physician immediately.

The ideal screening protocol would be sensitive, inexpensive, and noninvasive. Radiographic imaging provides a convenient and relatively inexpensive evaluation of the abnormalities associated with impingement. However, the radiation exposure would not be appropriate for large-scale screening in asymptomatic subjects, especially adolescents. In Chapter 3, clinical exams, such as those outlined in Section 1.3.2, are evaluated as a noninvasive tool to screen for asymptomatic FAI abnormalities. While the exams have a high sensitivity in symptomatic FAI patients, it is unknown if they could be used to screen for FAI in subjects who do not currently have hip pain but may have underlying FAI abnormalities.[36] Measuring ROM during rotational exams may also be useful as a screening tool, but the correlation between ROM and underlying FAI morphology has not yet been described in asymptomatic subjects.

Regression analysis completed in Chapter 3 between radiographic measures of FAI and range of motion identified a significant but weak correlation between cam FAI and internal rotation. In addition, the impingement exam, which has a high reported sensitivity in FAI patients, was not positive in the majority of subjects with underlying but asymptomatic FAI abnormalities. These results, quantified by a goniometer and a subjective report of pain, provide an abstracted understanding of FAI kinematics. To fully understand how FAI morphology restricts ROM and the mechanism behind pain generation in symptomatic subjects, accurate quantification, and visualization of detailed hip kinematics are needed. Further, a three-dimensional in vivo assessment of

impingement could confirm or refute the hypothesized mechanisms of chondrolabral damage described in Section 1.3.4.

As such, the second theme of this dissertation is the pursuit of accurate hip kinematics during clinical exams via dual-fluoroscopy and model-based tracking. While a number of other methods have previously been employed to quantify or simulate the impingement process, each has had its limitations, as described in Section 1.4. Dual fluoroscopy and model-based tracking can accurately quantify joint motion to submillimeter accuracy without assumptions of joint centers, axes of rotation, or bony collision and is not subject to error due to skin motion artifact or a limited frame rate.

Dual fluoroscopy and model-based tracking methods have been validated for the native hip during simulated walking and rising from a chair.[156,157] In addition, the shape-based tracking of total hip arthroplasty implants has been validated during simulated walking.[158] The reported bias and precision of joint angles and translations in these studies have been less than one millimeter and one degree, respectively. Since only motions occurring primarily in the sagittal plane were validated, there is limited applicability to the study of FAI. Specifically, impingement is hypothesized to occur at terminal range of motion or complicated motions which also incorporate rotation in the coronal and axial planes. Supine clinical exams, such as the impingement and FABER test, which combine rotation, flexion and ab/adduction may be more relevant to the study of FAI.

In Chapter 4, dual fluoroscopy and model-based tracking of the hip joint are validated for supine clinical exams. In this chapter, model-based tracking results are compared to the reference standard, dynamic radiostereometric analysis, in a cadaveric

experiment to quantify the bias and precision of outcome measures derived from this technique. In addition, the methodology is extended to one normal subject to demonstrate the feasibility of the translating this technique to the study of live subjects.

In Chapter 5, dual fluoroscopy and model-based tracking methodology are extended to a cohort of asymptomatic subjects with normal hip morphology and three subjects with differing FAI morphology. This chapter establishes baseline joint angles, translations and bone-bone distances during clinical exams for the normal population. Kinematics of the three patients are then compared to the mean results of the normal subjects and discussed in the context of each patient's clinical presentation and surgical treatment. Quantifying what may be subtle differences in joint kinematics due to FAI will be the first step in understanding the relationship between altered kinematics, soft-tissue damage, and OA. The results presented in this chapter can be used for future comparisons to additional patients with FAI or patients with other hip pathologies.

Finally, Chapter 6 is a summary of this dissertation. It summarizes the conclusions of this dissertation as a body of work, and interprets key findings of the earlier research (Chapter 2 and 3) in the context of studies published since the completion of this work. Finally, it discusses suggestions for future directions.

1.7 References

1. Chen FS, Frenkel SR, Di Cesare PE. 1999. Repair of articular cartilage defects: part I. Basic Science of cartilage healing. Am J Orthop 28: 31-33.

2. Bhosale AM, Richardson JB. 2008. Articular cartilage: structure, injuries and review of management. Br Med Bull 87: 77-95.

3. Buckwalter JA, Mankin HJ. 1998. Articular cartilage: tissue design and chondrocyte-matrix interactions. Instr Course Lect 47: 477-486.

4. Pearle AD, Warren RF, Rodeo SA. 2005. Basic science of articular cartilage and osteoarthritis. Clin Sports Med 24: 1-12.

5. Makela JT, Huttu MR, Korhonen RK. 2012. Structure-function relationships in osteoarthritic human hip joint articular cartilage. Osteoarthritis Cartilage 20: 1268-1277.

6. Seldes RM, Tan V, Hunt J, et al. 2001. Anatomy, histologic features, and vascularity of the adult acetabular labrum. Clin Orthop Relat Res: 232-240.

7. Tan V, Seldes RM, Katz MA, et al. 2001. Contribution of acetabular labrum to articulating surface area and femoral head coverage in adult hip joints: an anatomic study in cadavera. Am J Orthop 30: 809-812.

8. Hlavacek M. 2002. The influence of the acetabular labrum seal, intact articular superficial zone and synovial fluid thixotropy on squeeze-film lubrication of a spherical synovial joint. J Biomech 35: 1325-1335.

9. Shibutani N. 1988. Three-dimensional architecture of the acetabular labrum--a scanning electron microscopic study. J Jpn Orthop 62: 321-329.

10. Fuss FK, Bacher A. 1991. New aspects of the morphology and function of the human hip joint ligaments. Am J Anat 192: 1-13.

11. Ito H, Song Y, Lindsey DP, et al. 2009. The proximal hip joint capsule and the zona orbicularis contribute to hip joint stability in distraction. J Orthop Res 27: 989-995.

12. Gilroy AM, MacPherson BR, Ross LM. 2008. Atlas of Anatomy. New York: Thieme Medical Publishers, Inc.; 672 p.

13. Murphy LB, Helmick CG, Schwartz TA, et al. 2010. One in four people may develop symptomatic hip osteoarthritis in his or her lifetime. Osteoarthritis Cartilage 18: 1372-1379.

14. Lane NE. 2007. Clinical practice. Osteoarthritis of the hip. N Engl J Med 357: 1413-1421.

15. Altman RD, Gold GE. 2007. Atlas of individual radiographic features in osteoarthritis, revised. Osteoarthritis Cartilage 15 Suppl A: A1-56.

16. Tonnis D, Heinecke A. 1999. Acetabular and femoral anteversion: relationship with osteoarthritis of the hip. J Bone Joint Surg Am 81: 1747-1770.

17. Crawford RW, Murray DW. 1997. Total hip replacement: indications for surgery and risk factors for failure. Ann Rheum Dis 56: 455-457.

18. Mandelbaum B, Waddell D. 2005. Etiology and pathophysiology of osteoarthritis. Orthopedics 28: s207-214.

19. Sandell LJ, Aigner T. 2001. Articular cartilage and changes in arthritis. An introduction: cell biology of osteoarthritis. Arthritis Res 3: 107-113.

20. Ganz R, Parvizi J, Beck M, et al. 2003. Femoroacetabular impingement: a cause for osteoarthritis of the hip. Clin Orthop Relat Res: 112-120.

21. Beck M, Kalhor M, Leunig M, et al. 2005. Hip morphology influences the pattern of damage to the acetabular cartilage: femoroacetabular impingement as a cause of early osteoarthritis of the hip. J Bone Joint Surg Br 87: 1012-1018.

22. Murray RO. 1965. The aetiology of primary osteoarthritis of the hip. Br J Radiol 38: 810-824.

23. Murray RO, Duncan C. 1971. Athletic activity in adolescence as an etiological factor in degenerative hip disease. J Bone Joint Surg Br 53: 406-419.

24. Harris WH. 1986. Etiology of osteoarthritis of the hip. Clin Orthop Relat Res: 20-33.

25. Stulberg S, Cordell L, Harris W, et al. 1975. Unrecognized childhood hip disease: a major cause of idiopathic osteoarthritis of the hip. The Hip Proceedings of the Third Open Scientific Meeting of the Hip Society: St. Louis, 212-228.

26. Solomon L. 1972. Pathogenesis of osteoarthritis. Lancet 1: 1072.

27. Solomon L. 1975. Proceedings: Osteoarthritis of the hip: pathological changes and their implications for treatment. J Bone Joint Surg Br 57: 258.

28. Solomon L, Schnitzler CM, Browett JP. 1982. Osteoarthritis of the hip: the patient behind the disease. Ann Rheum Dis 41: 118-125.

29. Ito K, Minka MA, 2nd, Leunig M, et al. 2001. Femoroacetabular impingement and the cam-effect. A MRI-based quantitative anatomical study of the femoral head-neck offset. J Bone Joint Surg Br 83: 171-176.

30. Tonnis D. 1987. Congenital dysplasia and dislocation of the hip in children and adults. Berlin: Springer-Verlag; 538 p.

31. Reynolds D, Lucas J, Klaue K. 1999. Retroversion of the acetabulum. A cause of hip pain. J Bone Joint Surg Br 81: 281-288.

32. Parvizi J, Leunig M, Ganz R. 2007. Femoroacetabular impingement. J Am Acad Orthop Surg 15: 561-570.

33. Dy CJ, Thompson MT, Crawford MJ, et al. 2008. Tensile strain in the anterior part of the acetabular labrum during provocative maneuvering of the normal hip. J Bone Joint Surg Am 90: 1464-1472.

34. Zebala LP, Schoenecker PL, Clohisy JC. 2007. Anterior femoroacetabular impingement: a diverse disease with evolving treatment options. Iowa Orthop J 27: 71-81.

35. Philippon M, Schenker M, Briggs K, et al. 2007. Femoroacetabular impingement in 45 professional athletes: associated pathologies and return to sport following arthroscopic decompression. Knee Surg Sports Traumatol Arthrosc 15: 908-914.

36. Philippon MJ, Maxwell RB, Johnston TL, et al. 2007. Clinical presentation of femoroacetabular impingement. Knee Surg Sports Traumatol Arthrosc 15: 1041-1047.

37. Klaue K, Durnin CW, Ganz R. 1991. The acetabular rim syndrome. A clinical presentation of dysplasia of the hip. J Bone Joint Surg Br 73: 423-429.

38. Clohisy JC, Nunley RM, Otto RJ, et al. 2007. The frog-leg lateral radiograph accurately visualized hip cam impingement abnormalities. Clin Orthop Relat Res 462: 115-121.

39. Tannast M, Siebenrock KA, Anderson SE. 2007. Femoroacetabular impingement: radiographic diagnosis--what the radiologist should know. Am J Roentgenol 188: 1540-1552.

40. Meyer DC, Beck M, Ellis T, et al. 2006. Comparison of six radiographic projections to assess femoral head/neck asphericity. Clin Orthop Relat Res 445: 181-185.

41. Gosvig KK, Jacobsen S, Sonne-Holm S, et al. 2010. Prevalence of malformations of the hip joint and their relationship to sex, groin pain, and risk of osteoarthritis: a population-based survey. J Bone Joint Surg Am 92: 1162-1169.

42. Raynor CM, Bryant D, Spouge A, et al. 2009. Presence of Markers of Femoroacetabular Impingement in the Asymptomatic Population. FASEB J 23: 822-827.

43. Clohisy JC, Carlisle JC, Beaule PE, et al. 2008. A systematic approach to the plain radiographic evaluation of the young adult hip. J Bone Joint Surg Am 90 Suppl 4: 47-66.

44. Gosvig KK, Jacobsen S, Palm H, et al. 2007. A new radiological index for assessing asphericity of the femoral head in cam impingement. J Bone Joint Surg Br 89: 1309-1316.

45. Neumann M, Cui Q, Siebenrock KA, et al. 2009. Impingement-free hip motion: the 'normal' angle alpha after osteochondroplasty. Clin Orthop Relat Res 467: 699-703.

46. Notzli HP, Wyss TF, Stoecklin CH, et al. 2002. The contour of the femoral head-neck junction as a predictor for the risk of anterior impingement. J Bone Joint Surg Br 84: 556-560.

47. Beaule P, Hack K, Rakhra K, et al. 2009. Prevalence of CAM Type FAI Morphology in 200 Asymptomatic Volunteers (SS-29) Arthroscopy 25: Supplement 1, e16.

48. Hong SJ, Shon WY, Lee CY, et al. 2010. Imaging findings of femoroacetabular impingement syndrome: focusing on mixed-type impingement. Clin Imaging 34: 116-120.

49. Johnston TL, Schenker ML, Briggs KK, et al. 2008. Relationship between offset angle alpha and hip chondral injury in femoroacetabular impingement. Arthroscopy 24: 669-675.

50. Anderson LA, Peters CL, Park BB, et al. 2009. Acetabular cartilage delamination in femoroacetabular impingement. Risk factors and magnetic resonance imaging diagnosis. J Bone Joint Surg Am 91: 305-313.

51. Hack K, Di Primio G, Rakhra K, et al. 2010. Prevalence of cam-type femoroacetabular impingement morphology in asymptomatic volunteers. J Bone Joint Surg Am 92: 2436-2444.

52. Gosvig KK, Jacobsen S, Sonne-Holm S, et al. 2008. The Prevalence of Cam-Type Deformity of the Hip Joint: A Survey of 4151 Subjects of the Copenhagen Osteoarthritis Study. Acta Radiologica 49: 436-441.

53. Kang AC, Gooding AJ, Coates MH, et al. 2010. Computed tomography assessment of hip joints in asymptomatic individuals in relation to femoroacetabular impingement. Am J Sports Med 38: 1160-1165.

54. Harris MD, Reese SP, Peters CL, et al. 2013. Three-dimensional Quantification of Femoral Head Shape in Controls and Patients with Cam-type Femoroacetabular Impingement. Ann Biomed Eng 41: 1162-1171.

55. Hansen BJ, Harris MD, Anderson LA, et al. 2011. Correlation between radiographic measures of acetabular morphology with 3D femoral head coverage in patients with acetabular retroversion. Acta Orthop 83: 233-239.

56. Schmid MR, Notzli HP, Zanetti M, et al. 2003. Cartilage lesions in the hip: diagnostic effectiveness of MR arthrography. Radiology 226: 382-386.

57. Apprich S, Mamisch TC, Welsch GH, et al. 2012. Evaluation of articular cartilage in patients with femoroacetabular impingement (FAI) using T2* mapping at different time points at 3.0 Tesla MRI: a feasibility study. Skeletal Radiol 41: 987-995.

58. Beaule PE, Hynes K, Parker G, et al. 2012. Can the alpha angle assessment of cam impingement predict acetabular cartilage delamination? Clin Orthop Relat Res 470: 3361-3367.

59. Wenger DE, Kendell KR, Miner MR, et al. 2004. Acetabular labral tears rarely occur in the absence of bony abnormalities. Clin Orthop Relat Res: 145-150.

60. Clohisy JC, Baca G, Beaule PE, et al. 2013. Descriptive epidemiology of femoroacetabular impingement: a north american cohort of patients undergoing surgery. Am J Sports Med 41: 1348-1356.

61. Ito K, Leunig M, Ganz R. 2004. Histopathologic features of the acetabular labrum in femoroacetabular impingement. Clin Orthop Relat Res: 262-271.

62. Leunig M, Beck M, Kalhor M, et al. 2005. Fibrocystic changes at anterosuperior femoral neck: prevalence in hips with femoroacetabular impingement. Radiology 236: 237-246.

63. Pfirrmann CW, Mengiardi B, Dora C, et al. 2006. Cam and pincer femoroacetabular impingement: characteristic MR arthrographic findings in 50 patients. Radiology 240: 778-785.

64. Beaule PE, O'Neill M, Rakhra K. 2009. Acetabular labral tears. J Bone Joint Surg Am 91: 701-710.

65. Bedi A, Dolan M, Hetsroni I, et al. 2011. Surgical treatment of femoroacetabular impingement improves hip kinematics: a computer-assisted model. Am J Sports Med 39 Suppl: 43S-49S.

66. Bedi A, Dolan M, Leunig M, et al. 2011. Static and dynamic mechanical causes of hip pain. Arthroscopy 27: 235-251.

67. Pollard TC, Villar RN, Norton MR, et al. 2010. Genetic influences in the aetiology of femoroacetabular impingement: a sibling study. J Bone Joint Surg Br 92: 209-216.

68. Baker-Lepain JC, Lynch JA, Parimi N, et al. 2012. Variant alleles of the Wnt antagonist FRZB are determinants of hip shape and modify the relationship between hip shape and osteoarthritis. Arthritis Rheum 64: 1457-1465.

69. Waarsing JH, Kloppenburg M, Slagboom PE, et al. 2011. Osteoarthritis susceptibility genes influence the association between hip morphology and osteoarthritis. Arthritis Rheum 63: 1349-1354.

70. Dudda M, Kim YJ, Zhang Y, et al. 2011. Morphologic differences between the hips of Chinese women and white women: could they account for the ethnic difference in the prevalence of hip osteoarthritis? Arthritis Rheum 63: 2992-2999.

71. Hogervorst T, Eilander W, Fikkers JT, et al. 2012. Hip ontogenesis: how evolution, genes, and load history shape hip morphotype and cartilotype. Clin Orthop Relat Res 470: 3284-3296.

72. Johnson JK, Renner JB, Dahners LE. 2012. Anteroposterior thickening of the femoral neck with aging decreases the "offset" in men. Am J Sports Med 40: 2213-2217.

73. Ganz R, Leunig M, Leunig-Ganz K, et al. 2008. The etiology of osteoarthritis of the hip: an integrated mechanical concept. Clin Orthop Relat Res 466: 264-272.

74. Siebenrock KA, Wahab KH, Werlen S, et al. 2004. Abnormal extension of the femoral head epiphysis as a cause of cam impingement. Clin Orthop Relat Res: 54-60.

75. Carsen S, Moroz PJ, Rakhra K, et al. 2013. The Otto Aufranc Award. On the Etiology of the Cam Deformity: A Cross-sectional Pediatric MRI Study. Clin Orthop Relat Res [Epub ahead of print].

76. Agricola R, Bessems JH, Ginai AZ, et al. 2012. The development of Cam-type deformity in adolescent and young male soccer players. Am J Sports Med 40: 1099-1106.

77. Siebenrock KA, Ferner F, Noble PC, et al. 2011. The cam-type deformity of the proximal femur arises in childhood in response to vigorous sporting activity. Clin Orthop Relat Res 469: 3229-3240.

78. Kocher MS, Tucker R. 2006. Pediatric athlete hip disorders. Clin Sports Med 25: 241-253, viii.

79. Fadul DA, Carrino JA. 2009. Imaging of femoroacetabular impingement. J Bone Joint Surg Am 91 Suppl 1: 138-143.

80. Bardakos NV, Villar RN. 2009. Predictors of progression of osteoarthritis in femoroacetabular impingement: a radiological study with a minimum of ten years follow-up. J Bone Joint Surg Br 91: 162-169.

81. Hartofilakidis G, Bardakos NV, Babis GC, et al. 2011. An examination of the association between different morphotypes of femoroacetabular impingement in asymptomatic subjects and the development of osteoarthritis of the hip. J Bone Joint Surg Br 93: 580-586.

82. Audenaert EA, Peeters I, Van Onsem S, et al. 2011. Can we predict the natural course of femoroacetabular impingement? Acta Orthop Belg 77: 188-196.

83. Wall PD, Fernandez M, Griffin DR, et al. 2013. Nonoperative treatment for femoroacetabular impingement: a systematic review of the literature. Pm R 5: 418-426.

84. Matsuda DK, Carlisle JC, Arthurs SC, et al. 2011. Comparative systematic review of the open dislocation, mini-open, and arthroscopic surgeries for femoroacetabular impingement. Arthroscopy 27: 252-269.

85. Botser IB, Smith TW, Jr., Nasser R, et al. 2011. Open surgical dislocation versus arthroscopy for femoroacetabular impingement: a comparison of clinical outcomes. Arthroscopy 27: 270-278.

86. Bedi A, Zaltz I, De La Torre K, et al. 2011. Radiographic comparison of surgical hip dislocation and hip arthroscopy for treatment of cam deformity in femoroacetabular impingement. Am J Sports Med 39 Suppl: 20S-28S.

87. Cohen SB, Huang R, Ciccotti MG, et al. 2012. Treatment of femoroacetabular impingement in athletes using a mini-direct anterior approach. Am J Sports Med 40: 1620-1627.

88. Siebenrock KA, Schoeniger R, Ganz R. 2003. Anterior femoro-acetabular impingement due to acetabular retroversion. Treatment with periacetabular osteotomy. J Bone Joint Surg Am 85-A: 278-286.

89. Peters CL, Anderson LA, Erickson JA, et al. 2011. An algorithmic approach to surgical decision making in acetabular retroversion. Orthopedics 34: 10.

90. Larson CM. 2010. Arthroscopic management of pincer-type impingement. Sports Med Arthrosc 18: 100-107.

91. Larson CM, Giveans MR, Stone RM. 2012. Arthroscopic debridement versus refixation of the acetabular labrum associated with femoroacetabular impingement: mean 3.5-year follow-up. Am J Sports Med 40: 1015-1021.

92. Krych AJ, Thompson M, Knutson Z, et al. 2013. Arthroscopic labral repair versus selective labral debridement in female patients with femoroacetabular impingement: a prospective randomized study. Arthroscopy 29: 46-53.

93. Clohisy JC, St John LC, Schutz AL. 2010. Surgical treatment of femoroacetabular impingement: a systematic review of the literature. Clin Orthop Relat Res 468: 555-564.

94. Karthikeyan S, Roberts S, Griffin D. 2012. Microfracture for acetabular chondral defects in patients with femoroacetabular impingement: results at second-look arthroscopic surgery. Am J Sports Med 40: 2725-2730.

95. Harris JD, Erickson BJ, Bush-Joseph CA, et al. 2013. Treatment of femoroacetabular impingement: a systematic review [published online ahead of print June 7 2013]. Current reviews in musculoskeletal medicine.

96. Philippon MJ, Briggs KK, Yen YM, et al. 2009. Outcomes following hip arthroscopy for femoroacetabular impingement with associated chondrolabral dysfunction: minimum two-year follow-up. J Bone Joint Surg Br 91: 16-23.

97. Clohisy JC, Knaus ER, Hunt DM, et al. 2009. Clinical presentation of patients with symptomatic anterior hip impingement. Clin Orthop Relat Res 467: 638-644.

98. Peters CL, Erickson JA, Anderson L, et al. 2009. Hip-preserving surgery: understanding complex pathomorphology. J Bone Joint Surg Am 91 Suppl 6: 42-58.

99. Lavigne M, Parvizi J, Beck M, et al. 2004. Anterior femoroacetabular impingement: part I. Techniques of joint preserving surgery. Clin Orthop Relat Res: 61-66.

100. Buckwalter JA. 1996. Effects of early motion on healing of musculoskeletal tissues. Hand Clin 12: 13-24.

101. Finsterbush A, Friedman B. 1975. Reversibility of joint changes produced by immobilization in rabbits. Clin Orthop Relat Res: 290-298.

102. Salter RB. 1989. The biologic concept of continuous passive motion of synovial joints. The first 18 years of basic research and its clinical application. Clin Orthop Relat Res: 12-25.

103. Williams JM, Moran M, Thonar EJ, et al. 1994. Continuous passive motion stimulates repair of rabbit knee articular cartilage after matrix proteoglycan loss. Clin Orthop Relat Res: 252-262.

104. Pfirrmann CW, Duc SR, Zanetti M, et al. 2008. MR arthrography of acetabular cartilage delamination in femoroacetabular cam impingement. Radiology 249: 236-241.

105. Kelly BT, Bedi A, Robertson CM, et al. 2012. Alterations in internal rotation and alpha angles are associated with arthroscopic cam decompression in the hip. Am J Sports Med 40: 1107-1112.

106. Kennedy MJ, Lamontagne M, Beaule PE. 2009. Femoroacetabular impingement alters hip and pelvic biomechanics during gait Walking biomechanics of FAI. Gait Posture 30: 41-44.

107. Brisson N, Lamontagne M, Kennedy MJ, et al. 2012. The effects of cam femoroacetabular impingement corrective surgery on lower-extremity gait biomechanics. Gait Posture 37: 258-263.

108. Rylander JH, Shu B, Andriacchi TP, et al. 2011. Preoperative and postoperative sagittal plane hip kinematics in patients with femoroacetabular impingement during level walking. The American journal of sports medicine 39 Suppl: 36S-42S.

109. Lenaerts G, Bartels W, Gelaude F, et al. 2009. Subject-specific hip geometry and hip joint centre location affects calculated contact forces at the hip during gait. J Biomech 42: 1246-1251.

110. Piazza SJ, Erdemir A, Okita N, et al. 2004. Assessment of the functional method of hip joint center location subject to reduced range of hip motion. J Biomech 37: 349-356.

111. Audenaert EA, Mahieu P, Pattyn C. 2011. Three-dimensional assessment of cam engagement in femoroacetabular impingement. Arthroscopy 27: 167-171.

112. Tannast M, Kubiak-Langer M, Langlotz F, et al. 2007. Noninvasive three-dimensional assessment of femoroacetabular impingement. J Orthop Res 25: 122-131.

113. Kubiak-Langer M, Tannast M, Murphy SB, et al. 2007. Range of motion in anterior femoroacetabular impingement. Clin Orthop Relat Res 458: 117-124.

114. Lee CB, Clark J. 2011. Fluoroscopic demonstration of femoroacetabular impingement during hip arthroscopy. Arthroscopy 27: 994-1004.

115. Wassilew GI, Janz V, Heller MO, et al. 2013. Real time visualization of femoroacetabular impingement and subluxation using 320-slice computed tomography. J Orthop Res 31: 275-281.

116. Bey MJ, Kline SK, Tashman S, et al. 2008. Accuracy of biplane x-ray imaging combined with model-based tracking for measuring in-vivo patellofemoral joint motion. J Orthop Surg 3: 38.

117. Bey MJ, Zauel R, Brock SK, et al. 2006. Validation of a new model-based tracking technique for measuring three-dimensional, in vivo glenohumeral joint kinematics. J Biomech Eng 128: 604-609.

118. Seibert JA. 1997. The AAPM/RSNA physics tutorial for residents. X-ray generators. Radiographics 17: 1533-1557.

119. Zink FE. 1997. X-ray tubes. Radiographics 17: 1259-1268.

120. Balter S. 2001. Interventional Fluoroscopy: Physics, Technology, and Safety. New York: Wiley-Liss; 284 p.

121. Wang J, Blackburn TJ. 2000. The AAPM/RSNA physics tutorial for residents: X-ray image intensifiers for fluoroscopy. Radiographics 20: 1471-1477.

122. Tashman S. 2008. Comments on "validation of a non-invasive fluoroscopic imaging technique for the measurement of dynamic knee joint motion". J Biomech 41: 3290-3291: author reply 3292-3293.

123. Seibert JA. 2006. Flat-panel detectors: how much better are they? Pediatr Radiol 36 Suppl 2: 173-181.

124. Cowen AR, Davies AG, Sivananthan MU. 2008. The design and imaging characteristics of dynamic, solid-state, flat-panel x-ray image detectors for digital fluoroscopy and fluorography. Clin Radiol 63: 1073-1085.

125. Gronenschild E. 1997. The accuracy and reproducibility of a global method to correct for geometric image distortion in the x-ray imaging chain. Med Phys 24: 1875-1888.

126. Liu RR, Rudin S, Bednarek DR. 1999. Super-global distortion correction for a rotational C-arm x-ray image intensifier. Med Phys 26: 1802-1810.

127. Reimann DA, Flynn MJ. 1992. Automated distortion correction of X-ray image intensifier images. pp. 1339-1341.

128. Rudin S, Bednarek DR, Wong R. 1991. Accurate characterization of image intensifier distortion. Med Phys 18: 1145-1151.

129. Cerveri P, Forlani C, Borghese NA, et al. 2002. Distortion correction for x-ray image intensifiers: local unwarping polynomials and RBF neural networks. Med Phys 29: 1759-1771.

130. Reimann DA, Flynn MJ. 1992. Automated Distortion Correction of X-ray Image Intensifier Images. IEEE Nuclear Science Symposium and Medical Imaging Conference. Orlando, FL: IEEE; pp. 1339-1341.

131. Soimu D, Badea C, Pallikarakis N. 2003. A novel approach for distortion correction for X-ray image intensifiers. Comput Med Imaging Graph 27: 79-85.

132. Kwon YM. DLT Method. http://www.kwon3d.com/theory/dlt/dlt.html. Accessed July 29, 2013.

133. Choo AM, Oxland TR. 2003. Improved RSA accuracy with DLT and balanced calibration marker distributions with an assessment of initial-calibration. J Biomech 36: 259-264.

134. Tashman S, Anderst W. 2003. In-vivo measurement of dynamic joint motion using high speed biplane radiography and CT: application to canine ACL deficiency. J Biomech Eng 125: 238-245.

135. You BM, Siy P, Anderst W, et al. 2001. In vivo measurement of 3-D skeletal kinematics from sequences of biplane radiographs: application to knee kinematics. IEEE Trans Med Imaging 20: 514-525.

136. Bingham JT. 2006. An Automated Matching Algorithm for Dual Orthogonal Fluoroscopy. Massachusettes Institute of Technology, Cambridge, MA.

137. Li G, Van de Velde SK, Bingham JT. 2008. Validation of a non-invasive fluoroscopic imaging technique for the measurement of dynamic knee joint motion. J Biomech 41: 1616-1622.

138. Anderst WJ, Vaidya R, Tashman S. 2008. A technique to measure three-dimensional in vivo rotation of fused and adjacent lumbar vertebrae. Spine J 8: 991-997.

139. Bingham JT, Papannagari R, Van de Velde SK, et al. 2008. In vivo cartilage contact deformation in the healthy human tibiofemoral joint. Rheumatology 47: 1622-1627.

140. Boyer PJ, Massimini DF, Gill TJ, et al. 2008. In vivo articular cartilage contact at the glenohumeral joint: preliminary report. J Orthop Sci 13: 359-365.

141. Caputo AM, Lee JY, Spritzer CE, et al. 2009. In vivo kinematics of the tibiotalar joint after lateral ankle instability. Am J Sports Med 37: 2241-2248.

142. Kozanek M, Wang S, Passias PG, et al. 2009. Range of motion and orientation of the lumbar facet joints in vivo. Spine J 34: E689-696.

143. Li G, Papannagari R, Nha KW, et al. 2007. The coupled motion of the femur and patella during in vivo weightbearing knee flexion. J Biomech Eng 129: 937-943.

144. Lu TW, Tsai TY, Kuo MY, et al. 2008. In vivo three-dimensional kinematics of the normal knee during active extension under unloaded and loaded conditions using single-plane fluoroscopy. Med Eng Phys 30: 1004-1012.

145. Moynihan AL, Varadarajan KM, Hanson GR, et al. 2010. In vivo knee kinematics during high flexion after a posterior-substituting total knee arthroplasty. Int Orthop 34: 497-503.

146. Nha KW, Papannagari R, Gill TJ, et al. 2008. In vivo patellar tracking: clinical motions and patellofemoral indices. J Orthop Res 26: 1067-1074.

147. Wan L, de Asla RJ, Rubash HE, et al. 2008. In vivo cartilage contact deformation of human ankle joints under full body weight. J Orthop Res 26: 1081-1089.

148. Deneweth JM, Bey MJ, McLean SG, et al. 2010. Tibiofemoral joint kinematics of the anterior cruciate ligament-reconstructed knee during a single-legged hop landing. Am J Sports Med 38: 1820-1828.

149. McDonald CP, Bachison CC, Chang V, et al. 2010. Three-dimensional dynamic in vivo motion of the cervical spine: assessment of measurement accuracy and preliminary findings. Spine J 10: 497-504.

150. Martin DE, Greco NJ, Klatt BA, et al. 2011. Model-based tracking of the hip: implications for novel analyses of hip pathology. The Journal of arthroplasty 26: 88-97.

151. Myers CA, Torry MR, Peterson DS, et al. 2011. Measurements of tibiofemoral kinematics during soft and stiff drop landings using biplane fluoroscopy. Am J Sports Med 39: 1714-1722.

152. Anderst WJ, Tashman S. 2003. A method to estimate in vivo dynamic articular surface interaction. J Biomech 36: 1291-1299.

153. Li G, Wuerz TH, DeFrate LE. 2004. Feasibility of using orthogonal fluoroscopic images to measure in vivo joint kinematics. J Biomech Eng 126: 314-318.

154. Li G, DeFrate LE, Park SE, et al. 2005. In vivo articular cartilage contact kinematics of the knee: an investigation using dual-orthogonal fluoroscopy and magnetic resonance image-based computer models. Am J Sports Med 33: 102-107.

155. Wan L, de Asla RJ, Rubash HE, et al. 2006. Determination of in-vivo articular cartilage contact areas of human talocrural joint under weightbearing conditions. Osteoarthritis Cartilage 14: 1294-1301.

156. Martin DE, Greco NJ, Klatt BA, et al. 2011. Model-based tracking of the hip: implications for novel analyses of hip pathology. J Arthroplasty 26: 88-97.

157. Lin H, Wang S, Tsai TY, et al. 2013. In-vitro validation of a non-invasive dual fluoroscopic imaging technique for measurement of the hip kinematics. Med Eng Phys 35: 411-416.

158. Tsai TY, Li JS, Wang S, et al. 2013. A novel dual fluoroscopic imaging method for determination of THA kinematics: in-vitro and in-vivo study. J Biomech 46: 1300-1304.

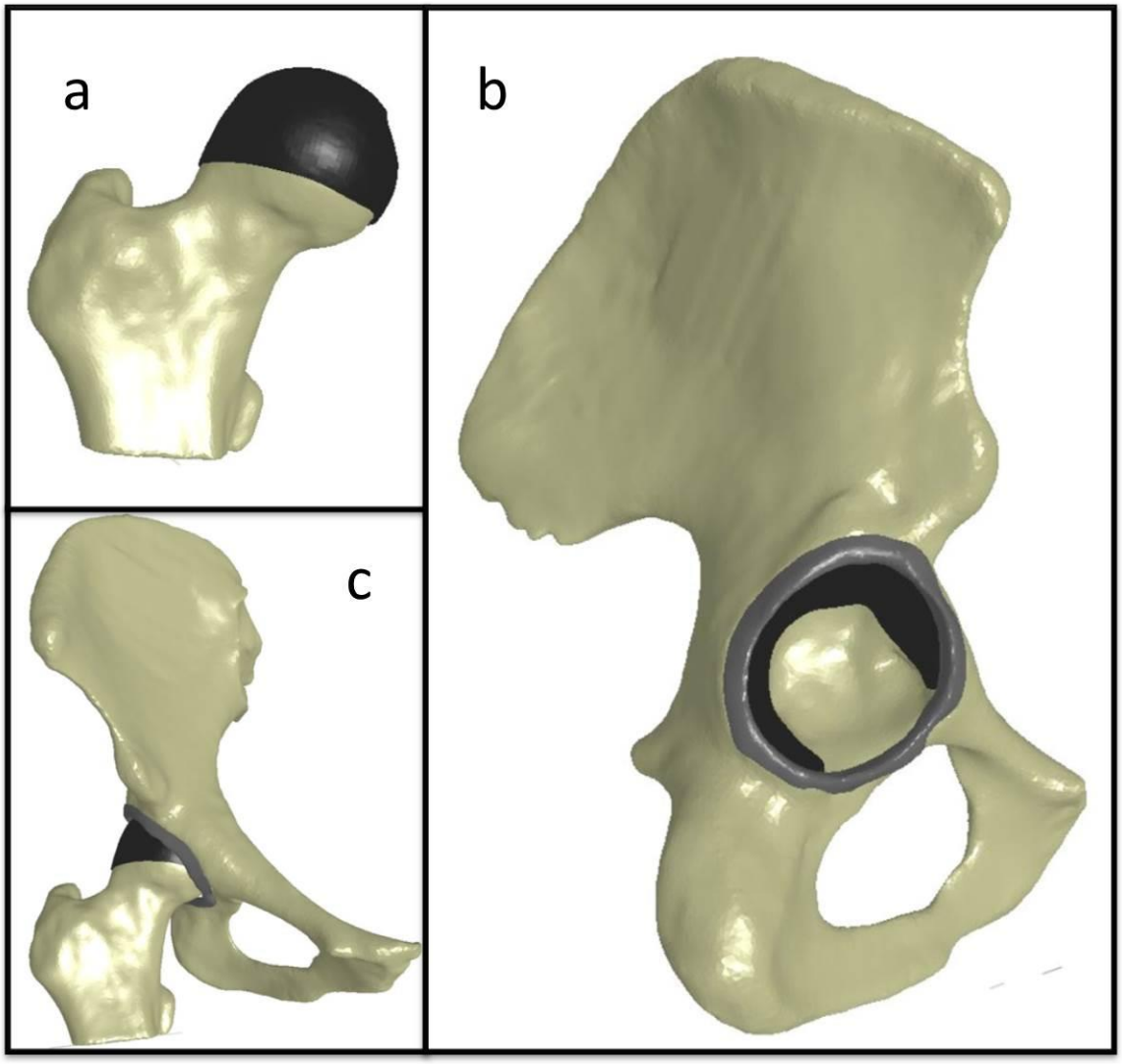

Figure 1.1. Schematic of a normal right hip joint. a) Anterior view of proximal femur with femoral cartilage (dark grey). b) Medial view of hemipelvis with acetabular cartilage on the lunate surface (dark grey) and acetabular labrum with transverse acetabular ligament attached to the acetabular rim (light grey). c) Anterior view of pelvis and femur in neutral position (midstance of walking).

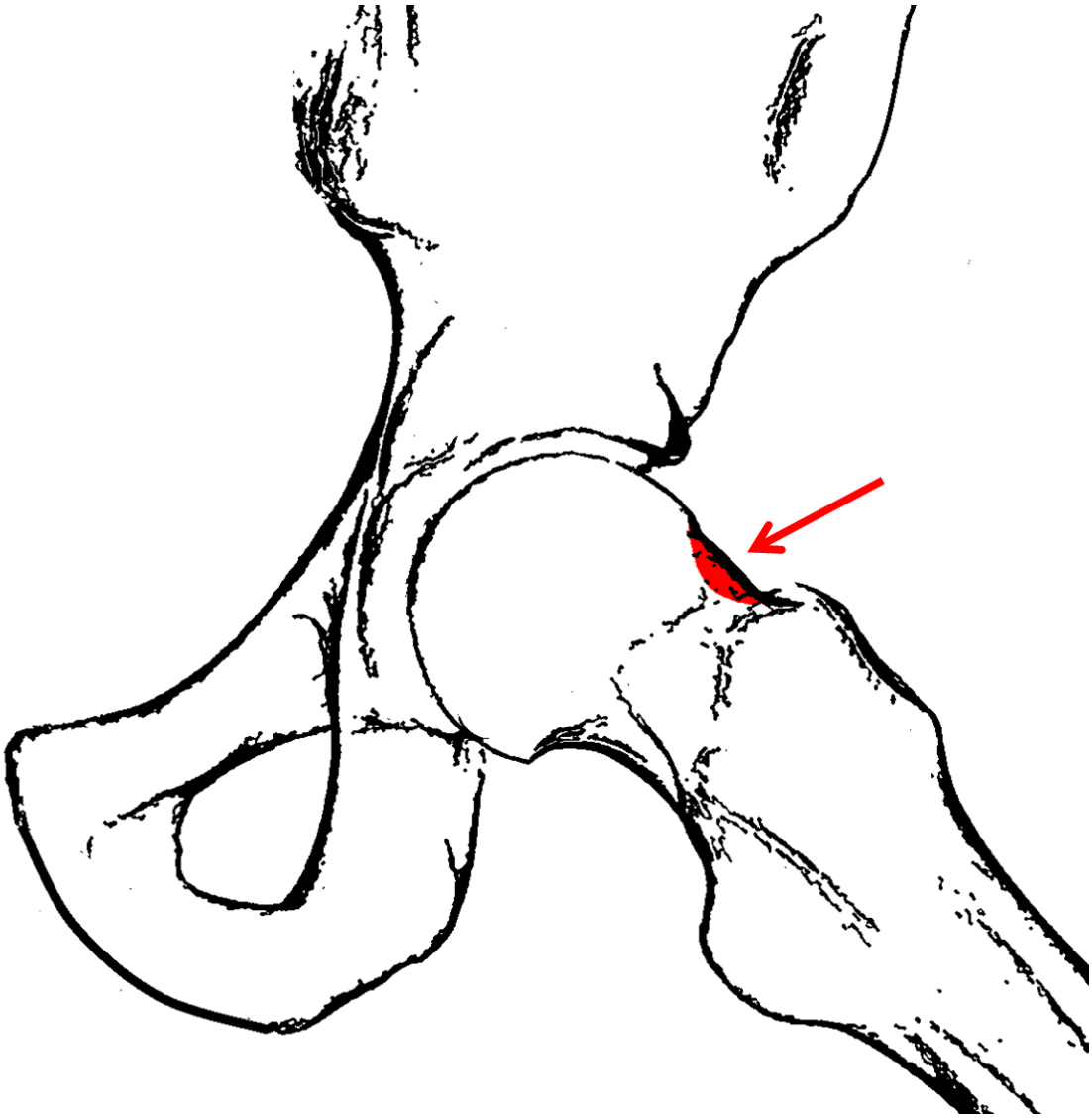

Figure 1.2. Schematic of cam femoroacetabular impingement. Frog-leg lateral view of the femur. Arrow points to highlighted section of excess bone on the femoral neck.

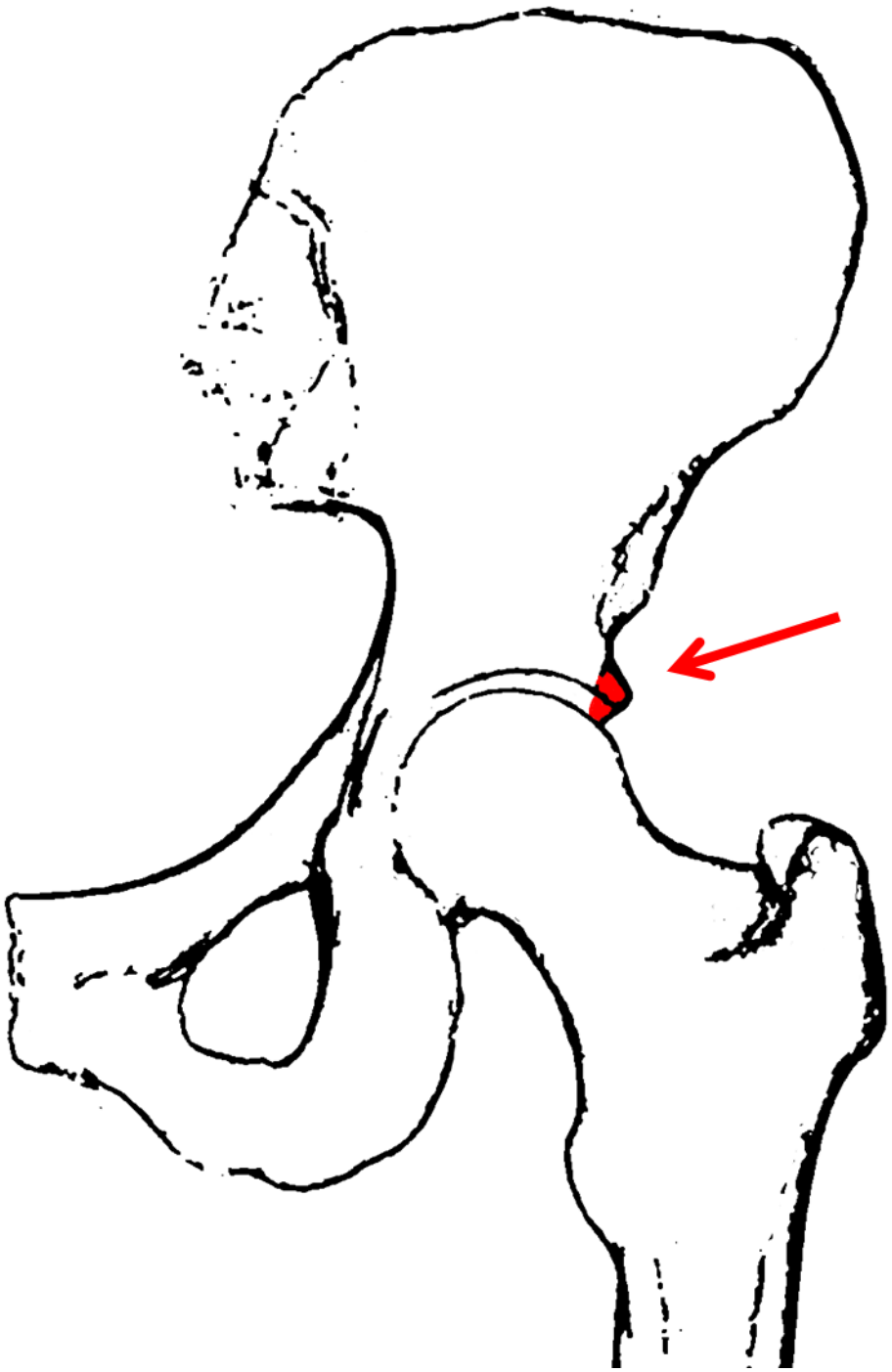

Figure 1.3. Schematic of pincer femoroacetabular impingement. Anteroposterior view of the pelvis. Arrow points to highlighted section of excess bone on the superior acetabular rim.

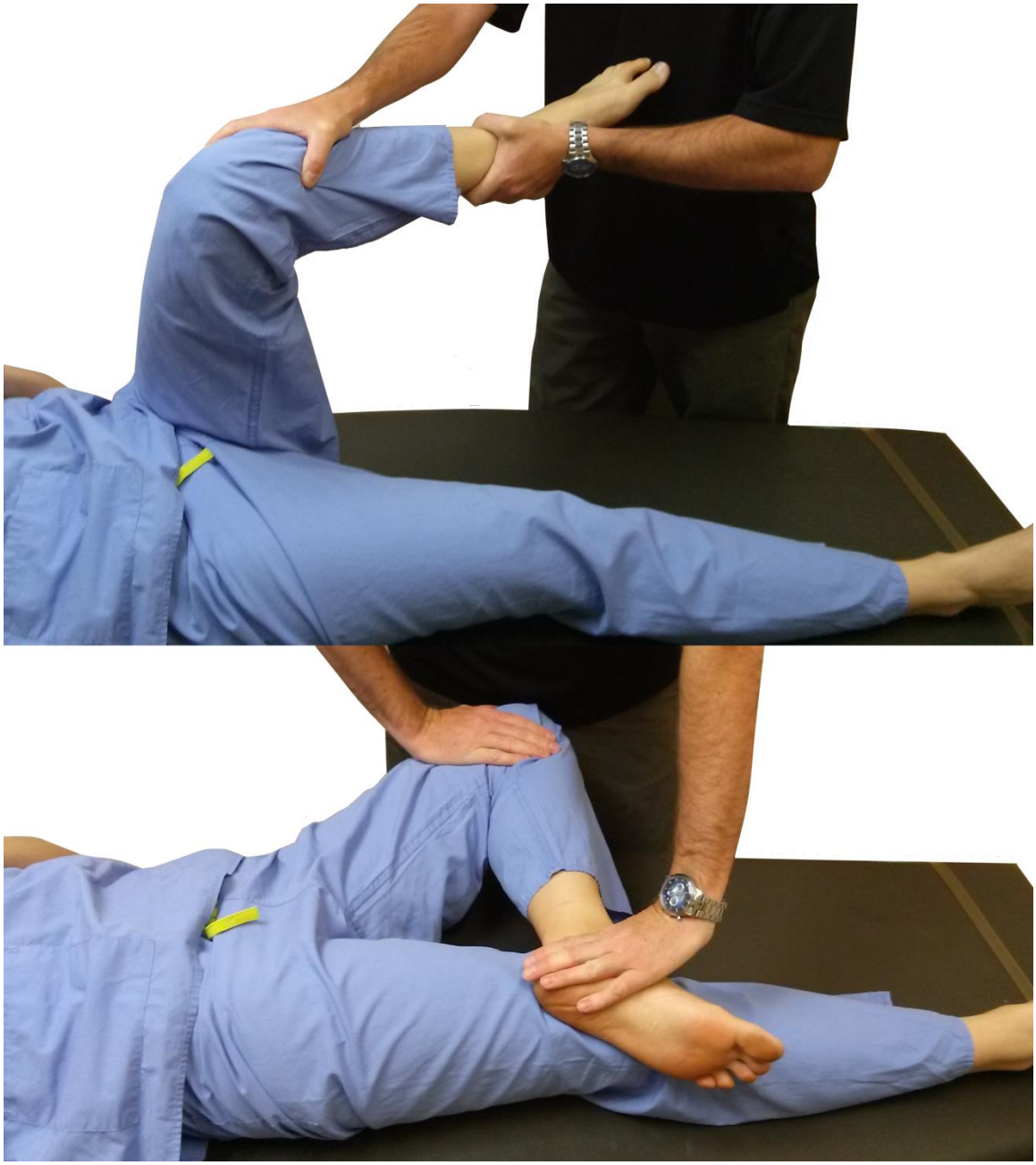

Figure 1.4. Photographs of patient and examiner during clinical exams commonly used to assess FAI patients. Top: Terminal position of impingement exam, in which the hip is flexed and then internally rotated and adducted. Bottom: Terminal position of the Flexion-Abduction-External Rotation (FABER) Test, in which the subject's leg is in a figure-four position, with hip external rotation and abduction.

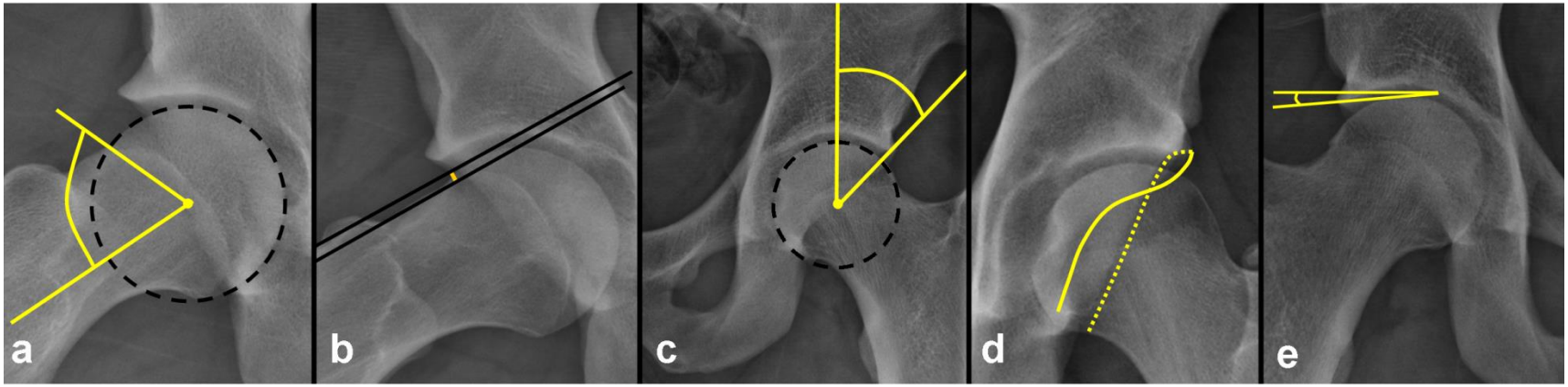

Figure 1.5. Radiographic measures commonly used in the diagnosis of FAI. a) Alpha angle - the angle between the longitudinal axis of the femoral neck and a line connecting the femoral head center and the point where the head deviates from a best fit circle. b) Head-neck offset - the difference in radius between the femoral head and neck. c) Lateral center edge angle - angle formed by a vertical line and a line connecting the femoral head center with the lateral edge of the acetabulum. d) Crossover sign - the posterior wall of the acetabulum (dashed line) crosses the anterior wall (solid line) on anteroposterior radiographs. e) Acetabular index - angle formed by a horizontal line and a line connecting the medial point of the sclerotic zone with the lateral center of the acetabulum.

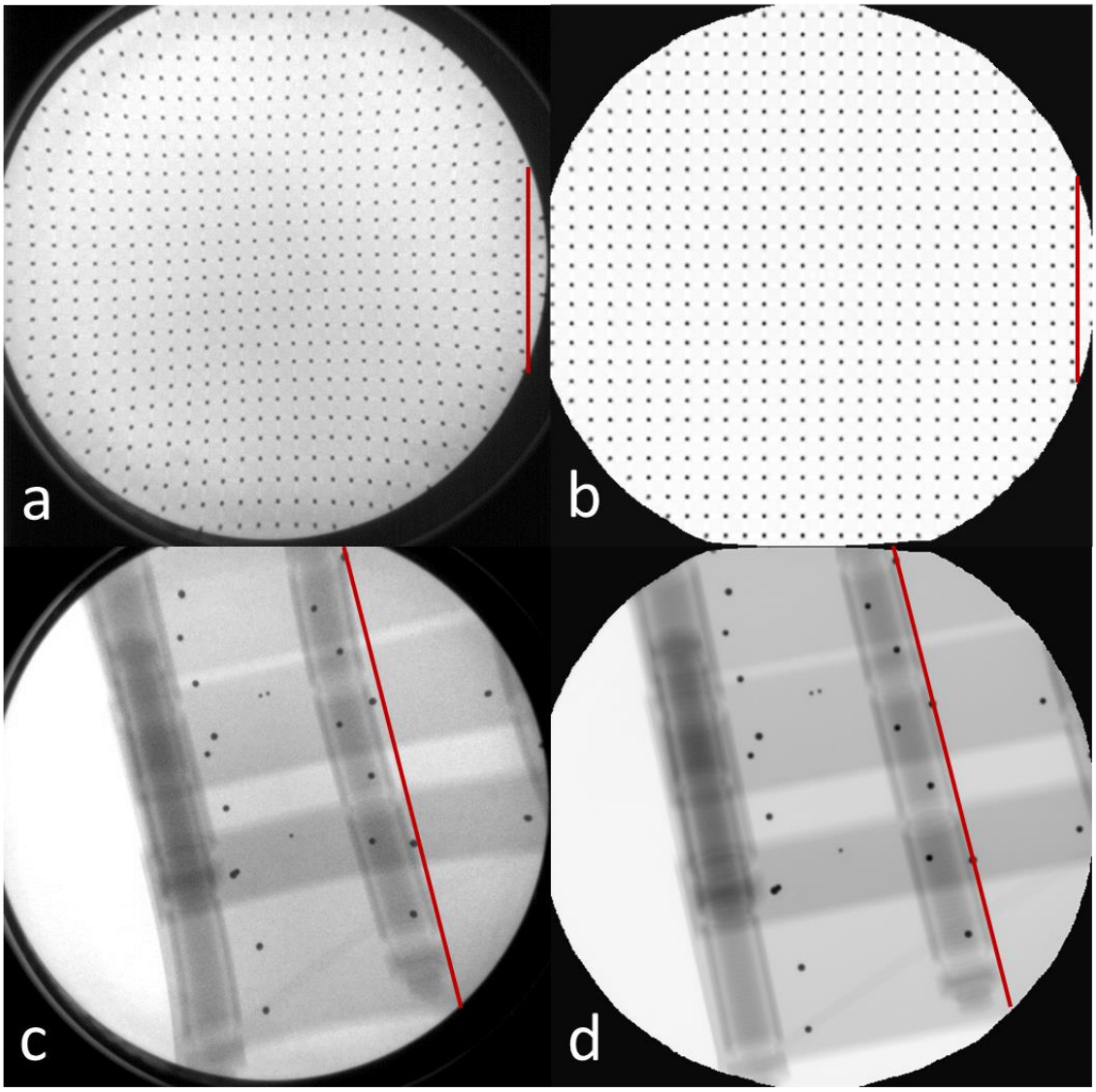

Figure 1.6. Example of distorted fluoroscope images and corrected images. a) Distorted image of grid of radioopaque beads spaced one millimeter apart. Note pincushion distortion. This image is used in image processing software to establish the transformation required to correct distortion. b) Corrected grid, note regular spacing. After the image processing software established the require transformation for the grid, the transformation can be applied to correct all images collected from the same fluoroscope. c) Distorted image of calibration frame. d) Corrected image of calibration frame. On all images, note reference line highlighting curvature in distorted images and corrected geometry in processed images.

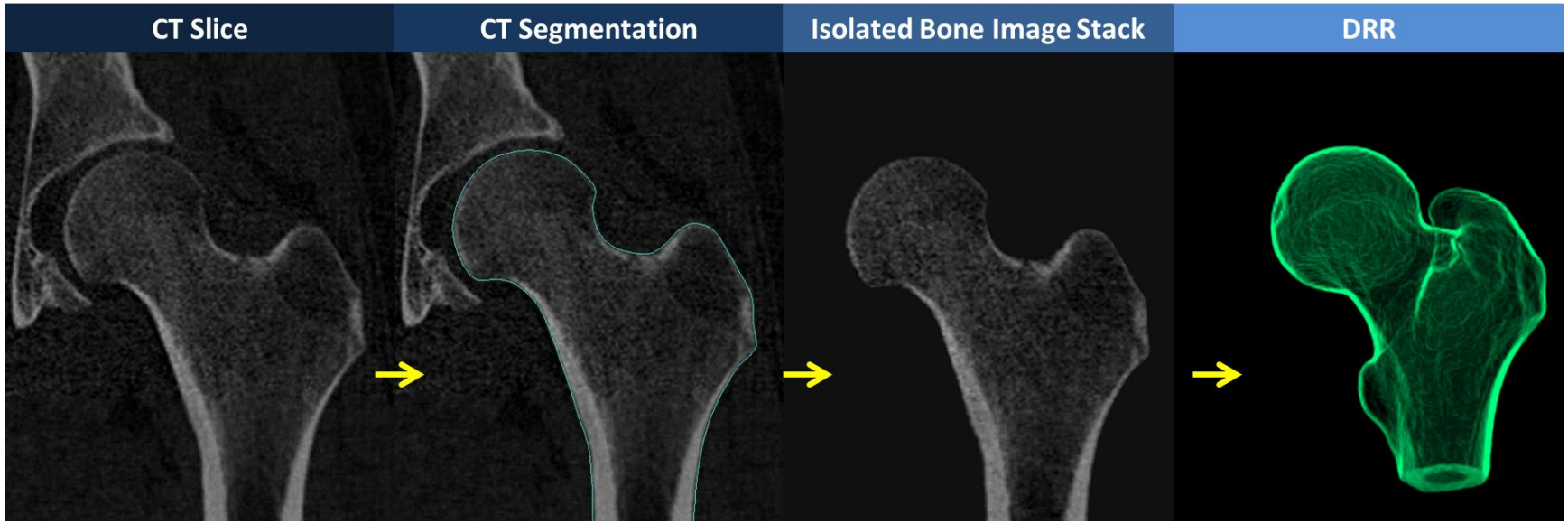

Figure 1.7. Generation of digitally reconstructed radiographs (DRRs). CT images are acquired of the joint of interest. Each bone is segmented semi-automatically. A Boolean operation applied the CT data set and segmented image labels generates an image stack containing the pixels of a single bone. Ray trace projection through this isolated image stack generates a digitally reconstructed radiograph of the bone of interest.

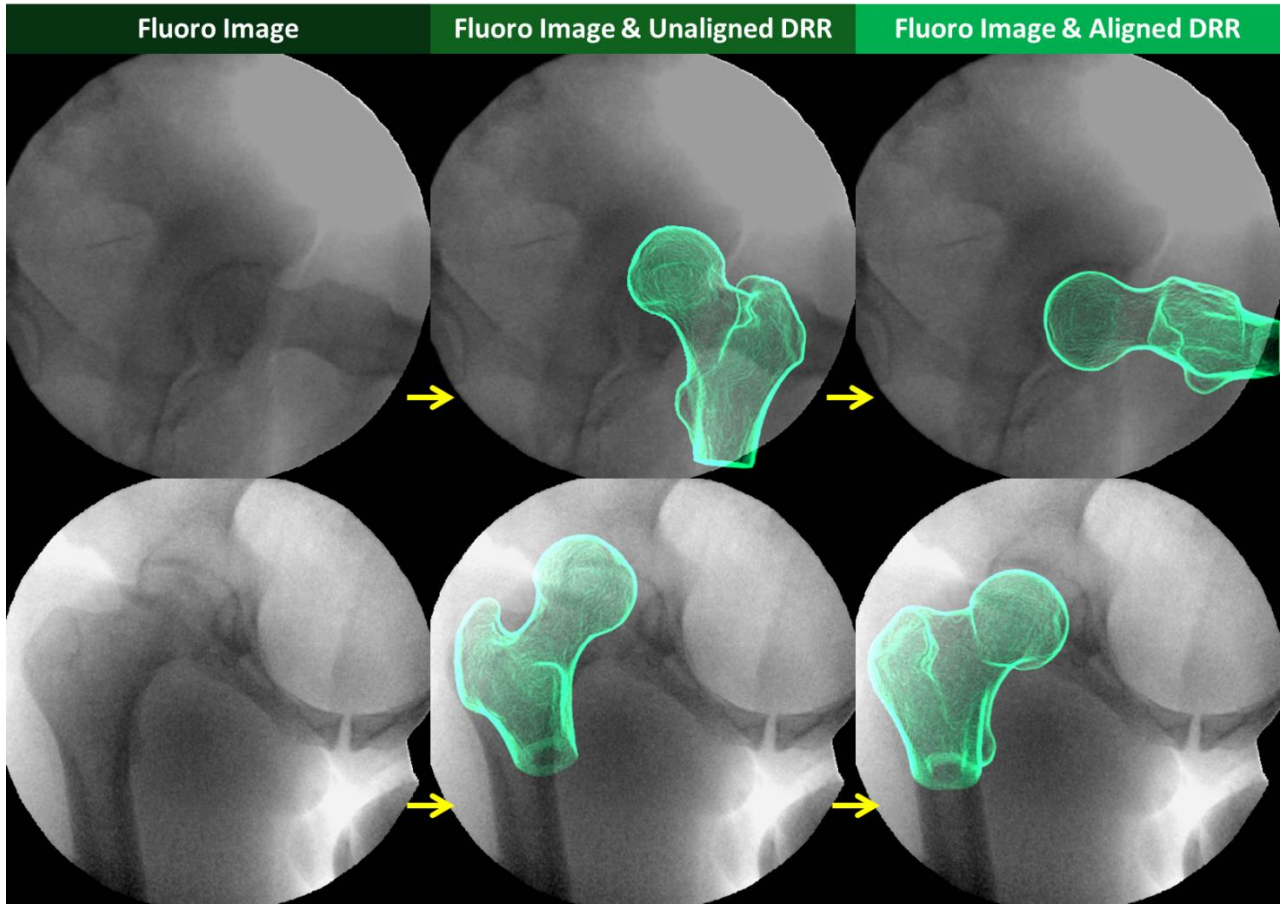

Figure 1.8. Model-based tracking. Images of the same joint are acquired by two synced fluoroscopes (top and bottom rows) and loaded into model-based tracking software. Previous calibration steps established the relative configuration and perspective of the two fluoroscopes, and the user interface is initialized with digitally reconstructed radiographs (DRRs) of the bone of interest overlaid on the fluoroscopy images in an unaligned position. The model-based tracking software then optimizes the pixel intensity agreement between the DRR and the original video to align the bone to its in vivo position. The process is repeated for all frames of the video.

CHAPTER 2

RADIOGRAPHIC PREVALENCE OF FEMOROACETABULAR IMPINGEMENT IN COLLEGIATE FOOTBALL PLAYERS

Ashley L. Kapron, Andrew E. Anderson, Stephen K. Aoki,
Lee G. Phillips, David J. Petron, Robert Toth,
Christopher L Peters

The Journal of Bone and Joint Surgery, 2011;93(e111):1-10

e111(1)

AAOS
AMERICAN ACADEMY OF ORTHOPAEDIC SURGEONS

EXHIBIT SELECTION

Radiographic Prevalence of Femoroacetabular Impingement in Collegiate Football Players

AAOS Exhibit Selection

Ashley L. Kapron, BS, Andrew E. Anderson, PhD, Stephen K. Aoki, MD, Lee G. Phillips, MD, David J. Petron, MD, Robert Toth, PA-C, and Christopher L. Peters, MD

Investigation performed at the University of Utah, Salt Lake City, Utah

Background: The prevalence of femoroacetabular impingement may be greater in athletes than in the general population because of increased loading of the hip during sports. This study evaluated the radiographs of collegiate football players in order to quantify the prevalence of femoroacetabular impingement in asymptomatic athletes.

Methods: Sixty-seven male collegiate football players (age, 21 ± 1.9 years) participated in this prospective study. Both hips (n = 134) were evaluated independently by two orthopaedic surgeons for radiographic signs of femoroacetabular impingement. The alpha angle and femoral head-neck offset were measured on frog-leg lateral radiographs. The lateral center-edge angle, acetabular index, crossover sign, and alpha angle were measured on anteroposterior radiographs. Data for continuous variables were averaged between observers prior to assessing prevalence. Cam femoroacetabular impingement was considered to be present if the femoral head-neck offset was <8 mm and/or the alpha angle was >50° on either radiograph. Pincer femoroacetabular impingement was considered to be present if the lateral center-edge angle was >40°, the acetabular index was <0°, and/or a positive crossover sign was detected by both observers.

Results: Ninety-five percent of the 134 hips had at least one sign of cam or pincer impingement, and 77% had more than one sign. Twenty-one percent had only one sign of cam femoroacetabular impingement and 57% had both signs. Fifty-two percent had only one sign of pincer femoroacetabular impingement, 10% had two, and 4% had all three signs. Specifically, 72% had an abnormal alpha angle, 64% had a decreased femoral head-neck offset, 61% had a positive crossover sign, 16% had a decreased acetabular index, and 7% had an increased lateral center-edge angle. Fifty percent of all hips had at least one sign of pincer femoroacetabular impingement and at least one sign of cam impingement. Interobserver and intraobserver repeatability was moderate or better for each measure (range, 0.59 to 0.85).

Conclusions: Morphologic abnormalities associated with cam and pincer femoroacetabular impingement were common in these collegiate football players. The prevalence of cam and pincer femoroacetabular impingement was substantially higher than the previously reported prevalence in the general population.

Femoroacetabular impingement, the reduction of clearance between the femoral head and the acetabulum, may be the principal cause of idiopathic hip osteoarthritis[1-6]. Femoroacetabular impingement has two predominant forms: pincer, defined as anterior acetabular overcoverage; and cam, defined as asphericity of the femoral head or the head-neck

Disclosure: None of the authors received payments or services, either directly or indirectly (i.e., via his or her institution), from a third party in support of any aspect of this work. One or more of the authors, or his or her institution, has had a financial relationship, in the thirty-six months prior to submission of this work, with an entity in the biomedical arena that could be perceived to influence or have the potential to influence what is written in this work. No author has had any other relationships, or has engaged in any other activities, that could be perceived to influence or have the potential to influence what is written in this work. The complete **Disclosures of Potential Conflicts of Interest** submitted by authors are always provided with the online version of the article.

TABLE I Descriptive Analysis of Demographic, Questionnaire, and Continuous Radiographic Parameters

	Mean and Std. Dev.	Range
Age *(yr)*	21 ± 1.9	17 to 26
Height *(cm)*	185 ± 6.3	170 to 197
Weight *(kg)*	102 ± 19	75 to 144
Body mass index *(kg/m²)*	30 ± 4.5	23 to 40
Hip Outcome Score *(%)*		
Activities of daily living	99 ± 3.8	72 to 100
Sports	98 ± 4.4	78 to 100
Lateral center-edge angle *(deg)*	30 ± 6.6	13 to 45
Acetabular index *(deg)*	4.9 ± 5.4	−7.0 to 17
Head-neck offset *(mm)*	6.5 ± 3.1	−0.8 to 14
Alpha angle *(deg)*		
Frog-leg lateral	52 ± 10	34 to 83
Anteroposterior	55 ± 12	38 to 88

junction. Fifty to seventy-five percent of patients with femoroacetabular impingement have been reported to exhibit evidence of both forms of impingement[1]. Cam impingement is believed to cause damage to the labrum and adjacent cartilage as the nonspherical femoral head is repeatedly forced into a generally spherical acetabulum[3]. Pincer impingement is believed to cause premature contact between the femoral head-neck junction and the protruding rim of the acetabulum that can result in labral tears, cartilage lesions, and damage to the posteroinferior region of the acetabulum[3].

It has been suggested that femoral remodeling due to increased loading may result in femoroacetabular impingement deformities[7,8]. Football players have greater musculature and body mass than most other athletes, and may therefore be at greater risk for femoroacetabular impingement. Collegiate and professional football players are likely to start football and other sports at a young age. Thus, high physical demands placed on their joints during the critical stages of hip development or at later times may initiate remodeling, leading to abnormalities consistent with femoroacetabular impingement. In addition, continued sports participation could cause femoroacetabular impingement to become symptomatic as the increased loading exacerbates the labral or articular cartilage damage. In fact, femoroacetabular impingement has been cited as an underlying factor responsible for hip injuries in National Football League players[9].

Understanding the prevalence of femoroacetabular impingement in athletes such as football players would increase awareness among health-care providers of the potential vulnerability of this population, leading to earlier diagnosis and treatment. In a 1971 study, the prevalence of deformities similar to those seen in hips with cam femoroacetabular impingement was estimated to be 24% in asymptomatic, athletic men[10]. However, the radiographic definition of femoroacetabular impingement used in this early study was not consistent with current criteria for defining the presence of femoroacetabular impingement. To our knowledge, the only other studies regarding femoroacetabular impingement in athletes have involved patients who presented with hip pain[11,12]. Thus, the present study evaluated the radiographs of collegiate football players in order to quantify the prevalence of femoroacetabular impingement in asymptomatic athletes.

Materials and Methods

Subject Selection

Ninety-six male football players from the University of Utah Division 1A collegiate football team were invited to participate in this prospective study, which was approved by our institutional review board. Sixty-seven players provided informed consent and were included in the study.

Radiographic Evaluation

Pelvic anteroposterior and frog-leg lateral radiographs of both hips (n = 134) were made in the supine position with gonad shielding. Each hip was evaluated independently in a digital environment (iSite PACS; Philips Healthcare, Andover, Massachusetts) by two orthopaedic surgeons (L.G.P. and S.K.A.) for radiographic signs of femoroacetabular impingement. One of the surgeons (L.G.P.) repeated the evaluation ten weeks later.

Femoral sphericity was assessed on both the frog-leg lateral and the anteroposterior radiograph with use of the alpha angle[13] (Fig. 1, *top*, and 2, *bottom*). The alpha angle is the angle between the longitudinal axis of the femoral neck and a line connecting the center of the femoral head with the point where the femoral head deviates from a best-fit sphere. The femoral head-neck offset, which is the difference in radius between the femoral head and neck, was measured on the frog-leg lateral radiograph[14] (Fig. 1, *bottom*).

TABLE II Occurrence of Abnormal Radiographic Findings Indicative of Femoroacetabular Impingement

Type of Impingement	Abnormality	Left Hips *(no.)*	Right Hips *(no.)*	% Bilateral	% of All Hips
Cam					
	Alpha angle >50°				
	Frog-leg lateral	37	36	88	54
	Anteroposterior	40	34	84	55
	Head-neck offset <8 mm	46	40	91	64
Pincer					
	Crossover sign	42	40	90	61
	Lateral center-edge angle >40°	6	4	60	7
	Acetabular index <0°	14	7	48	16

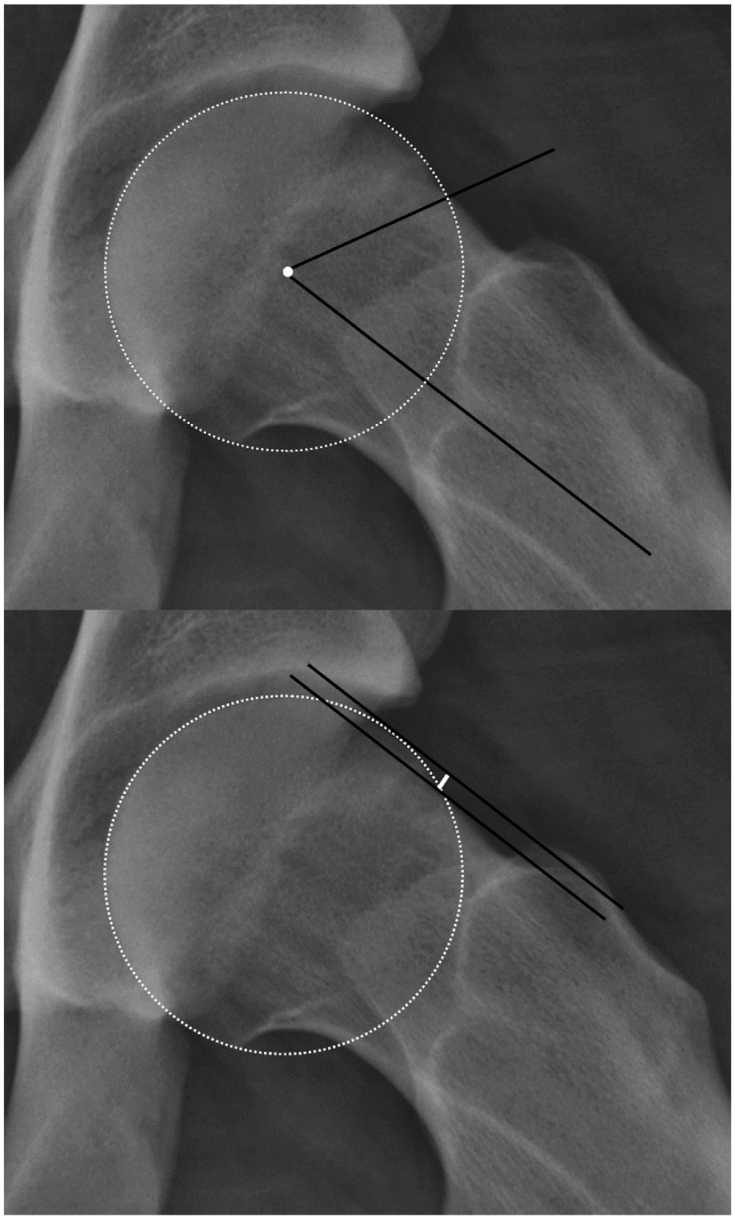

Fig. 1

Frog-leg lateral radiograph of the left hip of a twenty-two-year-old man with moderate cam femoroacetabular impingement abnormalities. *Top:* The alpha angle (62°) is measured between the longitudinal axis of the femoral neck and a line connecting the center of the femoral head and the point where the head deviates from a best-fit sphere. *Bottom:* The femoral head-neck offset (3.1 mm) is measured between two lines, one tangent to the most anterolateral aspect of the femoral neck and one tangent to the femoral head, that are both parallel to the longitudinal axis of the femoral neck.

Acetabular coverage was evaluated on the anteroposterior radiograph with use of the lateral center-edge angle and the acetabular index. The lateral center-edge angle is formed by a line connecting the lateral edge of the acetabulum with the center of the femoral head and a line perpendicular to the line connecting the ischial tuberosities[14] (Fig. 2, *top*, left side of image). The acetabular index, or "acetabular roof angle," is the angle formed by a line parallel to the line connecting the ischial tuberosities and a line connecting the medial point of the sclerotic zone with the lateral edge of the acetabulum[14] (Fig. 2, *top*, right side of image). Acetabular coverage was also evaluated on the anteroposterior radiograph with use of the crossover sign, in which the posterior wall of the acetabulum crosses the anterior wall, indicating acetabular retroversion (Fig. 2, *bottom*).

Radiographic signs of osteoarthritis in each hip were graded according to the Tönnis system[15], in which 0 indicates "no signs of osteoarthritis," 1 indicates "slight narrowing of joint space, slight lipping at joint margin, slight sclerosis of femoral head or acetabulum," 2 indicates "small cysts in femoral head or acetabulum, increasing narrowing of joint space, moderate loss of

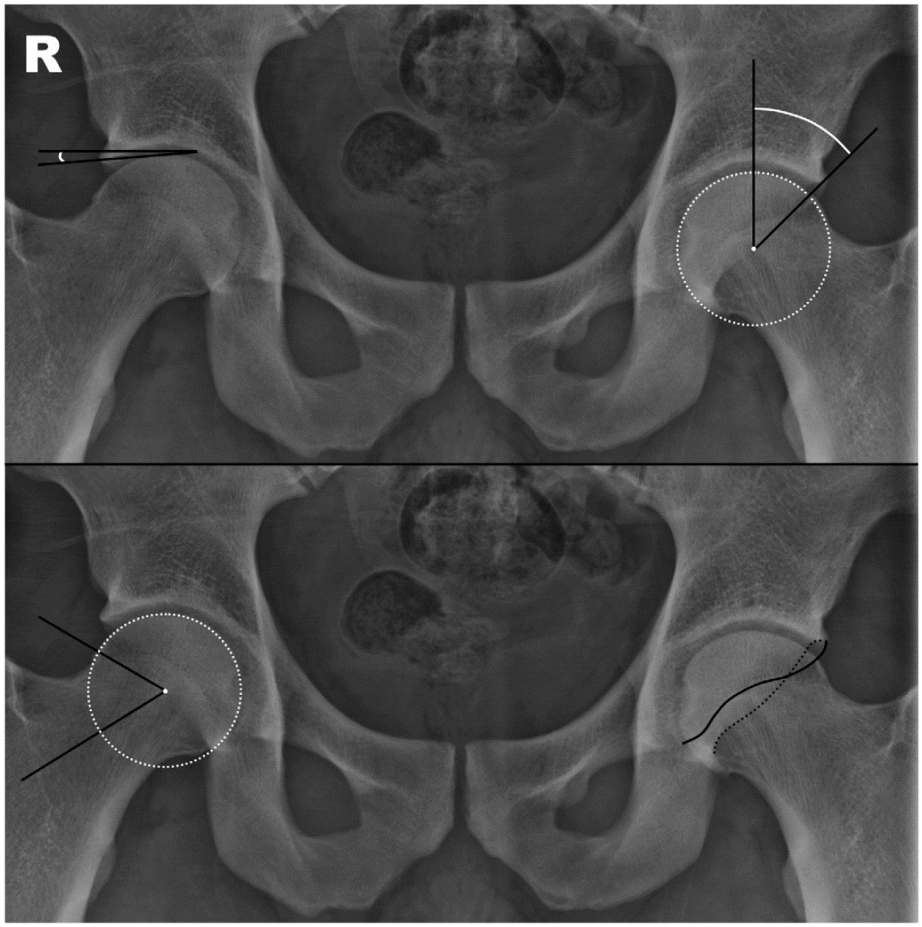

Fig. 2

Anteroposterior pelvic radiograph of a nineteen-year-old man with mixed femoroacetabular impingement abnormalities. *Top:* As shown on the left side of the image, the acetabular index (−3.5°) is measured between the line parallel to the line connecting the ischial tuberosities and a line connecting the medial point of the sclerotic zone with the lateral edge of the acetabulum. As shown on the right side of the image, the lateral center-edge angle (45°) is measured between a line perpendicular to the line connecting the ischial tuberosities and a line connecting the center of the femoral head with the lateral edge of the acetabulum. *Bottom:* The presence of lateral cam deformities is demonstrated by the abnormal alpha angle of 61° in each hip (as illustrated on the left side of the image). The right side of the image demonstrates the presence of the crossover sign, as the posterior acetabular rim (dashed line) crosses the anterior acetabular rim (solid line).

sphericity of femoral head," and 3 indicates "large cysts, severe narrowing or obliteration of joint space, severe deformity of femoral head, or avascular necrosis [osteonecrosis]."

Determining the Prevalence of Femoroacetabular Impingement

For continuous variables (e.g., the alpha angle), the value recorded by each of the two observers during the initial evaluation was averaged. The crossover sign was considered to be present only if it was detected by both observers. For the Tönnis grade, the highest score reported by either observer was used, representing the worst-case evaluation.

A risk score, equal to the number of radiographic abnormalities associated with cam and pincer femoroacetabular impingement, was calculated for each hip. The two possible cam abnormalities were an alpha angle of >50° (on either the anteroposterior or the frog-leg lateral radiograph) and a head-neck offset of <8 mm[13,14]. The three possible pincer abnormalities were the presence of the crossover sign, an abnormally sloping acetabular roof (acetabular index of <0°)[16], and acetabular overcoverage (lateral center-edge angle of >40°)[17]. The prevalence of femoroacetabular impingement was assessed on the basis of the percentage of hips at each risk level (0, 1, or 2 signs of cam impingement and 0, 1, 2, or 3 signs of cam impingement). The presence of at least one cam sign and at least one pincer sign was considered to indicate mixed impingement.

Questionnaire

Each subject completed a short questionnaire on the same day that the radiographs were made. This questionnaire was based on the validated Hip Outcome Score and was designed to ascertain the condition of the hip during the previous week[18,19]. The "activities of daily living" and "sports" subscores were calculated, with higher values representing greater function.

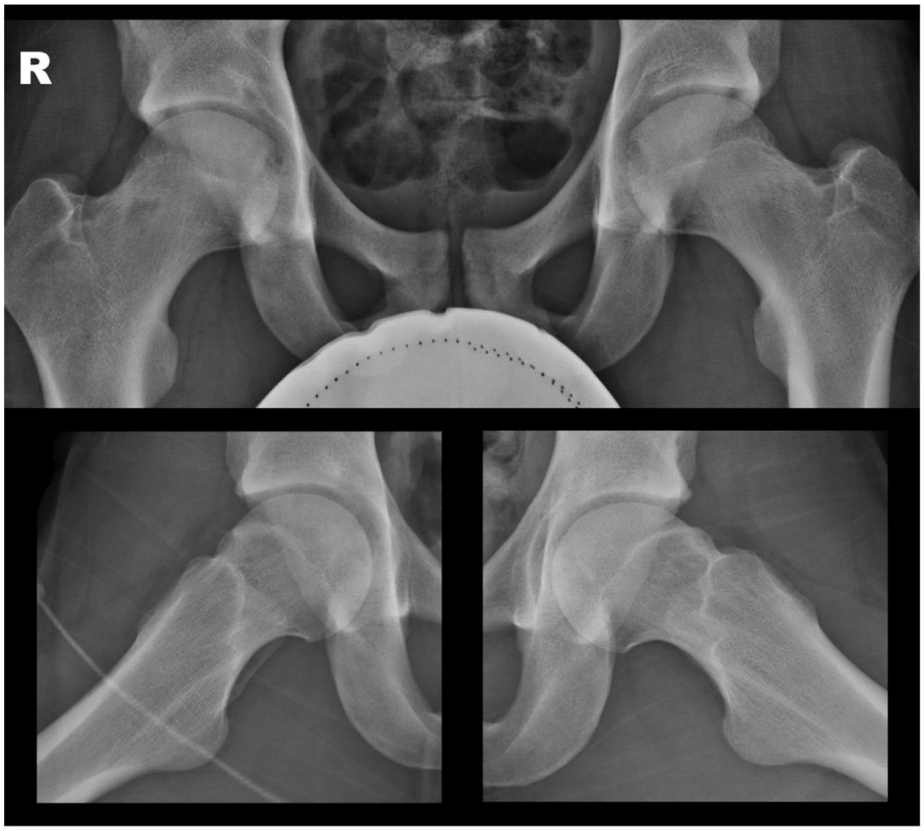

Fig. 3

Radiographs of a twenty-one-year-old man with mixed femoroacetabular impingement abnormalities. This man was the only subject whose activities of daily living (ADL) subscore was <90%. (His ADL subscore was 72% and his sports subscore was 78%.) *Top:* Anteroposterior radiograph showing an abnormal alpha angle in both the right hip (left side of image, 62°) and the left hip (right side of image, 65°). *Bottom:* Frog-leg lateral radiographs showing the lowest femoral head-neck offset of any subject in the study (right hip [left panel], 2.1 mm; left hip [right panel], −0.8 mm) and an elevated alpha angle (right hip, 68°; left hip, 74°).

Statistical Analysis

Interobserver and intraobserver repeatability was assessed with use of the interclass correlation coefficient (ICC) for continuous variables and the kappa statistic for dichotomous variables (Stata version 11; StataCorp, College Station, Texas). Observer agreement was considered slight if the ICC or kappa value was <0.21, fair if it was 0.21 to 0.40, moderate if it was 0.41 to 0.60, substantial if it was 0.61 to 0.80, and almost perfect if it was >0.80[13,20]. Histograms of the alpha angle (on the anteroposterior and the frog-leg lateral radiograph) and of the lateral center-edge angle were also generated with use of Stata.

The Fisher-Freeman-Halton test was used to compare study participation by player position. The ten position groups included cornerback, defensive line, linebacker, offensive line, quarterback, running back, safety, special team, tight end, and wide receiver. The Fisher-Freeman-Halton test is a generalization of the Fisher exact test to greater than 2×2 crosstabulation tables[21]. This test was also used to determine whether the prevalence of the previously defined radiographic abnormalities differed significantly among player position groups.

The relationship between each continuous radiographic measure (alpha angle on the anteroposterior and the frog-lateral radiograph, acetabular index, lateral center-edge angle, and femoral head-neck offset) and each demographic measure (height, weight, and body mass index [BMI]) was assessed with use of a random-effects linear regression model that accounted for the nonindependence of the comparisons involving a player's left and right hips. A p value of <0.05 was considered to indicate that the regression coefficient (slope) was significantly different from zero. The correlation coefficient (r value) was computed with use of the method of Bland and Altman[22], which also accounts for the nonindependence of the measurements on the left and right sides. Finally, a t test was used to determine whether the height, weight, or BMI differed between subjects with a crossover sign in either hip and subjects without a crossover sign.

Source of Funding

There was no external funding source for this study.

Results

Demographics and Symptoms

The mean age (and standard deviation) of the sixty-seven football players was 21 ± 1.9 years, the height was 185 ± 6.3 cm, the weight was 102 ± 19 kg, and the BMI was 30 ± 4.5 kg/m^2. Study participation did not differ significantly by player position.

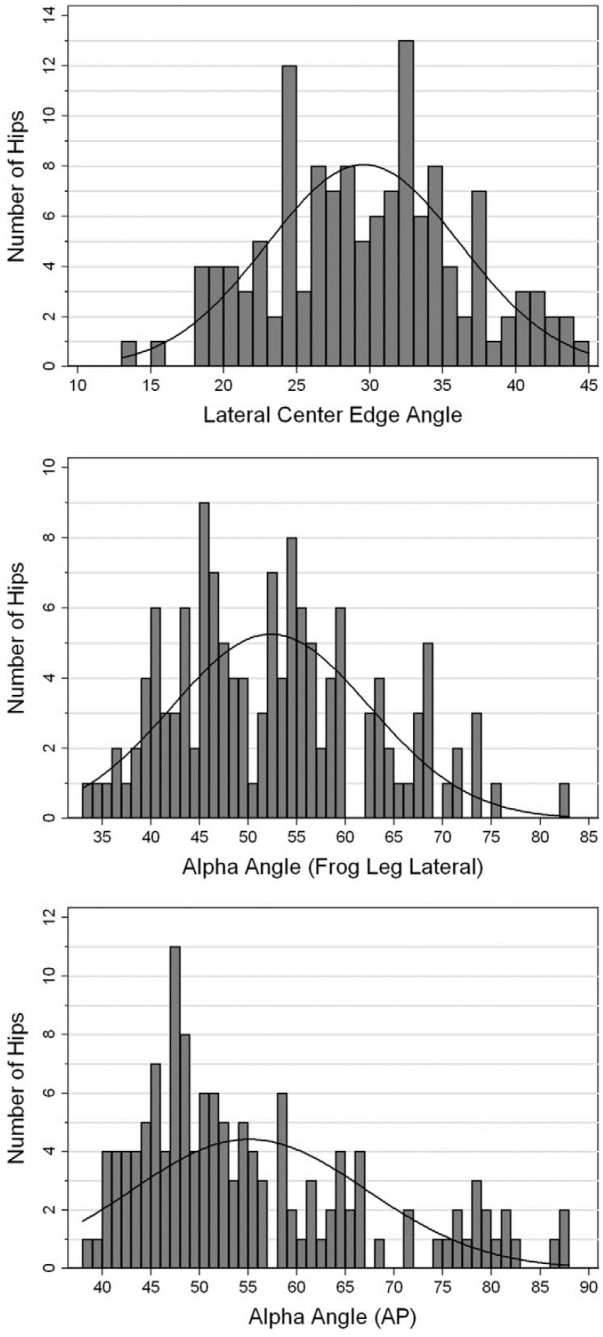

Fig. 4
Histograms showing the distribution of the lateral center-edge angle (top) and of the alpha angle measured on the frog-leg lateral (middle) and the anteroposterior (AP) (bottom) radiograph. The solid curve shows the best-fit normal distribution.

In general, the players were asymptomatic at the time of the study according to the self-reported Hip Outcome Score questionnaire (Table I). Only one player had an activities of daily living subscore of <90%; the activities of daily living subscore for this player was 72%, and the sports subscore was 78%. This subject's radiographs exhibited both cam and pincer

TABLE III Prevalence of Femoroacetabular Impingement According to Risk Score

Type of Impingement	Risk Score*	No. of Hips	% of All Hips
Cam			
	0	29	22
	1	28	21
	2	77	57
Pincer			
	0	45	34
	1	70	52
	2	14	10
	3	5	4
Mixed†			
	0	67	50
	1	67	50

*The risk score was calculated by summing the number of radiographic abnormalities present. The two possible cam abnormalities were an alpha angle of >50° (on either the anteroposterior or the frog-leg lateral radiograph) and a head-neck offset of >8 mm. The three possible pincer abnormalities were the presence of the crossover sign, an acetabular index of <0°, and a lateral center-edge angle of >40°. †Mixed abnormalities were defined by the presence of at least one cam abnormality and at least one pincer abnormality.

abnormalities, including the lowest femoral head-neck offset in this cohort (Fig. 3). Four additional players had a sports subscore between 80% and 90%; the remaining sixty-two players had sports and activities of daily living subscores of >90%. Slight osteoarthritis (Tönnis grade 1) was detected in 16% (twenty-two) of the 134 hips; the remaining hips had no signs of osteoarthritis.

Radiographic Evidence of Femoroacetabular Impingement

Table II summarizes the prevalence of each radiographic abnormality describing cam and pincer impingement among the 134 hips. At least 48% of the subjects with a particular radiographic abnormality had the same type of abnormality in both hips (Table II). The distribution of the lateral center-edge and alpha angles is depicted in Figure 4.

Ninety-five percent of the 134 hips had at least one sign of cam or pincer impingement, and 77% had more than one sign. Seventy-eight percent had at least one sign of cam abnormality, and 66% had at least one sign of pincer abnormality (Table III). Fifty percent had mixed impingement. Specifically, 72% had an abnormal alpha angle (detected on the anteroposterior and/or the frog-leg lateral radiograph), 64% had a decreased femoral head-neck offset, 61% had a positive crossover sign, 16% had a decreased acetabular index, and 7% had an increased lateral center-edge angle (Table II).

There were significant ($p < 0.05$) but weak ($r = 0.24$ to 0.32) correlations between some demographic and radiographic measures. Specifically, both weight and BMI were correlated with the alpha angle (on both the anteroposterior and the frog-leg lateral radiograph) and with the femoral head-neck offset. Height was correlated with the lateral center-edge angle. The other combinations of demographic and radiographic measures were not significantly correlated. Height ($p = 0.342$), weight ($p = 0.466$), and BMI ($p = 0.593$) did not differ significantly between subjects with and without a crossover sign.

TABLE IV Interobserver and Intraobserver Repeatability of Radiographic Measures

Measure	Repeatability	
	Interobserver	Intraobserver
Crossover sign*	0.59	0.68
Alpha angle†		
Frog-leg lateral	0.71	0.76
Anteroposterior	0.72	0.59
Head-neck offset†	0.74	0.81
Acetabular index†	0.76	0.80
Lateral center-edge angle†	0.85	0.85

*Kappa value. †Intraclass correlation coefficient.

Repeatability

Interobserver repeatability was almost perfect for the lateral center-edge angle; substantial for the acetabular index, femoral head-neck offset, and alpha angle on both radiographs; and moderate for the crossover sign (Table IV). Intraobserver repeatability was almost perfect for the femoral head-neck offset and lateral center-edge angle; substantial for the crossover sign, alpha angle on the frog-leg lateral radiograph, and acetabular index; and moderate for the alpha angle on the anteroposterior radiograph (Table IV).

Discussion

In younger subjects, hip pain and labral tears occur more frequently in joints with femoroacetabular impingement abnormalities[23,24]. Thus, the high percentage of players with radiographic signs of cam and pincer impingement in the present study suggests that football players may have a high propensity to develop symptomatic femoroacetabular impingement. In fact, femoroacetabular impingement is a recognized cause of hip pain in professional football players[9,11]. In the present study of collegiate football players, 95% (127) of the 134 hips had at least one sign of cam or pincer impingement, with 66% having pincer deformities, 78% having cam deformities, and 50% having mixed femoroacetabular impingement deformities. When a sign of femoroacetabular impingement was present in a player, it occurred bilaterally at least 48% of the time.

The prevalence of cam impingement reported in the present study is three times greater than the 24% prevalence of cam-like deformities reported in a 1971 study of asymptomatic, athletic men[10]. The osseous abnormalities evaluated in this early study were described as femoral tilt deformity or mild

slipped capital femoral epiphysis, similar to the modern description of cam femoroacetabular impingement. However, femoroacetabular impingement had not been formally described in 1971, and the radiographic measures used in the early study were different from those that are commonly applied today. Nevertheless, our findings are consistent with this earlier study in demonstrating a link between abnormal femoral morphology and high-level sports participation in males.

The estimated prevalence of femoroacetabular impingement in the athletes evaluated in the present study is much higher than the previously reported prevalence in asymptomatic members of the general population[25-29]. In one study of 200 asymptomatic volunteers, 25% of the eighty-nine male subjects had at least one hip with a cam deformity, defined as an alpha angle of >50.5°[25]. Of the 1332 male participants in the Copenhagen Osteoarthritis Study, 15.2% had a pincer abnormality (lateral center-edge angle >45°) and 19.6% had a pistol grip deformity consistent with cam femoroacetabular impingement (triangular index ≥0 mm)[27]. In abdominal computed tomography scans of twenty-three men undergoing imaging for symptoms unrelated to the hip, 52% had at least one pincer abnormality (acetabular version angle <15°, presence of a crossover sign, or lateral center-edge angle >40°) or cam abnormality (alpha angle >55° or head-neck offset <8 mm)[29]. The majority of the abnormalities detected during imaging in both the latter study of asymptomatic individuals and a study of patients who had sought treatment for a hip condition[30] were present bilaterally, which is consistent with the findings in the present study.

The broad range of cutoff values that have been used to define cam femoroacetabular impingement can result in discrepancies between the prevalence reported in the present study and that in previous studies. For example, although a cutoff of >50° was chosen to define an abnormal alpha angle in the present study, as this angle corresponds to the most commonly used value in the literature[14,31-34], other investigators have used cutoff values ranging from 42° to 68°[16,35]. A cutoff of 43° has been proposed as the average alpha angle that allowed impingement-free motion after surgical debridement[36]. Sixty degrees has been proposed as the cutoff value for developing hip pain[30]. Another study made the distinction between normal (<68°), borderline (68° to 83°), and pathologic (>83°) alpha angles[35]. Applying the cutoffs proposed in the latter three studies, all but two of the hips in the present study may have impinged motion, 33% may develop hip pain, and 2% would be classified as "pathologic." Similar discrepancies exist for pincer femoroacetabular impingement. For example, reported cutoff values for a normal lateral center-edge angle range from 35° to 45°[27,28]. In the present study, a lateral center-edge angle of >40°[17], representing the midrange of previously reported cutoffs, was chosen to define overcoverage. Raynor et al. investigated the effect of cutoff values on the estimated prevalence of femoroacetabular impingement in eighty-eight asymptomatic subjects by evaluating alpha angles of 45°, 50°, and 55° and lateral center-edge angles of 35° and 40°. The estimated prevalence of femoroacetabular impingement depended greatly on the cutoff value that was used, ranging from 24% to 67%[28].

Thus, differences in the cutoff values used to diagnose femoroacetabular impingement could potentially account for some of the differences in prevalence between the present study and previous studies of the general population. However, the higher prevalence of femoroacetabular impingement in football players in the present study compared with the reported prevalence in the general population in previous studies may also be related to the greater loads resulting from the greater body mass and activity level in the select population in our study. Indeed, BMI and weight were significantly correlated with measures of cam femoroacetabular impingement in our study, although the strength of the correlation was weak. Since all of the subjects in our study had a similar activity level, it is unclear whether BMI or activity level contributed more strongly to the increased prevalence of femoroacetabular impingement in this population. It has been shown that cam impingement lesions in young athletic males may be due to subclinical physeal injury and subsequent femoral head remodeling[34,37]. Athletes who participate aggressively in sports during adolescence, when a relative weakness of the physis occurs[38], may be susceptible to the insidious development of cam deformities[39]. In addition, an elevated BMI may increase the risk of slipped capital femoral epiphysis[40] and may therefore have a similar impact on the risk of cam femoroacetabular impingement. The origins of the increased prevalence of pincer abnormalities in athletic subjects are more speculative. Acetabular abnormalities may develop in response to femoral head remodeling, with cam deformities provoking the formation of pincer deformities. A cam lesion may cause repeated microtrauma to the labrum, which can subsequently ossify, extending the acetabular rim and increasing coverage[37,41]. However, the incidence of labral ossification was not quantified in our study.

One strength of our study lies in its prospective nature. In addition, all radiographs were made with use of a single protocol designed specifically for this investigation. Interobserver and intraobserver repeatability of most radiographic measures was substantial or almost perfect, and was similar to that in previous studies[13,42,43]. Although the crossover sign only had a moderate kappa value for interobserver repeatability, our protocol ensured that a crossover sign was considered to be present only if both observers noted it. Thus, the reported prevalence of the crossover sign represents a conservative estimate. The remaining radiographic measures evaluated in our study were reported as the average of the first reads of both observers, to reduce the effect of interobserver variation. An additional strength of our study was the homogeneity of the cohort that was analyzed. The subjects were all male, represented a well-defined age range, and had very similar activity levels. Also, the participation rate did not depend significantly on player position. Finally, although most subjects had femoroacetabular impingement abnormalities, all had either no or only slight osteoarthritic changes (Tönnis grade 0 or 1). Furthermore, the modified Hip Outcome Score confirmed that most subjects were asymptomatic at the time of the study; only one player had an activities of daily living subscore of <90%.

Our study had several limitations. First, the supine anteroposterior radiographs were not corrected for pelvic tilt,

which can influence radiographic measures such as the crossover sign[14,44-49]. Although we acknowledge that specialized software (Hip²Norm; University of Bern, Bern, Switzerland[45,46,50]) is available to correct for pelvic tilt, the present study was performed without it, in accordance with the standard diagnostic procedure for patients in our clinic and with the majority of published studies. Furthermore, to achieve best results from Hip²Norm, calibration of individual pelvic tilt with use of a pure-lateral radiograph is recommended, and this radiograph was not obtained in our study.

In addition, it is well known that the three-dimensional abnormalities present in femoroacetabular impingement are best characterized with use of computed tomography or magnetic resonance imaging[31,51,52]. Although three-dimensional imaging was not used in our study, both anteroposterior and frog-leg lateral radiographs were made, thus visualizing two different regions of the femoral head-neck junction[13]. Since cam deformities can present differently on these two views, we diagnosed an abnormality if the alpha angle surpassed the cutoff value on either radiograph.

Another limitation involves the cutoff values used to diagnose abnormalities. Since the normal ranges for the radiographic parameters have yet to be established, the criteria used in the present study could overestimate or underestimate the prevalence of impingement. However, we have included histograms showing the distribution of the alpha angle and the lateral center-edge angle so that readers can interpret the results on the basis of any alternate cutoff values that they prefer (Fig. 4). Although the majority of reported cutoff values, including those chosen for the present study, have been designed to identify the presence of osseous abnormalities in symptomatic patients who have already sought treatment, they may not be predictive of subjects who will develop pain in the future. Furthermore, male football players represent a unique population of athletes, with an elevated body mass and perhaps increased joint loading compared with athletes in other sports. Thus, the results should be extended with caution to other athletes. Finally, a control population was not utilized in the present study; however, a comparison with previously reported values for the general population[25-29] leads to the conclusion that these players have a much higher prevalence of osseous abnormalities consistent with femoroacetabular impingement than the general population has.

The present study provides the first insight into the prevalence of femoroacetabular impingement in young, asymptomatic athletic subjects as determined with use of modern radiographic criteria. The prevalence of femoroacetabular impingement reported in our study is clearly a function of the cutoff values selected. Our study suggests that the orthopaedic and sports community should strive to find agreement on diagnostic criteria for femoroacetabular impingement so that results can be interpreted consistently across centers. Nevertheless, the prevalence of morphologic deformities found in our study was substantially higher than that in previous reports involving the general public, suggesting that vigorous sports activity in adolescence may predispose the growing hip to the development of altered morphology. It would be interesting to follow these players over time to see which players, if any, develop symptomatic femoroacetabular impingement or osteoarthritis later in life. However, on the basis of the present findings, we recommend that all football players and other high-level athletes who present with hip pain be evaluated for osseous abnormalities to determine whether femoroacetabular impingement is an underlying factor in the pain. ■

NOTE: The authors acknowledge Greg Stoddard for assistance with statistical analysis and the University of Utah football team athletic trainers for assistance with execution of the data collection portion of this study.

Ashley L. Kapron, BS
Andrew E. Anderson, PhD
Stephen K. Aoki, MD
Lee G. Phillips, MD
David J. Petron, MD
Robert Toth, PA-C
Christopher L. Peters, MD
Departments of Bioengineering (A.L.K.) and Orthopaedics
(A.E.A., S.K.A., L.G.P., D.J.P., R.T., and C.L.P.),
University of Utah, 590 Wakara Way,
Salt Lake City, UT 84108.
E-mail address for A.L. Kapron: Ashley.Kapron@utah.edu.
E-mail address for A.E. Anderson: Andrew.Anderson@hsc.utah.edu.
E-mail address for S.K. Aoki: Stephen.Aoki@hsc.utah.edu.
E-mail address for L.G. Phillips: Lee.Phillips@hsc.utah.edu.
E-mail address for D.J. Petron: David.Petron@hsc.utah.edu.
E-mail address for R. Toth: Robert.Toth@hsc.utah.edu.
E-mail address for C.L. Peters: Chris.Peters@hsc.utah.edu

References

1. Beck M, Kalhor M, Leunig M, Ganz R. Hip morphology influences the pattern of damage to the acetabular cartilage: femoroacetabular impingement as a cause of early osteoarthritis of the hip. J Bone Joint Surg Br. 2005;87:1012-8.

2. Giori NJ, Trousdale RT. Acetabular retroversion is associated with osteoarthritis of the hip. Clin Orthop Relat Res. 2003;417:263-9.

3. Lavigne M, Parvizi J, Beck M, Siebenrock KA, Ganz R, Leunig M. Anterior femoroacetabular impingement: part I. Techniques of joint preserving surgery. Clin Orthop Relat Res. 2004;418:61-6.

4. Murphy S, Tannast M, Kim YJ, Buly R, Millis MB. Debridement of the adult hip for femoroacetabular impingement: indications and preliminary clinical results. Clin Orthop Relat Res. 2004;429:178-81.

5. Tanzer M, Noiseux N. Osseous abnormalities and early osteoarthritis: the role of hip impingement. Clin Orthop Relat Res. 2004;429:170-7.

6. Stulberg S, Cordell L, Harris W, Ramsey P, MacEwen G. Unrecognized childhood hip disease: a major cause of idiopathic osteoarthritis of the hip. In: The hip. Proceedings of the Third Open Scientific Meeting of the Hip Society. St. Louis: Mosby;1975. p 212-28.

7. Gelberman RH, Cohen MS, Shaw BA, Kasser JR, Griffin PP, Wilkinson RH. The association of femoral retroversion with slipped capital femoral epiphysis. J Bone Joint Surg Am. 1986;68:1000-7.

8. Galbraith RT, Gelberman RH, Hajek PC, Baker LA, Sartoris DJ, Rab GT, Cohen MS, Griffin PP. Obesity and decreased femoral anteversion in adolescence. J Orthop Res. 1987;5:523-8.

9. Feeley BT, Powell JW, Muller MS, Barnes RP, Warren RF, Kelly BT. Hip injuries and labral tears in the National Football League. Am J Sports Med. 2008;36:2187-95.

10. Murray RO, Duncan C. Athletic activity in adolescence as an etiological factor in degenerative hip disease. J Bone Joint Surg Br. 1971;53:406-19.

11. Philippon M, Schenker M, Briggs K, Kuppersmith D. Femoroacetabular impingement in 45 professional athletes: associated pathologies and return to sport following arthroscopic decompression. Knee Surg Sports Traumatol Arthrosc. 2007; 15:908-14.

12. Bizzini M, Notzli HP, Maffiuletti NA. Femoroacetabular impingement in professional ice hockey players: a case series of 5 athletes after open surgical decompression of the hip. Am J Sports Med. 2007;35:1955-9.

13. Clohisy JC, Nunley RM, Otto RJ, Schoenecker PL. The frog-leg lateral radiograph accurately visualized hip cam impingement abnormalities. Clin Orthop Relat Res. 2007;462:115-21.

14. Tannast M, Siebenrock KA, Anderson SE. Femoroacetabular impingement: radiographic diagnosis—what the radiologist should know. AJR Am J Roentgenol. 2007;188:1540-52.

15. Tönnis D, Heinecke A. Acetabular and femoral anteversion: relationship with osteoarthritis of the hip. J Bone Joint Surg Am. 1999;81:1747-70.

16. Clohisy JC, Carlisle JC, Beaulé PE, Kim YJ, Trousdale RT, Sierra RJ, Leunig M, Schoenecker PL, Millis MB. A systematic approach to the plain radiographic evaluation of the young adult hip. J Bone Joint Surg Am. 2008;90 Suppl 4: 47-66.

17. Anderson LA, Peters CL, Park BB, Stoddard GJ, Erickson JA, Crim JR. Acetabular cartilage delamination in femoroacetabular impingement. Risk factors and magnetic resonance imaging diagnosis. J Bone Joint Surg Am. 2009;91:305-13.

18. Martin RL, Kelly BT, Philippon MJ. Evidence of validity for the hip outcome score. Arthroscopy. 2006;22:1304-11.

19. Martin RL, Philippon MJ. Evidence of reliability and responsiveness for the hip outcome score. Arthroscopy. 2008;24:676-82.

20. Landis JR, Koch GG. The measurement of observer agreement for categorical data. Biometrics. 1977;33:159-74.

21. Conover WJ. Practical nonparametric statistics. New York: John Wiley & Sons, Inc; 1980.

22. Bland JM, Altman DG. Calculating correlation coefficients with repeated observations: Part 2—Correlation between subjects. BMJ. 1995;310:633.

23. Kang C, Hwang DS, Cha SM. Acetabular labral tears in patients with sports injury. Clin Orthop Surg. 2009;1:230-5.

24. Ochoa LM, Dawson L, Patzkowski JC, Hsu JR. Radiographic prevalence of femoroacetabular impingement in a young population with hip complaints is high. Clin Orthop Relat Res. 2010;468:2710-4.

25. Hack K, Di Primio G, Rakhra K, Beaulé PE. Prevalence of cam-type femoroacetabular impingement morphology in asymptomatic volunteers. J Bone Joint Surg Am. 2010;92:2436-44.

26. Gosvig KK, Jacobsen S, Sonne-Holm S, Gebuhr P. The prevalence of cam-type deformity of the hip joint: a survey of 4151 subjects of the Copenhagen Osteoarthritis Study. Acta Radiol. 2008;49:436-441.

27. Gosvig KK, Jacobsen S, Sonne-Holm S, Palm H, Troelsen A. Prevalence of malformations of the hip joint and their relationship to sex, groin pain, and risk of osteoarthritis: a population-based survey. J Bone Joint Surg Am. 2010;92: 1162-9.

28. Raynor CM, Bryant D, Spouge A, Birmingham TB, Willits K. Presence of markers of femoroacetabular impingement in the asymptomatic population. FASEB J. 2009; 23:822.7.

29. Kang AC, Gooding AJ, Coates MH, Goh TD, Armour P, Rietveld J. Computed tomography assessment of hip joints in asymptomatic individuals in relation to femoroacetabular impingement. Am J Sports Med. 2010;38:1160-5.

30. Allen D, Beaulé PE, Ramadan O, Doucette S. Prevalence of associated deformities and hip pain in patients with cam-type femoroacetabular impingement. J Bone Joint Surg Br. 2009;91:589-94.

31. Nötzli HP, Wyss TF, Stoecklin CH, Schmid MR, Treiber K, Hodler J. The contour of the femoral head-neck junction as a predictor for the risk of anterior impingement. J Bone Joint Surg Br. 2002;84:556-60.

32. Beaule P, Hack K, Rakhra K, DiPrimio G. Prevalence of CAM type FAI morphology in 200 asymptomatic volunteers (SS-29). Arthroscopy. 2009;25(Suppl 1):e16.

33. Hong SJ, Shon WY, Lee CY, Myung JS, Kang CH, Kim BH. Imaging findings of femoroacetabular impingement syndrome: focusing on mixed-type impingement. Clin Imaging. 2010;34:116-20.

34. Johnston TL, Schenker ML, Briggs KK, Philippon MJ. Relationship between offset angle alpha and hip chondral injury in femoroacetabular impingement. Arthroscopy. 2008;24:669-75.

35. Gosvig KK, Jacobsen S, Palm H, Sonne-Holm S, Magnusson E. A new radiological index for assessing asphericity of the femoral head in cam impingement. J Bone Joint Surg Br. 2007;89:1309-16.

36. Neumann M, Cui Q, Siebenrock KA, Beck M. Impingement-free hip motion: the 'normal' angle alpha after osteochondroplasty. Clin Orthop Relat Res. 2009;467:699-703.

37. Pollard TC, Villar RN, Norton MR, Fern ED, Williams MR, Murray DW, Carr AJ. Genetic influences in the aetiology of femoroacetabular impingement: a sibling study. J Bone Joint Surg Br. 2010;92:209-16.

38. Busconi B, McCarthy J. Hip and pelvic injuries in the skeletally immature athlete. Sports Med Arthrosc Rev. 1996;4:132-58.

39. Siebenrock KA, Wahab KH, Werlen S, Kalhor M, Leunig M, Ganz R. Abnormal extension of the femoral head epiphysis as a cause of cam impingement. Clin Orthop Relat Res. 2004;418:54-60.

40. Kocher MS, Tucker R. Pediatric athlete hip disorders. Clin Sports Med. 2006; 25:241-53,viii.

41. Fadul DA, Carrino JA. Imaging of femoroacetabular impingement. J Bone Joint Surg Am. 2009;91 Suppl 1:138-43.

42. Clohisy JC, Carlisle JC, Trousdale R, Kim YJ, Beaule PE, Morgan P, Steger-May K, Schoenecker PL, Millis M. Radiographic evaluation of the hip has limited reliability. Clin Orthop Relat Res. 2009;467:666-75.

43. Kappe T, Kocak T, Neuerburg C, Lippacher S, Bieger R, Reichel H. Reliability of radiographic signs for acetabular retroversion. Int Orthop. 2011;35:817-21.

44. Siebenrock KA, Kalbermatten DF, Ganz R. Effect of pelvic tilt on acetabular retroversion: a study of pelves from cadavers. Clin Orthop Relat Res. 2003;407:241-8.

45. Tannast M, Mistry S, Steppacher SD, Reichenbach S, Langlotz F, Siebenrock KA, Zheng G. Radiographic analysis of femoroacetabular impingement with Hip2Norm-reliable and validated. J Orthop Res. 2008;26:1199-205.

46. Tannast M, Murphy SB, Langlotz F, Anderson SE, Siebenrock KA. Estimation of pelvic tilt on anteroposterior X-rays—a comparison of six parameters. Skeletal Radiol. 2006;35:149-55.

47. Tannast M, Siebenrock KA. Conventional radiographs to assess femoroacetabular impingement. Instr Course Lect. 2009;58:203-12.

48. Tannast M, Zheng G, Anderegg C, Burckhardt K, Langlotz F, Ganz R, Siebenrock KA. Tilt and rotation correction of acetabular version on pelvic radiographs. Clin Orthop Relat Res. 2005;438:182-90.

49. Watanabe W, Sato K, Itoi E, Yang K, Watanabe H. Posterior pelvic tilt in patients with decreased lumbar lordosis decreases acetabular femoral head covering. Orthopedics. 2005;25:321-4.

50. Zheng G, Tannast M, Anderegg C, Siebenrock KA, Langlotz F. Hip2Norm: an object-oriented cross-platform program for 3D analysis of hip joint morphology using 2D pelvic radiographs. Comput Methods Programs Biomed. 2007;87:36-45.

51. Dudda M, Albers C, Mamisch TC, Werlen S, Beck M. Do normal radiographs exclude asphericity of the femoral head-neck junction? Clin Orthop Relat Res. 2009;467:651-9.

52. Konan S, Rayan F, Haddad FS. Is the frog lateral plain radiograph a reliable predictor of the alpha angle in femoroacetabular impingement? J Bone Joint Surg Br. 2010;92:47-50.

CHAPTER 3

HIP INTERNAL ROTATION IS CORRELATED TO RADIOGRAPHIC FINDINGS OF CAM FEMOROACETABULAR IMPINGEMENT IN COLLEGIATE FOOTBALL PLAYERS

Reprinted from Arthroscopy: The Journal of Arthroscopic & Related Surgery, 28(11), Ashley L. Kapron, Andrew E. Anderson, Christopher L Peters, Lee G. Phillips, Gregory J. Stoddard, David J. Petron, Robert Toth, Stephen K. Aoki, Hip Internal Rotation is Correlated to Radiographic Findings of Cam Femoroacetabular Impingement in Collegiate Football Players. 1661-1670, 2012, with permission from Elsevier.

Hip Internal Rotation Is Correlated to Radiographic Findings of Cam Femoroacetabular Impingement in Collegiate Football Players

Ashley L. Kapron, B.S., Andrew E. Anderson, Ph.D., Christopher L. Peters, M.D., Lee G. Phillips, M.D., Gregory J. Stoddard, M.P.H., David J. Petron, M.D., Robert Toth, P.A.-C., and Stephen K. Aoki, M.D.

Purpose: The objective of this study was to determine whether physical examinations (flexion–abduction–external rotation [FABER], impingement, range-of-motion profiles) could be used to detect the bony abnormalities of femoroacetabular impingement (FAI) in an athletic population. **Methods:** We performed a prospective study of 65 male collegiate football players. Both hips were evaluated by 2 orthopaedic surgeons for radiographic signs of FAI. The alpha angle and head-neck offset were measured on frog-leg lateral films. The center-edge angle, acetabular index, crossover sign, and alpha angle were measured on anteroposterior films. Measurements were averaged for both observers. Maximum hip range of motion in flexion (supine) and internal/external rotation (supine, sitting, and prone) was measured with a goniometer. Pain provoked by the impingement and FABER tests was also recorded. Examinations were completed at 2 of 4 stations (2 duplicates), each staffed by 2 clinicians (1 examined and 1 measured). The relation between each range-of-motion and radiographic measure was determined. Data from each station were assessed separately. Only those regressions significant ($P < .05$) for paired stations were considered clinically significant. **Results:** The alpha angle and head-neck offset measured on the frog-leg lateral films were significantly correlated (all $P < .01$) to supine, sitting, and prone internal rotation for all stations. Correlation coefficients ranged from -0.59 to -0.35 for alpha angle and 0.42 to 0.57 for head-neck offset. Although 95% of the hips had at least 1 radiographic sign of FAI, pain was reported in only 8.5% and 2.3% during the impingement and FABER tests, respectively. **Conclusions:** Internal rotation correlates to radiographic measures of cam FAI in this cohort of collegiate football players. Football players with diminished internal rotation in whom hip pain develops should be evaluated for underlying cam FAI abnormalities. **Level of Evidence:** Level IV, therapeutic case series.

Femoroacetabular impingement (FAI) describes bony abnormalities that cause mechanical abutment in the hip joint through acetabular overcoverage (pincer), femoral head/neck asphericity (cam), or a combination of the 2 (mixed). FAI abnormalities are thought to initiate cartilage and labral damage and may lead to hip osteoarthritis.[1-3]

FAI is a common cause of hip pain in athletes and can limit or end sports participation.[4] Arthroscopic and open surgical treatment of FAI seeks to reduce pain, improve

From the Departments of Bioengineering (A.L.K., A.E.A.), Orthopaedics (A.E.A., C.L.P., L.G.P., G.J.S., D.J.P., R.T., S.K.A.), Physical Therapy (A.E.A.), and Internal Medicine (G.J.S.), University of Utah, Salt Lake City, Utah, U.S.A.

The authors report that they have no conflicts of interest in the authorship and publication of this article.
Received October 28, 2011; accepted April 26, 2012.

Address correspondence to Stephen K. Aoki, M.D., Orthopaedic Center, University of Utah, 590 Wakara Way, Salt Lake City, UT 84108, U.S.A. E-mail: stephen.aoki@hsc.utah.edu

0749-8063/11709/$36.00
http://dx.doi.org/10.1016/j.arthro.2012.04.153

function, and prevent/delay osteoarthritis by restoring normal joint morphology and joint clearance. Early detection before end-stage osteoarthritis may be important to optimize clinical outcomes with these hip preservation approaches and facilitate the return to sport for athletic FAI patients.[5,6] Although the timeliness of a proper diagnosis continues to improve, misdiagnosis can occur by clinicians not familiar with FAI.

A screening protocol to identify subjects who may be at risk for the development of symptomatic FAI could limit misdiagnosis and improve surgical outcomes by reducing the time between onset of symptoms and treatment. The ideal screening protocol would be sensitive, inexpensive, and noninvasive. Radiographic imaging provides a method to quantify the type and extent of FAI abnormalities and is central to the diagnosis of patients presenting to the clinic with hip pain.[7] Interestingly, radiographic findings consistent with FAI are also present in asymptomatic members of the general and athletic populations, who may thus be at risk for the development of symptomatic FAI.[8-12] Although radiographic imaging could be used to identify these individuals directly, radiation exposure may not be appropriate for large-scale screening.

Clinical examinations may provide a noninvasive tool to screen for asymptomatic FAI abnormalities. The impingement and flexion–abduction–external rotation (FABER) tests have a high sensitivity for reproducing hip pain in symptomatic FAI patients.[13] In addition, symptomatic FAI patients often have limited hip range of motion (ROM), with decreases noted in flexion, abduction/adduction, and internal/external rotation.[13] Furthermore, internal rotation, external rotation, and abduction have been significantly correlated to the alpha angle in symptomatic FAI patients.[14] It is unknown, however, whether these tests could be used to screen for the bony abnormalities of FAI in an athletic population that is largely asymptomatic.

The objective of this study was to determine whether physical examinations could be used to detect radiographic FAI in collegiate football players. It was hypothesized that individuals with radiographic FAI abnormalities would have positive FABER and impingement tests and that ROM would be correlated to radiographic measures of FAI in this athletic population.

METHODS

Subject Selection

The University of Utah football team was invited to participate in this prospective, institutional review board–approved study (IRB 40479). Of 96 players, 67 provided informed consent and participated. As previously reported, each subject's hip condition was assessed with a questionnaire based on the validated Hip Outcome Score.[15,16]

Physical Examination

Physical examinations were completed on a single day during the routine pre-participation athletic evaluation. Examinations were performed at 4 stations. Stations A1 and B1 were each staffed by 2 orthopaedic surgeons. Stations A2 and B2 were each staffed by an orthopaedic surgeon and an orthopaedic physician assistant. At each station, the senior clinician manipulated the hip while the second clinician measured terminal ROM and distance using a goniometer and meter stick, respectively (Table 1).

The impingement test, FABER test, supine flexion examination, and supine internal/external rotation examinations were performed at stations A1 and A2. Internal rotation and external rotation in the sitting and prone positions were measured at stations B1 and B2. Players formed a single line and were assigned to the next available station, undergoing examinations at one A station and one B station. To determine interobserver repeatability, 16 players went to all 4 stations.

Radiographic Evaluation

The specifics of the radiographic evaluation have been reported previously.[11] In brief, within 3 days of the physical examinations, pelvic anteroposterior (AP) and frog-leg lateral radiographs of both hips were obtained for each player. Radiographs were obtained in the supine position with gonad shielding and independently evaluated by 2 orthopaedic surgeons (S.K.A. and L.G.P.) in a digital environment (picture archiving and communication system) (iSite PACS; Philips Healthcare Informatics, Foster City, CA). Interobserver and intraobserver repeatability of the radiographic measures was moderate or better.[11]

Cam FAI measures included the alpha angle (measured on all films) and head-neck offset (measured on the frog-leg lateral films only). Pincer FAI was evaluated on the AP radiographs with the lateral center-edge angle, acetabular index, and crossover sign. Abnormal radiographic findings were defined by use of the following cutoffs: acetabular index less than 0°, lateral center-edge angle greater than 40°, alpha angle greater than 50°, head-neck offset less than 8 mm, and presence of the crossover sign.[7,17-19] The Tönnis grade

Table 1. *Description of Physical Examinations*

Examination	Position	Method	Outcome	Reference
Impingement test	Supine	Passive flexion to approximately 90° with adduction/internal rotation	Verbal report of pain	9, 31
FABER test	Supine	Lower limb in figure-4 position: hip flexed, abducted, and externally rotated; lateral malleolus of affected limb sits superior to patella of extended contralateral knee; downward pressure applied to affected knee	(1) Vertical distance between lateral border of patella and examination table (2) Verbal report of pain	8, 24
Flexion	Supine	Passive manipulation to terminal hip flexion with knee flexed; downward pressure applied to extended contralateral knee to limit motion	Angle between table horizontal and midline of thigh	28
Internal/external rotation	Supine	Hip and knee in 90° flexion; abduction/adduction of hip limited through downward pressure applied to knee; ankle used to internally/externally rotate hip	Angle formed between midline of leg in neutral and terminal positions	26
Internal/external rotation	Sitting	Subject sitting at edge of examination table with lower legs hanging freely; abduction/adduction of hip limited through downward pressure applied to knee; ankle used to internally/externally rotate hip (knee-ankle treated as rigid body)	Angle formed between midline of leg in neutral and terminal positions	26
Internal/external rotation	Prone	Knee flexed to 90°; ankle used to internally/externally rotate hip (knee-ankle treated as rigid body); forearm applies downward pressure superior to buttocks to stabilize hip	Subtract 90° from angle between horizon and midline of leg in terminal position	26

was used to assess the osteoarthritic condition of the joint.[20]

Data and Statistical Analysis

Continuous radiographic data (e.g., alpha angle) were averaged between the first reads of both observers. The crossover sign was considered present only if it was detected by both observers. For the Tönnis grade, the highest score reported by either observer was used, representing the worst-case evaluation.

Physical examination data were not averaged between observers. Instead, statistical analysis was performed separately on examination data collected at each station (i.e., the alpha angle averaged between the 2 radiographic observers was correlated separately to flexion measured by observers at stations A1 and A2). For the impingement and FABER results, pain was considered present if it was detected by either observer.

All statistical analysis was performed by use of Stata software, version 11 (StataCorp, College Station, TX).

Groups Comparisons: Demographic and radiographic data were compared between groups to determine whether significant differences existed between players evaluated at stations A1 and B1 versus those evaluated at stations A2 and B2. An independent *t* test was used to determine differences in the demographic data (age, height, weight). A random-effects linear regression model was used to determine differences in the continuous radiographic data because dependent observations were included per subject (left and right side). The random-effects linear regression model was also used to compare physical examination results between those with the crossover sign and those without it.

Radiographic and Physical Examination Correlations: The relation between each continuous physical examination and radiographic measure was determined by the random-effects linear regression model. $P < .05$ indicated that the regression coefficient (slope) was significantly different from 0. Only those combinations with significant correlations for data from both physical examination stations were considered clinically significant. For those correlations, scatter plots with regression lines overlain were generated by use of StataIC 11 (StataCorp). The correlation coefficient (r) was computed using the method described by Bland and Altman,[21] which accounts for repeated measurements of both left and right sides.

Sensitivity and Specificity: For those correlations considered clinically significant, the physical examination threshold value that could detect an abnormal radiographic finding with a sensitivity of at least 80% (analogous to 80% power) was determined. The corresponding specificity was also calculated.

Repeatability: Interobserver repeatability and intraobserver repeatability for the continuous data (e.g., flexion) and dichotomous data (e.g., pain during impingement test) were assessed with the intraclass correlation coefficient (ICC) and κ statistic, respectively. Observer agreement, as quantified by the ICC and κ, was interpreted as slight if 0.20 or less, fair if 0.21 to 0.40, moderate if 0.41 to 0.60, substantial if 0.61 to 0.80, and almost perfect if greater than 0.80.[19,22]

Post Hoc Power Analysis: For the radiographic and physical examination correlations, a post hoc power analysis was used to determine the correlation coefficient that could be detected with 80% power using a 2-sided comparison ($\alpha = .05$). Because physical examination data from each station were analyzed separately, the power analysis was completed using the smallest number of subjects at a single station (80 hips clustered within 40 players, stations A2 and B1). The dependent observations (left and right hips) required that a design effect be applied to the power analysis. The design effect is $1 + (2 - 1) \times$ intraclass correlation coefficient of hips clustered within players, where 2 is the average cluster size (the number of hips analyzed per player).

For correlations between radiographic measures of cam FAI and ROM, the observed ICCs ranged from 0.47 to 0.81. For correlations between radiographic measures of pincer FAI and ROM, the observed ICCs ranged from 0.69 to 0.92. Using these ICCs in the design effect, the study had 80% power to detect a correlation coefficient as small as $r = 0.37$ to 0.40 for the cam measures and $r = 0.39$ to 0.41 for the pincer measures.

RESULTS

Subject Characteristics

Of the 67 football players who underwent radiographic evaluation in our previous study,[11] 2 were excluded because they did not complete the physical examinations. The remaining 65 football players were aged 21 ± 1.9 years with a mean height of 185 ± 6.4 cm and weight of 102 ± 19 kg. Overall, most of the players noted that their hips had no further symptoms at the time of this study, as self-reported on the questionnaire.[11] The mean (± standard deviation) activities–of–daily living and sports subscores were 99% ± 3.9% and 98% ± 4.4%, respectively.

The occurrence of each radiographic abnormality describing cam and pincer impingement was higher in these players than previously reported values for the general population.[11] In brief, of the 130 hips, 123 (95%) had at least 1 radiographic FAI abnormality. Specifically, 73 (54%) and 74 (55%) had an alpha angle greater than 50° on the frog-leg lateral and AP films, respectively. In addition, 86 (64%) had a head-neck offset less than 8 mm. Acetabular overcoverage was less prevalent: 10 hips (7%) had a lateral center-edge angle greater than 40°, and 21 (16%) hips had an acetabular index less than 0°. The crossover sign was present in 82 hips (61%). Slight osteoarthritis (Tönnis grade 1) was detected in 17% (22 of 130 hips); the remaining hips had no signs of osteoarthritis (Tönnis grade 0).

Physical Examinations

Descriptive statistics of the continuous physical examination data are shown in Table 2. Of the players, 25 went to stations A1 and B2, 24 went to stations A2 and B1, and 16 went to all 4 stations. There was no difference in both demographic and radiographic measures between players who went to stations A1 versus A2 and B1 versus B2 (all $P > .417$).

Among the 130 hips, pain was reported in 11 (8.5%) during the impingement test and 3 (2.3%) during the FABER test. All subjects who reported pain during the impingement and FABER tests had at least 1 radiographic abnormality.

Radiographic and ROM Correlations

Internal rotation, as measured in all 3 positions (supine, sitting, and prone) at both stations, was correlated ($P < .01$) to head-neck offset and alpha angle measured on the frog-leg lateral film (Table 3, Figs 1 and 2). For all internal rotation examinations, the threshold values that could detect a frog-leg lateral alpha angle greater than 50° or head-neck offset less than 8 mm with a sensitivity of at least 80% had a corresponding specificity no greater than 51% (Table 4).

Twelve additional combinations of physical examinations and radiographic measures were correlated ($P < .05$) for only 1 of the 2 physical examination stations (Table 5). The only difference in physical examination results between those with the crossover sign and those without it was for sitting external

TABLE 2. *Physical Examination Results From Cohort of 65 Collegiate Football Players*

	Station 1			Station 2			
Examination	Station	Mean ± SD	Range	Station	Mean ± SD	Range	ICC (n = 32)
Flexion	A1	92° ± 9.4°	70° to 110°	A2	113° ± 9.2°	91° to 136°	0.52
FABER distance	A1	22 mm ± 5.8 mm	10 mm to 34 mm	A2	29 mm ± 4.2 mm	20 mm to 37 mm	0.64
Internal rotation							
Supine	A1	15° ± 7.5°	−5° to 30°	A2	21° ± 8.1°	4° to 42°	0.73
Sitting	B1	36° ± 5.9°	23° to 49°	B2	36° ± 7.8°	20° to 59°	0.55
Prone	B1	37° ± 7.0°	20° to 53°	B2	33° ± 9.8°	9° to 63°	0.75
External rotation							
Supine	A1	33° ± 8.6°	15° to 55°	A2	45° ± 7.4°	28° to 63°	0.55
Sitting	B1	40° ± 6.0°	29° to 55°	B2	31° ± 7.1°	20° to 50°	0.71
Prone	B1	43° ± 7.4°	31° to 67°	B2	42° ± 10°	22° to 76°	0.66

NOTE. Examinations were completed at 4 stations. A1 was a duplicate station of A2, and B1 was a duplicate station of B2. All subjects went to one A and one B station. A subset of players went to duplicate stations to assess interobserver repeatability of the physical examination measurements, which was quantified by the ICC.

rotation measured at station B2. At this station, subjects with the crossover sign had significantly less external rotation than those without it ($P = .039$).

Repeatability

Physical examination repeatability was assessed using data from 16 players (32 hips) who completed physical examinations at all 4 stations. On the basis of the ICC, interobserver repeatability was substantial for supine/prone internal rotation, sitting/prone external rotation, and FABER distance (Table 2). Flexion, sitting internal rotation, and supine external rotation had moderate repeatability. Repeatability was substantial for the impingement test, with $\kappa = 0.62$. For the FABER test, $\kappa = 0$, because there were no cases of pain reported at both stations.

DISCUSSION

Prior knowledge of an increased risk for FAI may improve treatment outcomes by decreasing the time between the onset of symptoms and appropriate diagnosis, during which further chondrolabral damage may occur. The objective of this study was to determine whether physical examinations could be used to detect radiographic changes consistent with FAI in an athletic population, specifically collegiate football players. Internal rotation measured in supine, sitting, and prone positions negatively correlated to alpha angle and positively correlated to head-neck offset, both measured on frog-leg lateral radiographs. Because the severity of a cam deformity increases with an elevated alpha angle and

TABLE 3. *Relation Between Hip ROM and Radiographic Measures of FAI: Regression/Correlation Results for Combinations Significant for Both Physical Examination Stations*

Radiographic Measure	Internal Rotation	Station	Regression Coefficient (Slope)	Significance (*P*)	Correlation Coefficient (*r*)
Alpha angle	Supine	A1	–0.44	.004	–0.39
		A2	−0.43	.001	−0.47
	Sitting	B1	−0.69	< .001	−0.59
		B2	−0.41	.003	−0.35
	Prone	B1	−0.43	.006	−0.38
		B2	−0.42	< .001	−0.46
Head-neck offset	Supine	A1	0.11	.006	0.44
		A2	0.14	.001	0.48
	Sitting	B1	0.19	< .001	0.57
		B2	0.12	.002	0.44
	Prone	B1	0.14	< .001	0.42
		B2	0.13	< .001	0.48

reduced head-neck offset, the directions of these correlations are logical.

The alpha angle measured on the frog-leg lateral radiographs correlated to all measures of internal rotation ($r = -0.59$ to -0.35). However, the alpha angle from AP radiographs was only mildly correlated to supine internal rotation for station A1 ($r = -0.22$). A previous study of FAI patients (102 amateur and professional athletes) found that prone internal rotation was mildly correlated to the alpha angle measured on the cross-table lateral view ($P = .023$, $r =$

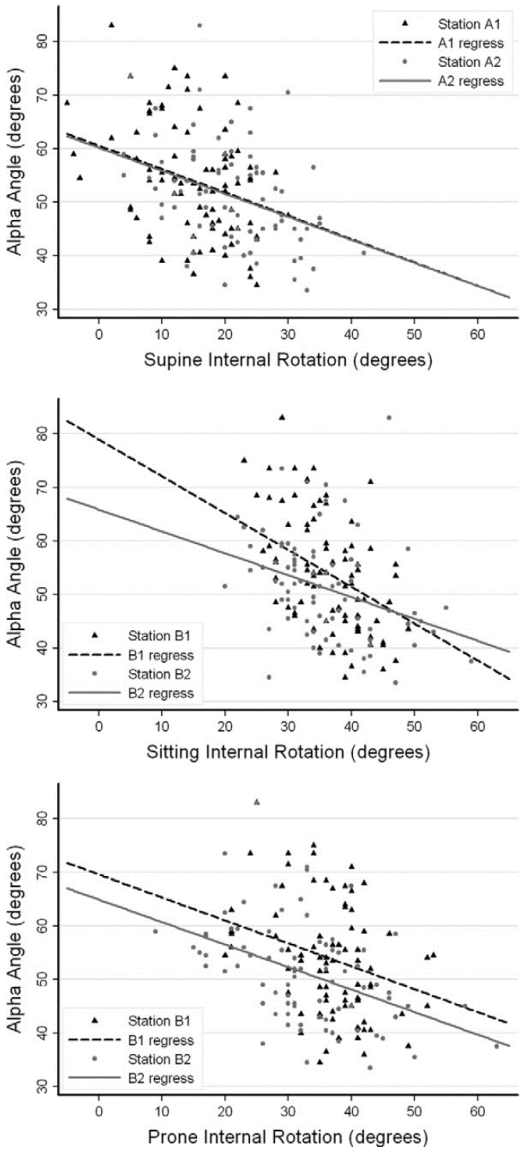

Figure 1. Scatterplots with regression lines overlain with frog-leg lateral alpha angle versus supine (top), sitting (middle), and prone (bottom) internal rotation from both stations.

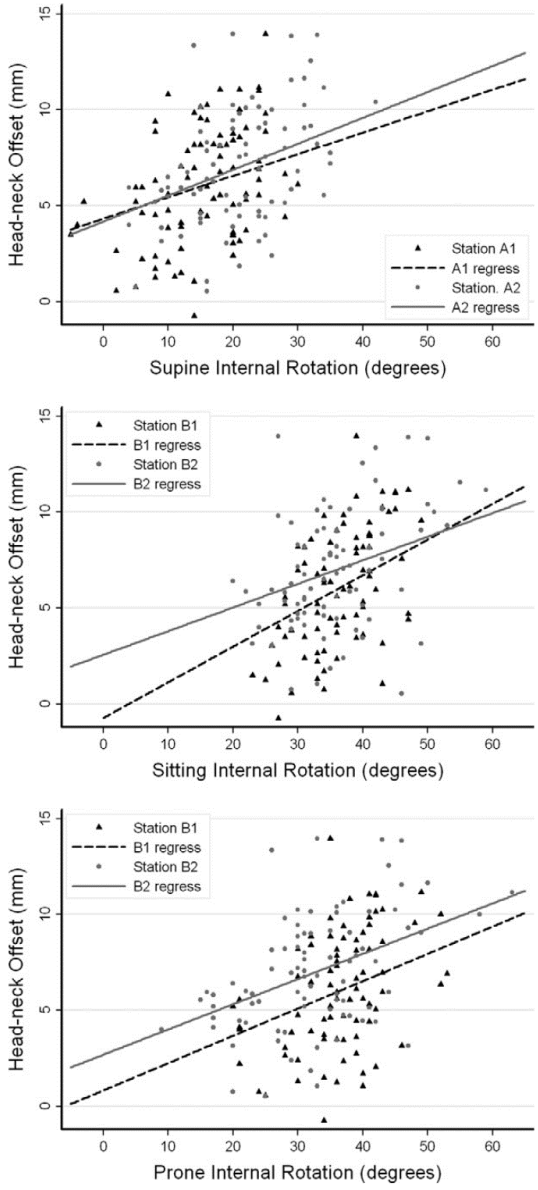

Figure 2. Scatterplots with regression lines overlain with head-neck offset versus supine (top), sitting (middle), and prone (bottom) internal rotation from both stations.

TABLE 4. *Internal Rotation Thresholds With at Least 80% Sensitivity to Detect Radiographic Abnormalities Consistent With Cam FAI*

Radiographic Abnormality	Internal Rotation	Station	Threshold	Sensitivity	Specificity
Alpha angle >50° (frog-leg lateral film)	Supine	A1	21°	82%	34%
		A2	25°	80%	46%
	Sitting	B1	41°	88%	47%
		B2	38°	81%	51%
	Prone	B1	41°	83%	44%
		B2	37°	81%	46%
Head-neck offset <8 mm (frog-leg lateral film)	Supine	A1	21°	80%	35%
		A2	26°	84%	47%
	Sitting	B1	41°	85%	50%
		B2	39°	81%	50%
	Prone	B1	41°	83%	50%
		B2	38°	83%	43%

–0.263).[14] The stronger correlation between the frog-leg lateral alpha angle and internal rotation may be attributed to the conclusion of Clohisy et al.[19] that the frog-leg lateral radiograph visualizes cam deformities better than the AP and cross-table lateral views. In addition, anterolateral abnormalities captured on frog-leg lateral radiographs may be more severe or have a greater impact on internal rotation than superolateral abnormalities quantified on AP radiographs.

In our study most subjects had radiographic findings consistent with FAI, but only a small fraction reported pain during the impingement and FABER tests. There were no false positives; all subjects who had pain during the tests had at least 1 abnormal radiographic finding. This is consistent with a study of 80 asymp-

TABLE 5. *Relation Between Physical Examinations and Radiographic Measures of FAI: Regression/Correlation Results for Combinations Significant for Only 1 of 2 Physical Examination Stations*

Radiographic Measure	Physical Examination	Station	Regression Coefficient (Slope)	Significance (*P*)	Correlation Coefficient (*r*)
Alpha angle	FABER distance	A1	0.44	.043	0.28
		A2	0.19	.462	0.07
	Sitting external	B1	−0.36	.076	−0.33
		B2	0.34	.030	0.25
	Prone external	B1	0.13	.440	0.00
		B2	0.27	.012	0.20
Acetabular index	Prone internal	B1	0.19	.005	−0.05
		B2	−0.02	.732	−0.05
AP alpha angle	FABER distance	A1	0.32	.223	0.21
		A2	0.81	.004	0.40
	Supine flexion	B1	−0.37	.012	−0.31
		B2	−0.13	.358	−0.18
	Supine internal	A1	−0.44	.017	−0.22
		A2	−0.19	.243	−0.08
	Supine external	A1	0.02	.904	−0.21
		A2	−0.44	.002	−0.24
	Sitting external	B1	−0.55	.021	−0.45
		B2	−0.05	.809	−0.11
Head-neck offset	Sitting external	B1	0.03	.630	0.27
		B2	−0.13	.006	−0.26
	Prone external	B1	−0.01	.860	−0.09
		B2	−0.07	.025	−0.25
Lateral center-edge angle	Prone internal	B1	−0.24	.001	0.03
		B2	−0.08	.160	−0.07

tomatic elite soccer and basketball players in which 13.8% reported pain during the impingement test but 43.8% had an alpha angle greater than 50°.[10] In contrast, positive results are almost always obtained in symptomatic FAI patients. In 1 study of 301 patients, 99% and 97% had positive impingement and FABER tests, respectively.[13] It is possible that pain is provoked only in individuals with underlying chondrolabral damage. Thus, whereas the impingement and FABER examinations do not have a high specificity to detect players with radiographic findings consistent with FAI, they may be suitable to identify subjects with underlying chondrolabral damage.

Relations between radiographic measures of pincer FAI and ROM were not clinically significant. The lack of correlation may be because of the low prevalence of hips with an abnormal lateral center-edge angle and acetabular index. Although the crossover sign was more prevalent, there were no clinically significant differences in ROM between those with the sign and those without it. The crossover sign may be indicative of localized acetabular overcoverage or posterior wall deficiency,[23] both of which may cause less restriction in ROM than cam deformities or general acetabular overcoverage quantified by the lateral center-edge angle and acetabular index. Finally, acetabular coverage and version were quantified on plain radiographs in this study. Measures of acetabular morphology from magnetic resonance imaging or computed tomography data may have correlated to the physical examination data.

There were no significant differences in demographic and radiographic results between subjects who were evaluated at separate stations. However, for some combinations, physical examinations and radiographic measures were significantly correlated for results from only 1 physical examination station and thus not considered clinically significant. Correlations and the level of significance may have varied between stations because of minor differences in the subjects evaluated (i.e., flexibility) or physical examination technique (i.e., applied pressure). In addition, ROM measurement with a goniometer has several limitations.[24] For example, visual alignment of the goniometer arms and fulcrum with appropriate anatomic landmarks can be difficult, especially in football players with above-average body mass indexes. Nonetheless, interobserver repeatability of all ROM measurements was moderate or better and similar to previous studies.[25,26]

Internal rotation threshold values that detected radiographic findings consistent with cam FAI in football players with 80% sensitivity ranged from 21° to 26° for supine, 37° to 41° for prone, and 38° to 41° for sitting internal rotation. These values are close to what is considered the reference range for normal internal rotation, specifically 30° to 40° for prone/supine[27] and 20° to 35° for sitting.[28] Because most subjects had radiographic findings consistent with FAI but fell within the normal internal rotation range, an internal rotation threshold that is higher than previous thresholds may be needed to screen for radiographic FAI abnormalities in football players.

Whereas internal rotation examinations show promise to screen for radiographic cam FAI in male football players, more research is required to develop a standardized screening protocol. One of the main barriers is the lack of consensus regarding radiographic cutoff values that would indicate a diagnosis of FAI and in which values would predict the development of symptomatic FAI. For example, the cutoff value for a normal alpha angle can range from 42° to 68°.[7,14,18,29] Applying these radiographic cutoffs to the results of our study would clearly change the internal rotation thresholds proposed earlier and corresponding examination sensitivity/specificity. Nonetheless, we believe that a lower cutoff value of 50° for alpha angle, in the context of a screening protocol, is suitable to identify all players who may have radiographic FAI abnormalities and thus be at risk to develop symptomatic FAI. It is possible that the risk of symptomatic FAI developing increases as the severity of a radiographic cam deformity increases. A previous study showed that symptomatic FAI patients with higher alpha angles are more likely to have chondral pathology at the time of surgery.[14] However, the relation between radiographic FAI morphology and predisposition to chondrolabral damage is unknown in the present population.

Whereas the internal rotation thresholds proposed earlier had a high sensitivity (80%) to detect FAI abnormalities, the corresponding specificity was no greater than 51%. For comparison, the forward-bending test for scoliosis, a commonly used screening examination in orthopaedics, has a reported sensitivity of 84% and specificity of 93%.[30] In this study sensitivity was maximized, not sensitivity and specificity together. This approach was chosen with a screening protocol in mind that could minimize misdiagnosis and improve the timeliness of treatment by informing individuals with positive examination findings of a possible risk for symptomatic FAI developing. With a high sensitivity, almost all individuals with underlying abnormalities would be identified. Diagnostic imaging would not be recommended unless hip pain during daily activities or sport was present. Thus falsely identifying a subject as at risk for FAI (which may

occur with a lower specificity) would have minimal consequences. Finally, whereas the internal rotation thresholds may be sufficient to minimize misdiagnosis, proactive monitoring would only be appropriate if a screening examination with higher specificity and sensitivity is identified.

The high prevalence of radiographic FAI abnormalities observed in collegiate football players made them an excellent study population. The wide range of hip morphology present in these athletes enabled a comprehensive evaluation of the physical examinations. It would be difficult to determine the relation between physical examinations and radiographic measures of FAI in a population with few radiographic FAI abnormalities. In addition, collegiate football players may be an ideal population to benefit from an FAI screening protocol, given that they have been identified as high risk and they currently have a mechanism in place for screening (pre-participation examinations). Similar findings may be obtained in athletes of similar stature and activity level, but results should be extended with caution.

This study has several limitations. As discussed earlier, these limitations include the use of radiographs alone to identify abnormalities consistent with FAI, the evaluation of a unique population, error and bias during physical examination, and the discrepancies regarding the cutoff values used to delineate morphologic abnormalities. In addition, the radiographs were not corrected for pelvic tilt, which may affect the radiographic findings (such as the prevalence of the crossover sign in this population). Moreover, the players may have under-reported pain during examination. Nonetheless, this study serves as an initial assessment of common physical examinations to detect radiographic FAI abnormalities in an athletic population. The methods used in our study will serve as a basis for testing more diverse populations.

CONCLUSIONS

Internal rotation correlates to radiographic measures of cam FAI in this cohort of collegiate football players. Football players with diminished internal rotation in whom hip pain develops should be evaluated for underlying cam FAI abnormalities.

Acknowledgment: The authors acknowledge Jill Erickson, Alexej Barg, Jesse Chrastil, and Clint Barnett for assistance with physical examination data collection.

REFERENCES

1. Giori NJ, Trousdale RT. Acetabular retroversion is associated with osteoarthritis of the hip. *Clin Orthop Relat Res* 2003:263-269.
2. Tanzer M, Noiseux N. Osseous abnormalities and early osteoarthritis: The role of hip impingement. *Clin Orthop Relat Res* 2004:170-177.
3. Beck M, Kalhor M, Leunig M, Ganz R. Hip morphology influences the pattern of damage to the acetabular cartilage: Femoroacetabular impingement as a cause of early osteoarthritis of the hip. *J Bone Joint Surg Br* 2005;87:1012-1018.
4. Byrd JW, Jones KS. Arthroscopic management of femoroacetabular impingement in athletes. *Am J Sports Med* 2011;39: 7S-13S (suppl).
5. Philippon M, Schenker M, Briggs K, Kuppersmith D. Femoroacetabular impingement in 45 professional athletes: Associated pathologies and return to sport following arthroscopic decompression. *Knee Surg Sports Traumatol Arthrosc* 2007; 15:908-914.
6. Larson CM, Giveans MR, Taylor M. Does arthroscopic FAI correction improve function with radiographic arthritis? *Clin Orthop Relat Res* 2011;469:1667-1676.
7. Tannast M, Siebenrock KA, Anderson SE. Femoroacetabular impingement: Radiographic diagnosis—What the radiologist should know. *AJR Am J Roentgenol* 2007;188:1540-1552.
8. Hack K, Di Primio G, Rakhra K, Beaulé PE. Prevalence of cam-type femoroacetabular impingement morphology in asymptomatic volunteers. *J Bone Joint Surg Am* 2010;92:2436-2444.
9. Gosvig KK, Jacobsen S, Sonne-Holm S, Palm H, Troelsen A. Prevalence of malformations of the hip joint and their relationship to sex, groin pain, and risk of osteoarthritis: A population-based survey. *J Bone Joint Surg Am* 2010;92:1162-1169.
10. Abellàn J, Esparza F, Blanco A, Martínez M, Merino GR, Lisón A. Radiological evidence of femoroacetabular impingement in asymptomatic athletes. *Br J Sports Med* 2011;45:333 (Abstr).
11. Kapron AL, Anderson AE, Aoki SK, et al. Radiographic prevalence of femoroacetabular impingement in collegiate football players: AAOS Exhibit Selection. *J Bone Joint Surg Am* 2011;93:e111(1-10).
12. Laborie LB, Lehmann TG, Engesaeter IO, Eastwood DM, Engesaeter LB, Rosendahl K. Prevalence of radiographic findings thought to be associated with femoroacetabular impingement in a population-based cohort of 2081 healthy young adults. *Radiology* 2011;260:494-502.
13. Philippon MJ, Maxwell RB, Johnston TL, Schenker M, Briggs KK. Clinical presentation of femoroacetabular impingement. *Knee Surg Sports Traumatol Arthrosc* 2007;15:1041-1047.
14. Johnston TL, Schenker ML, Briggs KK, Philippon MJ. Relationship between offset angle alpha and hip chondral injury in femoroacetabular impingement. *Arthroscopy* 2008;24:669-675.
15. Martin RL, Kelly BT, Philippon MJ. Evidence of validity for the hip outcome score. *Arthroscopy* 2006;22:1304-1311.
16. Martin RL, Philippon MJ. Evidence of reliability and responsiveness for the hip outcome score. *Arthroscopy* 2008;24:676-682.
17. Anderson LA, Peters CL, Park BB, Stoddard GJ, Erickson JA, Crim JR. Acetabular cartilage delamination in femoroacetabular impingement. Risk factors and magnetic resonance imaging diagnosis. *J Bone Joint Surg Am* 2009;91:305-313.
18. Clohisy JC, Carlisle JC, Beaulé PE, et al. A systematic approach to the plain radiographic evaluation of the young adult hip. *J Bone Joint Surg Am* 2008;90:47-66 (suppl 4).
19. Clohisy JC, Nunley RM, Otto RJ, Schoenecker PL. The frog-leg

lateral radiograph accurately visualized hip cam impingement abnormalities. *Clin Orthop Relat Res* 2007;462:115-121.
20. Tönnis D, Heinecke A. Acetabular and femoral anteversion: Relationship with osteoarthritis of the hip. *J Bone Joint Surg Am* 1999;81:1747-1770.
21. Bland JM, Altman DG. Calculating correlation coefficients with repeated observations: Part 2—Correlation between subjects. *BMJ* 1995;310:633.
22. Landis JR, Koch GG. The measurement of observer agreement for categorical data. *Biometrics* 1977;33:159-174.
23. Peters CL, Anderson LA, Erickson JA, Anderson AE, Weiss JA. An algorithmic approach to surgical decision making in acetabular retroversion. *Orthopedics* 2011;34:10.
24. Lea RD, Gerhardt JJ. Range-of-motion measurements. *J Bone Joint Surg Am* 1995;77:784-798.
25. Martin RL, Sekiya JK. The interrater reliability of 4 clinical tests used to assess individuals with musculoskeletal hip pain. *J Orthop Sports Phys Ther* 2008;38:71-77.
26. Wyss TF, Clark JM, Weishaupt D, Nötzli HP. Correlation between internal rotation and bony anatomy in the hip. *Clin Orthop Relat Res* 2007;460:152-158.
27. Scopp JM, Moorman CT III. The assessment of athletic hip injury. *Clin Sports Med* 2001;20:647-659.
28. Braly BA, Beall DP, Martin HD. Clinical examination of the athletic hip. *Clin Sports Med* 2006;25:199-210, vii.
29. Gosvig KK, Jacobsen S, Palm H, Sonne-Holm S, Magnusson E. A new radiological index for assessing asphericity of the femoral head in cam impingement. *J Bone Joint Surg Br* 2007;89:1309-1316.
30. Karachalios T, Sofianos J, Roidis N, Sapkas G, Korres D, Nikolopoulos K. Ten-year follow-up evaluation of a school screening program for scoliosis. Is the forward-bending test an accurate diagnostic criterion for the screening of scoliosis? *Spine* 1999;24:2318-2324.
31. Martin HD, Kelly BT, Leunig M, et al. The pattern and technique in the clinical evaluation of the adult hip: The common physical examination tests of hip specialists. *Arthroscopy* 2010;26:161-172.

CHAPTER 4

ACCURACY AND FEASIBILITY OF DUAL FLUOROSCOPY AND MODEL-BASED TRACKING TO QUANTIFY IN VIVO HIP KINEMATICS DURING CLINICAL EXAMS

4.1 Abstract

Accurate measurements of in vivo hip kinematics may elucidate the mechanisms responsible for impaired function and chondrolabral damage in hips with femoroacetabular impingement (FAI). The objectives of this study were to quantify the accuracy and demonstrate the feasibility of using dual fluoroscopy to measure in vivo hip kinematics during clinical exams used in the assessment of FAI. Steel beads were implanted into the pelvis and femur of two cadavers. Specimens were imaged under dual fluoroscopy during the impingement exam, FABER test, and rotational profile. Bead locations measured with model-based tracking were compared to those measured using dynamic radiostereometric analysis. Error was quantified by bias and precision, defined as the average and standard deviation of the differences between tracking methods, respectively. A normal male volunteer was also imaged during clinical exams. Bias and precision along a single axis did not exceed 0.17 and 0.21 mm, respectively. Comparing

kinematics, positional error was less than 0.48 mm and rotational error was less than 0.58°. For the volunteer, in vivo kinematics were successfully quantified and reported as joint angles and bone-to-bone distance. These results demonstrate that dual fluoroscopy and model-based tracking can accurately measure hip kinematics in living subjects during clinical exams of the hip.

4.2 Introduction

Chondrolabral damage in hips with femoroacetabular impingement (FAI) may result from motion conflict due to acetabular overcoverage, femoral head asphericity, or both. Three physical exams are used to evaluate FAI patients: 1) internal/external rotational profile, 2) impingement exam, and 3) flexion abduction external rotation (FABER) test.[1] These clinical exams place the hip into the limits of motion to initiate impingement. Range of motion during the exams is then quantified with a goniometer or estimated visually. However, without accurate measurements of hip kinematics for those motions believed to induce impingement, it remains unknown how, exactly, the altered anatomy in patients with FAI causes motion conflict. A more accurate methodology to measure and visualize hip kinematics in a research setting could confirm or refute the hypothesized mechanism of impingement, and provide data that could improve the diagnosis and treatment of FAI.

Researchers have employed skin marker motion analysis,[2-4] computer simulations,[5-8] dynamic CT[9], and single plane fluoroscopy[10] in the study of FAI. However, skin marker motion analysis assumes joint centers and axes, and markers are subject to substantial motion artifact. Computer simulations assume kinematics and

neglect bulk soft tissue restraints. Dynamic CT exhibits motion blur, and single plane fluoroscopy has poor out-of-plane accuracy.

Dual radiography and model-based tracking software could accurately quantify hip kinematics without the limitations of the aforementioned techniques.[11] However, previous applications of dual radiography to the native hip have investigated motions occurring primarily in the sagittal plane (walking, rising from a chair).[12,13] Quantifying motion during clinical exams that incorporate hip rotation and ab/adduction at extreme ranges of motion may be more applicable to the study of FAI. The objectives of this study were to quantify the accuracy and demonstrate the feasibility of using dual fluoroscopy to measure in vivo hip kinematics during clinical exams used in the assessment of FAI.

4.3 Methods

4.3.1 Dual Fluoroscopy System (DFS)

A custom DFS (Radiological Imaging Services, Hamburg, PA) was developed, which consisted of two x-ray emitters (Housing B-100/ Tube A-142, Varian, Salt Lake City, UT) and two 12" image intensifiers (T12964-P/S, Dunlee Inc., Aurora, IL), each mounted to a dedicated base. The DFS was positioned around a radiolucent table to image hips in the supine position (Figure 4.1). The fluoroscopy configuration was determined in preliminary cadaveric testing. The configuration enabled the clinician and subject to complete the exam without contact to the system, and minimized bone and soft tissue overlap in the images during all three exams. The source-to-image intensifier

distances of fluoroscopes 1 and 2 were 1100 and 1145 mm, respectively. The interbeam angle was 46° and the approximate imaging volume was 8500 cm^3.

All images in this study were acquired during continuous fluoroscopy using high-speed digital cameras (Phantom Miro 3, Vision Research, Wayne, NJ) at 100 Hz with 608x600 resolution and 3000 μs camera exposure. Images of a grid of steel beads corrected distortion.[14] An acrylic calibration frame housing 36 steel beads (3 mm diameter, spacing 6.35 cm, uncertainty 0.0036 mm) was used to define the position and orientation of the DFS in a laboratory coordinate system.

4.3.2 Validation of Dynamic Radiostereometric Analysis: Optimal Conditions

This study represented the first use of the described dual fluoroscopy system. Thus, a simple test was performed to quantify the accuracy of dynamic radiostereometric analysis (DRSA) under optimal conditions. An acrylic plate with steel beads spaced 30 mm (2 mm diameter, positional uncertainty 0.0013mm) was imaged during random motion.[15] 3D positions of the beads in laboratory coordinates were calculated using direct linear transform theory.[15] The bead intercentroid distances from DRSA were compared to known distances to quantify accuracy. Bias and precision was defined by the average and standard deviation of the differences for 400 frames, respectively.

4.3.3 Validation of Model-Based Tracking

Two pelvis-to-toe cadaveric specimens were acquired (Specimen 1: male, 57 years old, 170 cm, 70 kg, BMI 24.2; Specimen 2: female, 59 years old, 168 cm, 50 kg,

BMI 17.7). Steel beads (2 mm diameter) were implanted into the left hemipelvis and femur with a minimally invasive approach preserving all soft tissue (Figure 4.2). At least five beads were implanted into each bone. Bead locations were chosen so as to minimize disruption of soft tissue. Incisions were closed with suture. CT images of the entire pelvis, proximal femurs, and knees were acquired with a Siemens Somatom CT Scanner (0.7 mm slice thickness, Specimen 1/Specimen 2: 405/424 mm FOV, 512 x 512 matrix). Data were upsampled to 3x resolution to reduce staircase artifact.[16] Bones were segmented semi-automatically using Amira (5.4.1, Visage Imaging, San Diego, CA). Pixels representing the implanted beads were automatically segmented and fit to a sphere to define bead centroids in CT coordinates.

The pelvis was secured to the radiolucent table with Velcro™ straps. Fluoroscopy video was acquired for the impingement exam, FABER test, and supine straight legged int/external rotational profile. Three trials were collected per exam. Specimen 1 was imaged at 83 kVp/3.1 mA (fluoroscope 1) and 85 kVp/3.2 mA (fluoroscope 2). Specimen 2 was imaged at 73 kVp/ 2.9 mA (fluoroscope 1) and 74 kVp/2.5 mA (fluoroscope 2). The total number of frames for each exam was 331 ± 60.7 (average, standard deviation).

Using 3D bone reconstructions from the CT data, a pair of digitally reconstructed radiographs (DRRs) was generated using model-based tracking software.[11] CT pixels representing the beads and associated metal artifact (that was confined to immediate region of the bead only) were assigned intensities of surrounding bone. The position and orientation of the bones were calculated by optimizing agreement between the two DRRs and the fluoroscope images.[11] With the position of each bone and the relative location of each bead centroid known, the Cartesian coordinates of each bead centroid in laboratory

coordinates were calculated for each video frame. A custom PC with four graphics processing cards (Tesla C1060, Nvidia, Santa Clara, CA) completed the optimization for each frame in 0.1-1.0 s.

DRSA of the implanted beads served as the reference standard. There were a few frames in each exam for which all five beads were not clearly visible. Thus, the three most visible beads in each bone for each trial were tracked. Standard deviations of the interbead distances defined the in vitro precision of DRSA. Precision results were averaged across trials. For comparison to model-based tracking, the coordinates of the beads relative to the laboratory system were smoothed with a 4^{th}-order lowpass Butterworth filter with a cutoff frequency of 6 Hz.[17] Model-based tracking and filtered DRSA bead locations were compared for each trial. Bias and precision of the Euclidian distance between bead locations and the distance along each of the laboratory axes were calculated. Results were averaged across trials and specimens.

4.3.4 Anatomical Coordinate System Definition

Anatomical coordinate systems for the pelvis and femur were defined according to Wu *et al*.[18] Bony landmarks were selected automatically or semi-automatically using PreView and PostView.[19,20] Specifically, principal curvature automatically defined the lunate surface of the acetabulum, iliac crest and superior border of the sacroiliac joint on the pelvis and the femoral head, articulating surface of the femoral condyles, and ridges on the medial and lateral femoral epicondyles. The pelvic and femoral joint centers (PJC_{CT}, FJC_{CT}) were calculated as the center of the best fit sphere of the lunate surface of the acetabulum and femoral head, respectively (Figure 4.3). For the mediolateral axis of

the femur and midpoint of the knee, a plane was fit to the medial and lateral epicondyle ridges to isolate the posterior region of the condyles, which was then automatically fit to a cylinder (Figure 4.4). The center of the cylinder defined the midpoint of the knee.

The posterior superior iliac spine (PSIS) was defined as the posterior intersection of the superior border of the sacroiliac joint and the medial border of the iliac crest (Figure 4.5). The anterior superior iliac spine (ASIS) was defined as the anterior intersection between the medial and lateral borders of the iliac crest (Figure 4.5). While each of these of these borders was defined automatically by curvature, their intersections included a small number of nodes. The user selected a single node to represent the landmark. As the process was not fully automatic, a repeatability study was completed for the ASIS and PSIS. Specifically, three observers selected the landmarks three times to calculate inter- and intraobserver precision following the definition used by Victor *et al*.[21] The average position of each landmark across all nine selection trials was used in subsequent analyses. To evaluate the influence of landmark selection inconsistencies, the pelvic coordinate system was calculated using the average landmark positions and the positions from each selection trial. For each axis of the coordinate system, the angle between the average and trial configurations was calculated.

4.3.5 Validation of Joint Angles and Translations

Raw model-based tracking and DRSA results were converted into clinical joint angles and translations. The transformation matrix relating the pelvis and femur anatomical coordinate systems to the CT coordinate system (P_{anat}/CT and F_{anat}/CT) was defined using the landmarks described above. Not all bony landmarks required to define

the anatomical coordinate systems were visible in the dual fluoroscopy field of view. As such, a technical coordinate system was required for both the pelvis and femur, and established relative to the CT coordinate system using the three most visible beads (P_{tech}/CT and F_{tech}/CT). These technical coordinate systems were then tracked relative to laboratory coordinates (P_{tech}/Lab and F_{tech}/Lab) for each fluoroscopy frame for both model-based tracking and DRSA. The combination of these matrices provided the overall transformation from pelvis to femur anatomical coordinate systems for each frame, calculated as:

$$P_{anat}/CT \times CT/P_{tech} \times P_{tech}/Lab \times Lab/F_{tech} \times F_{tech}/CT \times CT/F_{anat} \quad [4.1]$$

The three joint angles (flexion/extension, abduction/adduction, internal/external rotation) were calculated from the resulting transformation matrix using a Grood and Suntay convention.[22]

To define translations, the position of the PJC and FJC was calculated in laboratory coordinates for each frame as follows (example for the PJC):

$$PJC_{Lab}=Lab/\ P_{tech} \times P_{tech}/CT \times PJC_{CT} \quad [4.2]$$

The vector from PJC to FJC was computed and then projected onto each of the pelvic coordinate axes (also recalculated for the current frame) to obtain medial/lateral, anterior/posterior, superior/inferior translations. Joint angles and translations derived from raw DRSA bead coordinates were filtered with a 6 Hz Butterworth filter. Bias and

precision were calculated between the filtered DRSA kinematics and raw model-based tracking kinematics.

Repeatability of the clinical exams was assessed at max external rotation (FABER), max internal rotation (Rotational Profile), and max internal rotation in flexion (for the Impingement Exam). Each time point was identified in the trial and the three joint angles were recorded. Exam repeatability was calculated as the standard deviation of each angle over the three trials.

4.3.6 Validation of Bone-to-Bone Distance

A custom tool was created in PostView[20] to visualize bone motion and bone-to-bone distance. For bone motion, the tool applied transformations from CT to laboratory coordinates for both the femur and pelvis for each time point to nodal coordinates defining the bone surfaces. For bone-to-bone distance, the user selected the faces representing the articulating regions of the acetabulum and femur. For each face, the tool calculated the nearest distance to the opposing surface (displayed as a fringe plot).

Bone-to-bone distance results were compared between DRSA and model-based tracking. For every 10^{th} frame of each exam, the root mean square (RMS) error was calculated between all nodes in the articulating region of the pelvis and femur (defined as nodes with a distance less than 10 mm measured by either tracking method). An average RMS error was calculated for each trial and then results were averaged across all specimens and exams.

4.3.7 Application to Live Human Subject

With IRB approval (#51053) and informed consent, one male with no history of hip pain or pathology was imaged (32 years old, 177 cm, 73 kg). An orthopaedic surgeon performed the three exams (Figure 4.6). 280 ± 5 frames were collected per exam. Radiation settings were 87 kVp/3.3 mA (fluoro 1) and 88 kVp/3.4 mA (fluoro 2). CT images of the entire pelvis, proximal femur, and knee were acquired with a Siemens SOMATOM Definition CT Scanner (0.7 mm slice thickness, 355 mm FOV, 512 x 512 matrix) and bones were segmented with Amira. Model-based tracking and filtering of results was completed as described above. Outcome measures included joint angles, translations, bone-to-bone distance, and videos of bone motion.

4.4 Results

Bias and precision of DRSA for the optimal conditions (beads in acrylic) were 0.017 and 0.113 mm, respectively. In vitro precision (± standard deviation across all trials and specimens) of DRSA was 0.159 ± 0.072 mm.

Average Euclidian bias of model-based tracking (± standard deviation across all trials and specimens) was 0.32 ± 0.08 mm for the pelvis and 0.30 ± 0.06 mm for the femur. Average Euclidian precision for the pelvis and femur were 0.13 ± 0.03 mm and 0.14 ± 0.04, respectively. Across exams, bias and precision of the distance difference along any one of the laboratory axes did not exceed 0.17 mm and 0.23 mm, respectively (Table 4.1).

For Specimen 1, Euclidian bias and precision across all trials were 0.35 ± 0.05 and 0.13 ± 0.02 for the pelvis, respectively, and 0.29 ± 0.04 mm and 0.13 ± 0.03 for the

femur, respectively. For Specimen 2, the Euclidian bias and precision across all trials were 0.30 ± 0.11 and 0.13 ± 0.04 for the pelvis, respectively, and 0.31 ± 0.09 mm and 0.15 ± 0.05 for the femur, respectively.

Intraobserver precision in landmark selection (± standard deviation across all observer trials) for the ASIS and PSIS were 0.18 ± 0.44 mm and 0.12 ± 0.37 mm, respectively. Interobserver precision was 0.18 ± 0.21 mm for the ASIS and 0.24 ± 0.38 mm for the PSIS. Comparing pelvic coordinate systems established using landmarks from each selection trial to the coordinate system established from the average position of each landmark, the average angle between respective axes was 0.07 ± 0.10°.

Comparing model-based tracking kinematics to DRSA kinematics, translation bias did not exceed 0.48 mm and angular bias did not exceed 0.58° (Table 4.2). Qualitatively, kinematics were nearly identical between DRSA and model-based tracking (visualized for the impingement exam on Specimen 1 in Figure 4.7). Exam repeatability ranged from 0.1° (for ab/adduction angle at the point of max internal rotation during the rotational profile) to 4.1° (for ab/adduction angle at the point of max external rotation during the FABER test). The average RMS error of bone-to-bone measurements (± standard deviation across all trials and specimens) was 0.52 ± 0.15 mm.

The total time used to position the live subject and image all exams was 21 seconds, resulting in an estimated dose exposure (EDE) from dual fluoroscopy of 0.32 mSv. Adding the CT scan, the total EDE was 9.74 mSv, or 19% of the annual exposure for research subjects stipulated by the Food and Drug Administration. For the three exams, joint angles were calculated and bone-to-bone distance was displayed in the articulating region (Figure 4.8). Greater external rotation than internal rotation was

achieved during the rotational profile. At maximum adduction during the impingement exam, the anterior femoral neck approximated the anterosuperior acetabular rim (shortest bone-to-bone distance was approximately 2 mm, Figure 4.8). For the FABER test, the femur achieved 65° of external rotation in the figure-four position.

Videos of bone motion and dynamic bone-to-bone distance fringe plots for all three exams were studied. During the impingement exam, the pelvis remained relatively stationary until the range of motion was reached, after which the force applied by the examiner caused posterior pelvic tilt and pelvic obliquity. During the FABER test, subtle subluxation occurred as the posterior femoral neck articulated against the posterior acetabular wall. For the rotational profile, internal rotation did not appear to be limited by articulation of the femoral head or neck with the acetabular rim.

4.5 Discussion

In this study, dual fluoroscopy and model-based tracking could measure hip kinematics during clinical exams to a bias and precision less than one millimeter and one degree, similar to other hip validation studies (Table 4.3). There were no substantial differences in tracking accuracy between exams. Exam repeatability for the cadavers was very good. The semi-automatic approach described for landmark selection had excellent repeatability; minor inconsistencies in landmark selection only slightly altered coordinate axes. A live subject was also successfully imaged. Joint angles, translations, and bone-to-bone distance results as well as videos of bone motion for the volunteer demonstrated the feasibility of using dual radiography and model-based tracking for future research.

The bias and precision of model-based tracking presented herein represent the upper bounds of error. Specifically, bead locations quantified by DRSA served as the reference standard, but beads implanted in bone are more difficult to visualize than those in a radiolucent material, like acrylic. As a result, the precision of DRSA was slightly worse in vitro than in the optimal conditions. In the past, inaccuracies in in vitro DRSA have been addressed by excluding those image frames with poor DRSA precision.[13]. By excluding frames, the accuracy of model-based tracking may be artificially improved. Rather than excluding frames in the present study, we chose to filter the in vitro DRSA data. We chose to filter the experimental data and retain the raw model-based tracking data as we believe this represents a worst case scenario.

There were a few limitations. First, while the study objective was to evaluate clinical exams utilized in the assessment of FAI, the live subject evaluated herein did not have FAI. However, normal subjects likely have a larger range of motion than FAI patients, which provides confidence that our DFS could quantify kinematics of FAI patients. The BMI of the cadaver specimens and volunteer were less than the United States average (28.7 kg/m^2).[23] However, Harris *et al*. reported a BMI of 24.5±2.6 kg/m^2 in a review of more than 2,000 FAI patients, making the results of this study relevant to the future study of FAI with dual fluoroscopy and model-based tracking.[24] Still, the radiation and imaging settings used in our study may not be applicable to persons with a BMI greater than ~25 kg/m^2. We chose to reduce radiation exposure to the human volunteer by performing a single trial. Therefore, a final limitation was that exam repeatability was accessed using the cadaveric specimens only.

In conclusion, by combining dual fluoroscopy with model-based tracking, we have shown that hip kinematics can be accurately quantified during clinical exams in vivo. The ability to accurately quantify joint angles, visualize bone motion and distance between bones could provide insight into how FAI alters hip kinematics and elucidate the mechanisms responsible for chondrolabral damage.

4.6 Acknowledgements

I would like to acknowledge my coauthors on this work, Stephen K. Aoki, Christopher L. Peters, Steve A. Maas, Michael J. Bey, Roger Zauel, and Andrew E. Anderson. I would also like to thank Kristin Ciarelli and Michael Kutschke for assistance with model-based tracking.

4.7 References

1. Philippon MJ, Maxwell RB, Johnston TL, et al. 2007. Clinical presentation of femoroacetabular impingement. Knee Surg Sports Traumatol Arthrosc 15: 1041-1047.

2. Kennedy MJ, Lamontagne M, Beaule PE. 2009. Femoroacetabular impingement alters hip and pelvic biomechanics during gait: Walking biomechanics of FAI. Gait Posture 30: 41-44.

3. Rylander JH, Shu B, Andriacchi TP, et al. 2011. Preoperative and postoperative sagittal plane hip kinematics in patients with femoroacetabular impingement during level walking. Am J Sports Med 39 Suppl: 36S-42S.

4. Brisson N, Lamontagne M, Kennedy MJ, et al. 2013. The effects of cam femoroacetabular impingement corrective surgery on lower-extremity gait biomechanics. Gait Posture 37: 258-263.

5. Audenaert EA, Mahieu P, Pattyn C. 2011. Three-dimensional assessment of cam engagement in femoroacetabular impingement. Arthroscopy 27: 167-171.

6. Tannast M, Kubiak-Langer M, Langlotz F, et al. 2007. Noninvasive three-dimensional assessment of femoroacetabular impingement. J Orthop Res 25: 122-131.

7. Kubiak-Langer M, Tannast M, Murphy SB, et al. 2007. Range of motion in anterior femoroacetabular impingement. Clin Orthop Relat Res 458: 117-124.

8. Bedi A, Dolan M, Hetsroni I, et al. 2011. Surgical treatment of femoroacetabular impingement improves hip kinematics: a computer-assisted model. Am J Sports Med 39 Suppl: 43S-49S.

9. Wassilew GI, Janz V, Heller MO, et al. 2013. Real time visualization of femoroacetabular impingement and subluxation using 320-slice computed tomography. J Orthop Res 31: 275-281.

10. Lee CB, Clark J. 2011. Fluoroscopic demonstration of femoroacetabular impingement during hip arthroscopy. Arthroscopy 27: 994-1004.

11. Bey MJ, Zauel R, Brock SK, et al. 2006. Validation of a new model-based tracking technique for measuring three-dimensional, in vivo glenohumeral joint kinematics. J Biomech Eng 128: 604-609.

12. Lin H, Wang S, Tsai TY, et al. 2013. In-vitro validation of a non-invasive dual fluoroscopic imaging technique for measurement of the hip kinematics. Med Eng Phys 35: 411-416.

13. Martin DE, Greco NJ, Klatt BA, et al. 2011. Model-based tracking of the hip: implications for novel analyses of hip pathology. J Arthroplasty 26: 88-97.

14. Reimann DA, Flynn MJ. 1992. Automated Distortion Correction of X-ray Image Intensifier Images. IEEE Nuclear Science Symposium and Medical Imaging Conference. Orlando, FL: IEEE; pp. 1339-1341.

15. Tashman S, Anderst W. 2003. In-vivo measurement of dynamic joint motion using high speed biplane radiography and CT: application to canine ACL deficiency. J Biomech Eng 125: 238-245.

16. Harris MD, Anderson AE, Henak CR, et al. 2012. Finite element prediction of cartilage contact stresses in normal human hips. J Orthop Res 30: 1133-1139.

17. Winter DA. 2005. Biomechanics and motor control of human movement, 3rd ed ed. Hoboken, NJ: John Wiley & Sons, Inc.; 325 p.

18. Wu G, Siegler S, Allard P, et al. 2002. ISB recommendation on definitions of joint coordinate system of various joints for the reporting of human joint motion--part I: ankle, hip, and spine. International Society of Biomechanics. J Biomech 35: 543-548.

19. Mass S, Rawlins D, Weiss JA. "PreView" Finite Element Pre-Processing. http://www.febio.org/preview. Accessed July 25, 2013.

20. Mass S, Rawlins D, Weiss JA. "PostView" Finite Element Post-Processing. http://www.febio.org/postview. Accessed July 25, 2013.

21. Victor J, Van Doninck D, Labey L, et al. 2009. How precise can bony landmarks be determined on a CT scan of the knee? Knee 16: 358-365.

22. Grood ES, Suntay WJ. 1983. A joint coordinate system for the clinical description of three-dimensional motions: application to the knee. J Biomech Eng 105: 136-144.

23. Flegal KM, Carroll MD, Kit BK, et al. 2012. Prevalence of obesity and trends in the distribution of body mass index among US adults, 1999-2010. JAMA 307: 491-497.

24. Harris JD, Erickson BJ, Bush-Joseph CA, et al. 2013. Treatment of femoroacetabular impingement: a systematic review. Curr Rev Musculoskelet Med 6: 207-218.

Table 4.1

Model-Based Tracking Bias and Precision of Sphere Centroid Locations

Bone		FABER Test		Impingement Exam		Rotational Profile	
		Bias	**Precision**	**Bias**	**Precision**	**Bias**	**Precision**
Pelvis	3D	0.35 (0.09)	0.15 (0.03)	0.35 (0.07)	0.14 (0.03)	0.26 (0.07)	0.11 (0.03)
	X	-0.14 (0.10)	0.14 (0.04)	-0.16 (0.13)	0.16 (0.04)	-0.06 (0.06)	0.14 (0.05)
	Y	0.03 (0.04)	0.09 (0.02)	0.04 (0.05)	0.09 (0.02)	0.07 (0.07)	0.08 (0.03)
	Z	0.12 (0.23)	0.17 (0.04)	0.09 (0.18)	0.17 (0.03)	0.06 (0.12)	0.15 (0.05)
Femur	3D	0.30 (0.06)	0.15 (0.04)	0.26 (0.05)	0.13 (0.05)	0.34 (0.07)	0.14 (0.03)
	X	0.07 (0.06)	0.13 (0.02)	0.11 (0.07)	0.11 (0.03)	0.03 (0.13)	0.13 (0.03)
	Y	-0.05 (0.09)	0.13 (0.04)	0.01 (0.05)	0.10 (0.02)	0.03 (0.06)	0.13 (0.03)
	Z	-0.04 (0.09)	0.23 (0.04)	0.04 (0.12)	0.17 (0.05)	0.17 (0.08)	0.21 (0.04)

All results in mm. Results are listed at average (standard deviation) for three beads tracked in two specimens for three trials per exam. 3D represents Euclidian distance between sphere centroids. X, Y, Z represent the difference along each of the laboratory axes.

Table 4.2

Model-based Tracking Bias and Precision of Joint Angles and Translations

Kinematic Parameter	FABER Test		Impingement Exam		Rotational Profile	
	Bias	**Precision**	**Bias**	**Precision**	**Bias**	**Precision**
Mediolateral Translation (mm)	0.35 (0.10)	0.32 (0.10)	0.36 (0.26)	0.48 (0.65)	0.23 (0.28)	0.42 (0.05)
Anteroposterior Translation (mm)	0.10 (0.27)	0.41 (0.11)	0.06 (0.31)	0.38 (0.07)	-0.22 (0.22)	0.51 (0.16)
Superoinferior Translation (mm)	0.27 (0.20)	0.47 (0.15)	0.48 (0.65)	0.59 (0.22)	0.03 (0.21)	0.25 (0.04)
Flexion-Extension (°)	0.28 (0.22)	0.78 (0.31)	0.26 (0.44)	0.54 (0.08)	0.49 (0.16)	0.57 (0.14)
Abduction-Adduction (°)	0.03 (0.32)	0.36 (0.12)	-0.06 (0.29)	0.44 (0.13)	0.55 (0.18)	0.38 (0.06)
Internal-External Rotation (°)	-0.14 (0.20)	0.71 (0.13)	-0.58 (0.66)	0.74 (0.23)	-0.21 (0.57)	0.76 (0.20)

Results are listed at average (standard deviation) of three trials for each exam completed for two specimens.

Table 4.3

Maximum Bias and Precision Comparison Between Studies

Maximum Reported Value	**Present Study**	**Martin *et al*., 2011**	**Lin *et al*., 2012**
Bias along a single laboratory axis (mm)	0.17	0.21	*
Precision along a single laboratory axis (mm)	0.21	0.24	*
Joint Angle Bias (°)	0.61	0.43	0.59
Joint Angle Precision (°)	0.81	1.27	0.82
Translation Bias (mm)	0.48	0.4	0.93
Translation Precision (mm)	0.59	0.45	1.13

* Lin *et al*. reported error along anatomical axes, not laboratory axes.

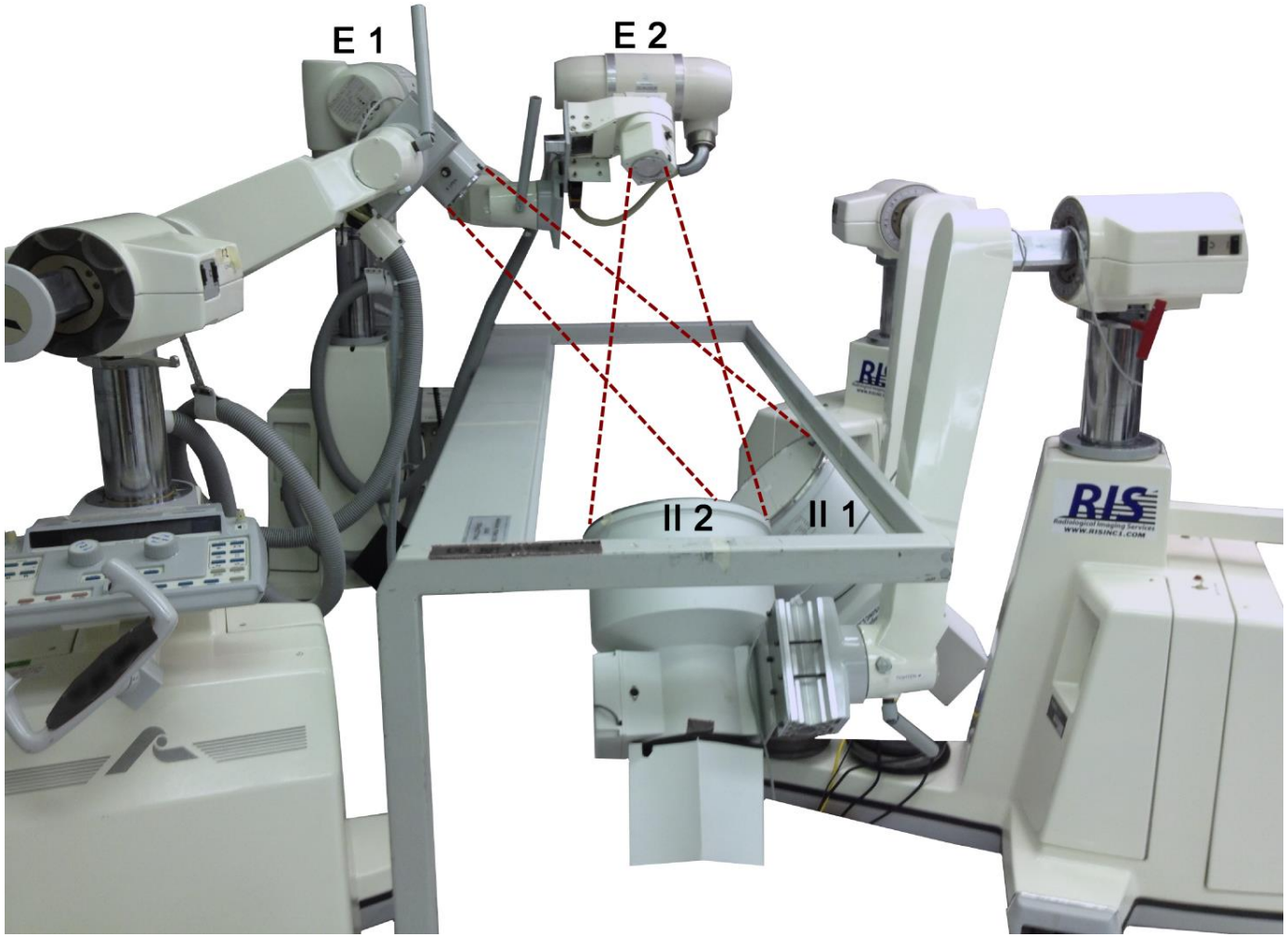

Figure 4.1. Dual fluoroscopy system configured to image the left hip during supine clinical exams. Dashed lines represent x-ray beam. E = emitter, II= image intensifier.

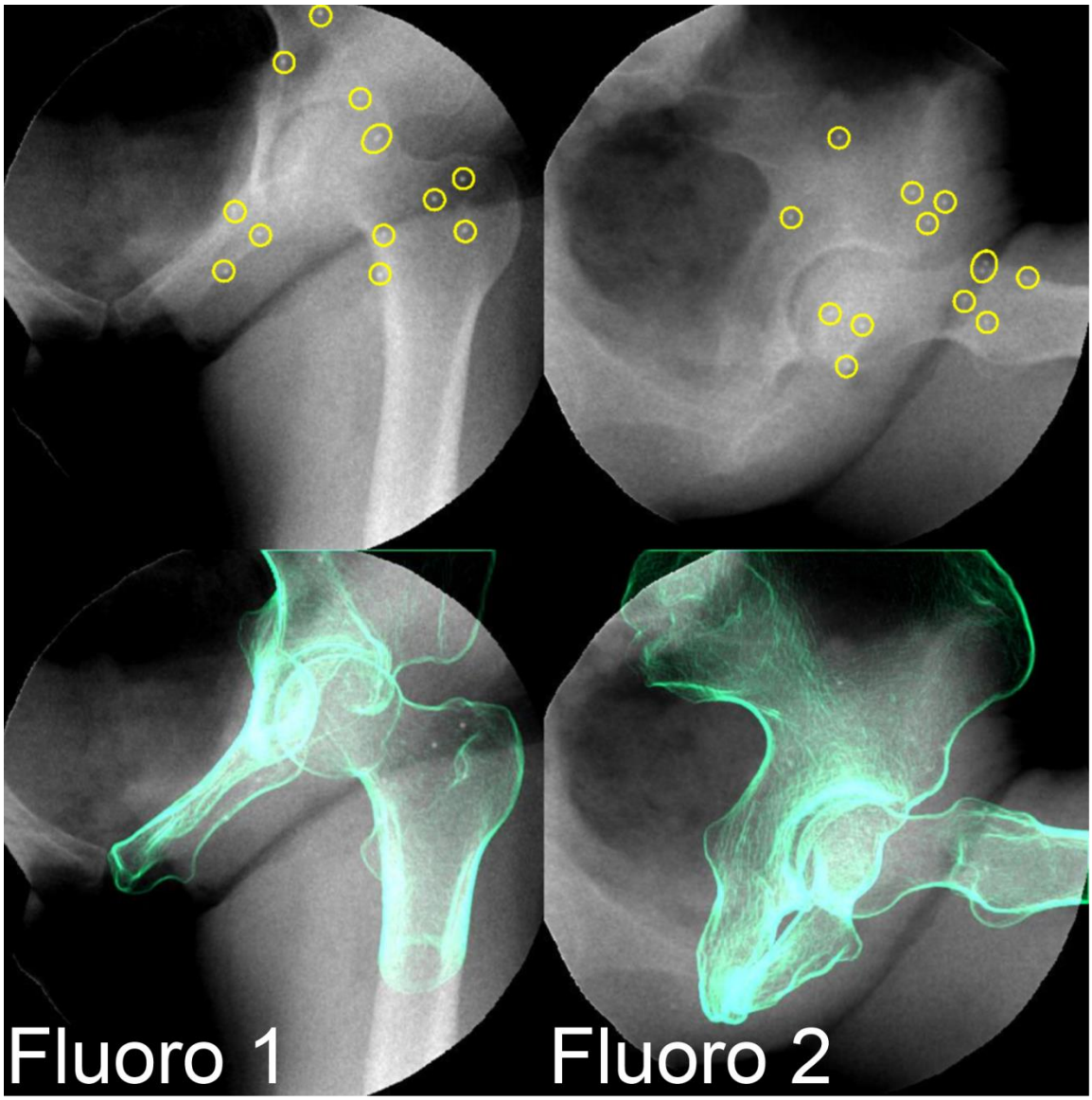

Figure 4.2. Fluoroscopy images from specimen 2 during the impingement exam. Point of max internal rotation at ~90° flexion is shown. Top: Fluoroscopy images with circles highlighting the beads implanted in pelvis and proximal femur. Bottom: Fluoroscopy images with digitally reconstructed radiographs of the pelvis and femur overlaid.

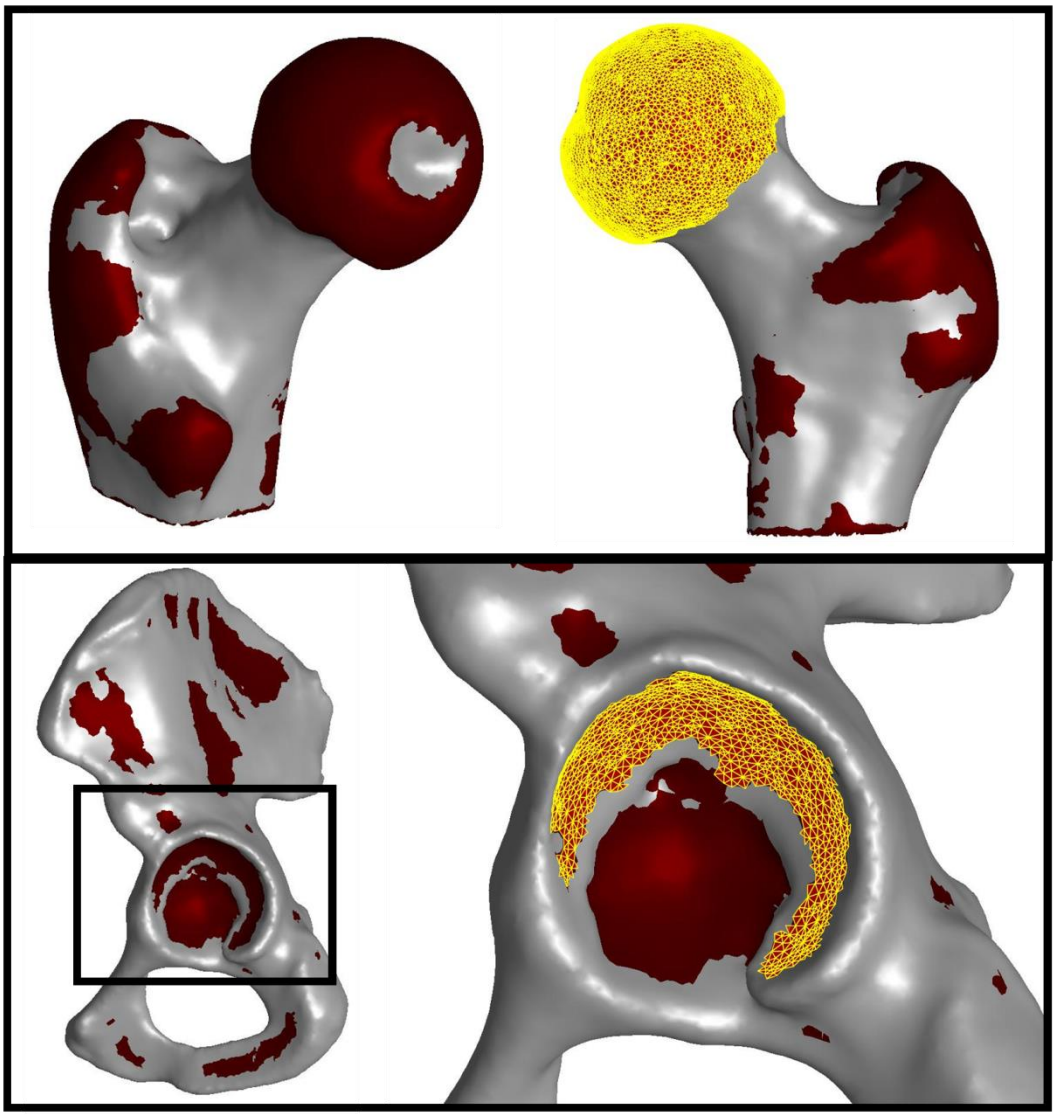

Figure 4.3. Methods to find pelvic and femoral joint centers. Second principal curvature automatically isolates femoral head (top) and lunate surface of the acetabulum (bottom). The pelvic and femoral joint centers were calculated as the center of the best fit sphere of the lunate surface of the acetabulum and femoral head, respectively.

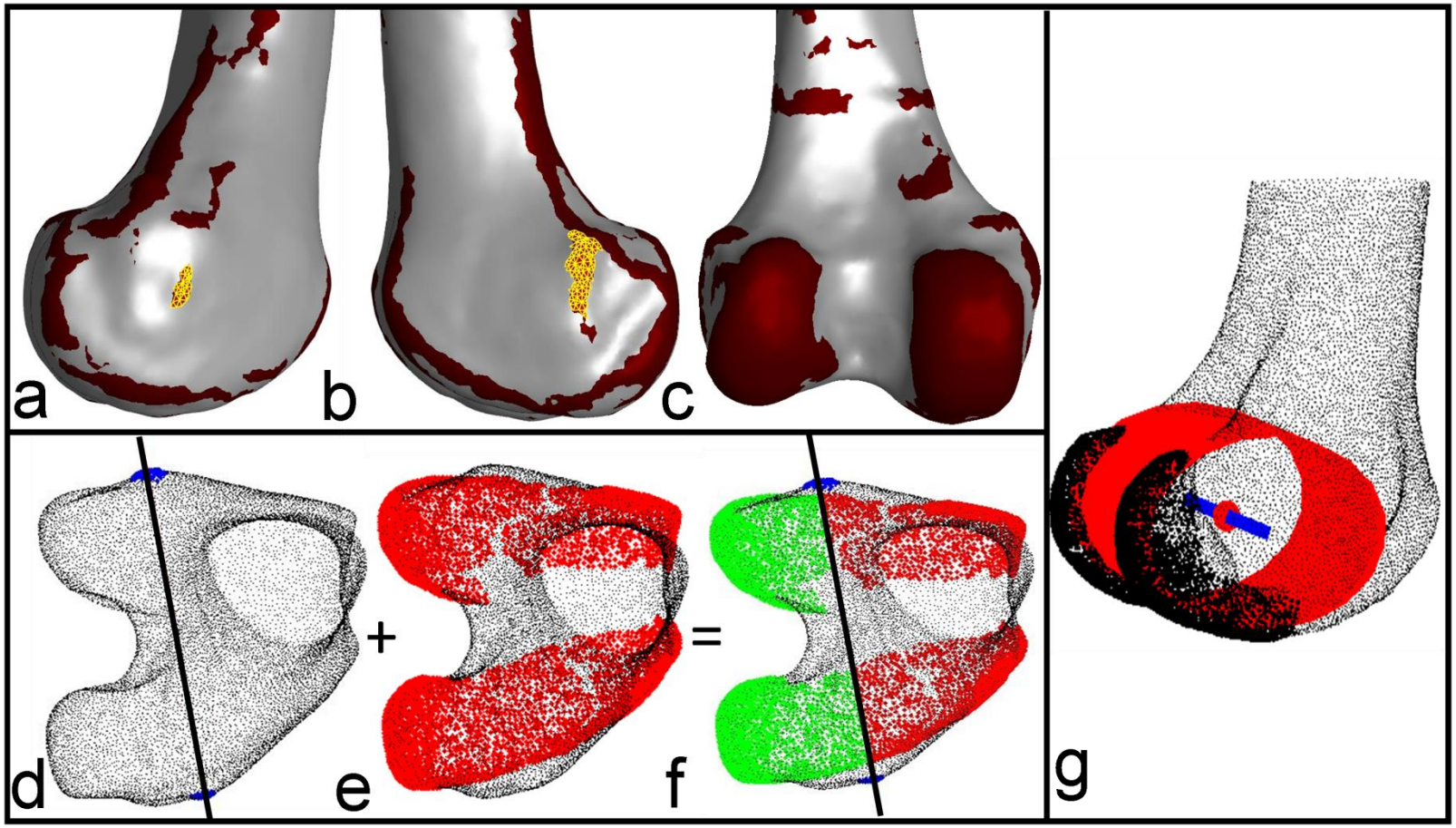

Figure 4.4. Methods to establish the mediolateral axis of the femur and midpoint of the knee. First principal curvature automatically defined the ridges on the medial and lateral femoral epicondyles [yellow selection in (a), (b)]. The articulating surface of the condyles was automatically defined using second principal curvature [red selection in (c), (e)]. A plane was fit to the medial and lateral epicondyle ridges [blue in (d)] to isolate the posterior condyles [green in (f)]. The isolated posterior condyles were fit to a cylinder [red in (g)] to define the mediolateral axis of the femur [blue in (g)]. The center of the cylinder defined the midpoint (g).

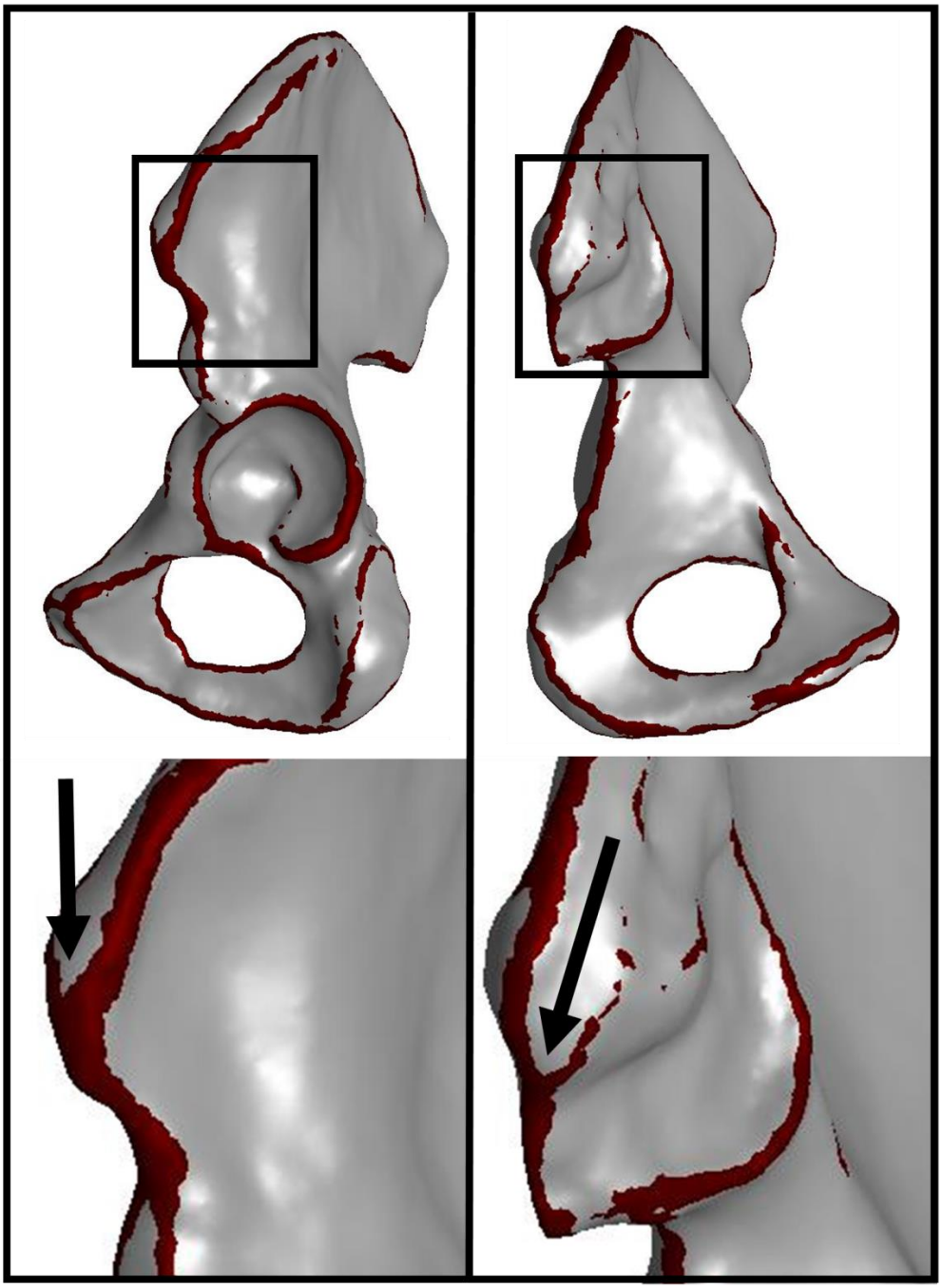

Figure 4.5. Methods to identify the anterior superior iliac spines (ASIS) and posterior superior iliac spines (PSIS). First principal curvature automatically defined the iliac crest and superior border of the sacroiliac joint. The ASIS was identified as a user-selected point at the anterior intersection between the medial and lateral borders of the iliac crest (arrow, left panel). The PSIS was identified as a user-selected point at the posterior intersection of the superior border of the sacroiliac joint and the medial border of the iliac crest (arrow, right panel).

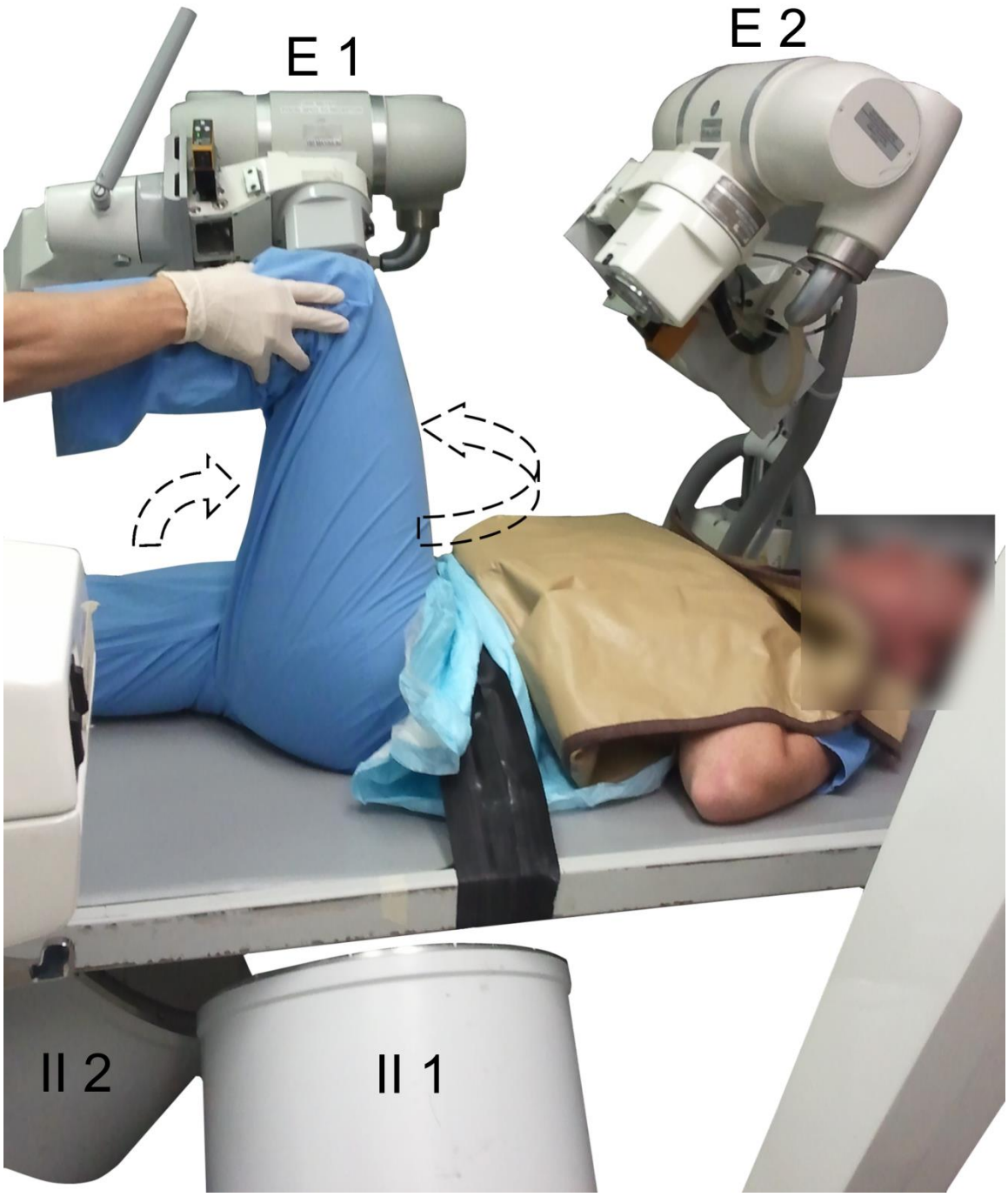

Figure 4.6. Live subject positioned in the dual fluoroscopy system with left hip flexed during impingement exam. Dashed arrows indicate the direction of motion during the impingement exam, specifically flexion to ~90° followed by internal rotation and adduction.

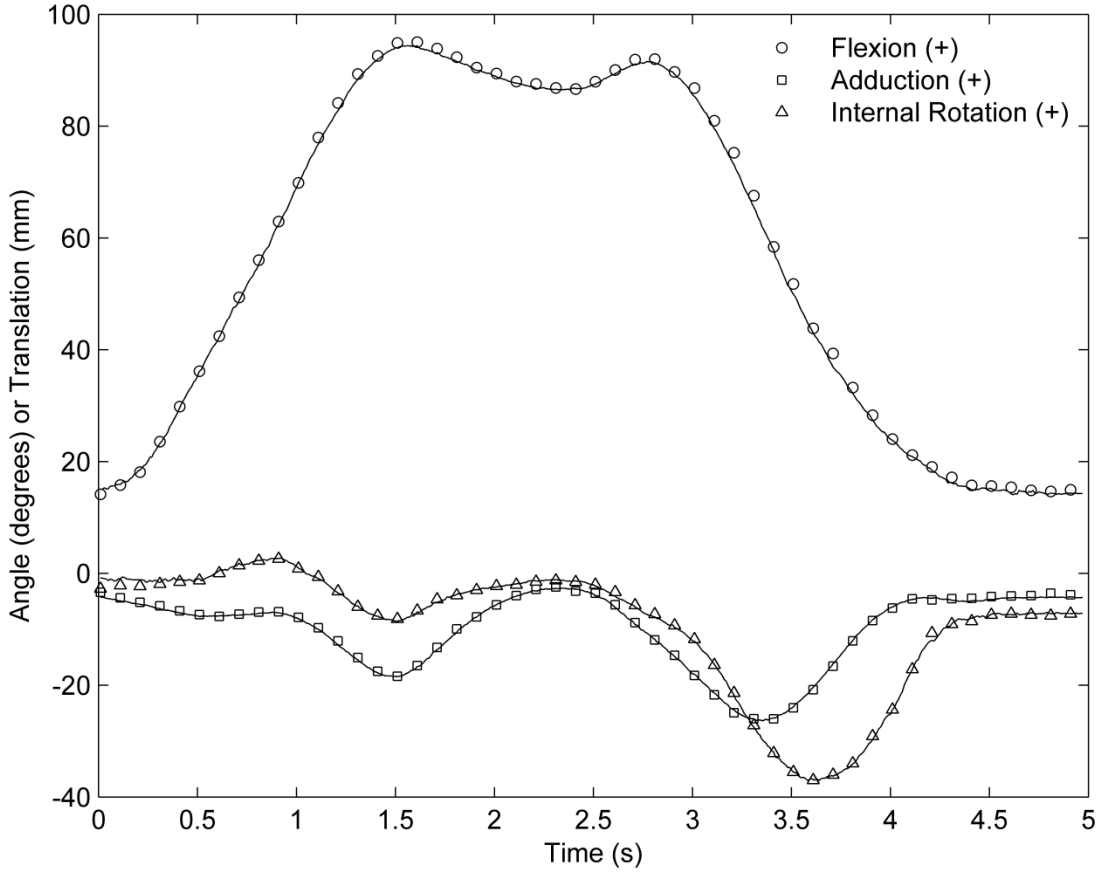

Figure 4.7. Results for specimen 1 during the impingement exam. Joint angles calculated via model-based tracking (lines) are compared to DRSA (shapes, plotted every 10th frame for clarity).

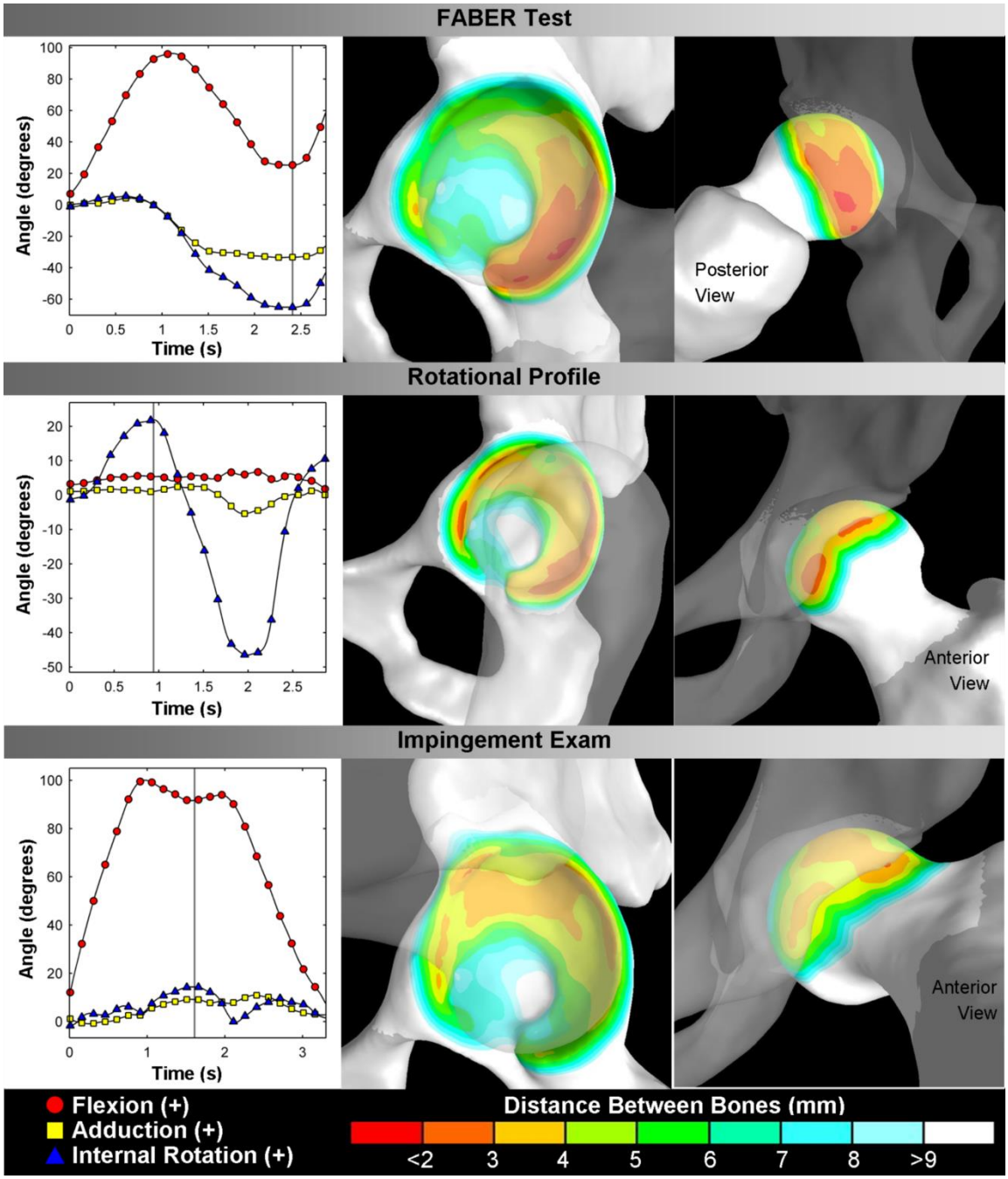

Figure 4.8. Joint angles calculated using model-based tracking during clinical exams on live subject (left column). Bone-to-bone distance (mm) is displayed on pelvis (middle column) and femur (right column) at time points indicated in joint angle plots by vertical grey line. Included time points are: max external rotation for the FABER test, max internal rotation for the rotational profile, and max internal rotation in flexion for the impingement exam.

CHAPTER 5

QUANTIFICATION OF IN VIVO HIP KINEMATICS DURING CLINICAL EXAMS USING DUAL FLUOROSCOPY AND MODEL-BASED TRACKING: APPLICATION TO THE STUDY OF FEMORACETABULAR IMPINGEMENT

5.1 Abstract

Abnormal articulation in hips with femoroacetabular impingement (FAI) may cause chondrolabral damage, but has not been accurately quantified. Dual fluoroscopy and model-based tracking can quantify 3D in vivo hip kinematics with errors less than one millimeter and one degree. The purpose of this study was to quantify and compare hip kinematics of a cohort of asymptomatic controls and patients with FAI during supine clinical exams. Dual fluoroscopy video was collected of six asymptomatic subjects and three patients with FAI during the impingement exam, rotational profile, and FABER test. Surfaces for the femur, pelvis, and labrum were segmented from CT arthrogram images. In vivo kinematics of the pelvis and femur were obtained from model-based tracking. Joint angles, joint translations, and relative pelvic angles were calculated. At the terminal position of the impingement exam, regions of minimum bone-to-bone distance and labrum-femur contact were identified. For the normal subjects, internal rotation averaged 9.1±4.4° (impingement exam) and 32±6.4° (rotational profile). External rotation

averaged 48±7.4° (FABER) and 36±8.2° (rotational profile). Comparatively, FAI patients demonstrated decreased range of motion. During all exams, hip articulation involved pelvic motion, and joint translation and no bone-to-bone contact. The region of minimum bone-to-bone distance coincided with the actual location of labrum-femur contact in only half the subjects. Results demonstrated joint articulation to be a highly complex process. Using dual fluoroscopy and model-based tracking, limitations in range of motion and the locations of impingement during clinical exams can be identified in FAI patients relative to normal subjects.

5.2 Introduction

Femoroacetabular impingement (FAI), a reduction in clearance between the femoral head and acetabulum, causes hip pain and damage to chondrolabral tissue and may initiate osteoarthritis (OA).[1] Morphologically, FAI presents as asphericity of the femoral head or neck (cam), acetabular overcoverage (pincer), or a combination of the two (mixed). Functionally, FAI presents as restricted and painful hip motion, which occurs in one or more anatomical planes.[1,2] Differing patterns of chondrolabral damage have led to separate hypothesized mechanisms of impingement for each subtype of FAI.[3-7] For example, in pincer FAI patients, labral tears perpendicular to the surface are suggested to originate as the labrum is compressed between the femoral neck and overcovered acetabulum. Cam FAI is predominately associated with labral tears and cartilage delamination at the chondrolabral boundary in the anterosuperior acetabulum, thought to originate as the aspherical head is forced into the acetabulum.

Clinical exams range the hip through motions thought to induce impingement, and are central to confirming functional impairments in patients with radiographic signs of FAI. In the impingement exam, the hip is flexed and then internally rotated and adducted. Patients with suspected FAI almost always report pain during the exam, which could be the result of contact to damaged tissue.[1,8,9] The flexion-abduction-external rotation (FABER) test, designed to test for posterior impingement, is also frequently positive in FAI patients.[9] Finally, range of motion is quantified during the rotational profile to identify possible restrictions in hip internal and external rotation.[10]

While valuable to the diagnosis of FAI, there is limited functional understanding of how hip pathoanatomy influences clinical exam findings. First, hip kinematics are measured with a goniometer or estimated visually.[11,12] Second, reports of pain are subjective. It is therefore difficult to objectively define an abnormal from normal exam finding. A detailed and accurate assessment of hip kinematics during clinical exams could serve several purposes. First, it could provide objective diagnostic criterion for these exams. Second, quantification of hip kinematics relative to the underlying 3D anatomy could be used for pre-operative planning. Finally, kinematic measurements during exams could lend valuable quantitative data to support hypothesized mechanisms of impingement and damage patterns observed clinically.

Previous kinematic studies have provided insights into altered function in FAI patients, but limitations in the chosen techniques have prohibited an accurate assessment of joint articulation. Skin marker motion analysis has identified gross reductions in range of motion during walking, squatting, and stair-climbing.[13-16] However, soft tissue artifact and inaccuracies in estimating the hip joint center limit the applicability of standard skin

marker tracking to identify subtle differences in joint articulation. Computer simulations have been used to predict the location of impingement and evaluate the effects of virtual surgery.[17-20] These models incorporate the true anatomy of the joint, derived from CT or MRI images. However, they assume a fixed center or axis of rotation for the femur. Further, range of motion is either estimated from the limits of bone-to-bone collision in the simulation, ignoring the contributions of surrounding soft tissue, or from magnetic-based tracking systems that are subject to the same limitations of skin marker motion analysis.

As shown in Chapter 4, dual fluoroscopy and model-based tracking can directly quantify hip kinematics during clinical exams with an error less than 0.48 mm and rotational error less than 0.58°. Prior to using this technique to ascertain hip kinematics of FAI patients during clinical exams, it is necessary to establish the same data in subjects who are asymptomatic for hip pain and have normal hip anatomy. Therefore, the first objective of this study was to use dual fluoroscopy to quantify hip kinematics of a cohort of asymptomatic controls during supine clinical exams (impingement exam, FABER test and neutral flexion rotational profile). The second objective was to demonstrate the utility of dual fluoroscopy and model-based tracking to study FAI by quantifying and comparing the kinematics of three patients with differing FAI morphology to results from the normal subjects.

5.3 Methods

5.3.1 Subjects

With IRB approval (#51053), eight asymptomatic subjects without a history of hip pain or pathology were screened for grossly abnormal morphology and signs of osteoarthritis with an anteroposterior (AP) radiograph. Six subjects passed the screening and were enrolled in the study as part of a normal cohort (2 females, age 25.5 ± 3.7 years, height: 177 ± 11.9 cm, weight: 64.9 ± 9.00 kg, BMI: 20.6 ± 1.18 kg/m^2, anteroposterior alpha angle 45 ± 2.6°, lateral center edge angle 34 ± 5.8°).

Three patients with symptomatic FAI were also enrolled in this study. The patients presented to the coauthor's (SKA) clinic with a history of left hip pain greater than two years, limiting exercise and activities of daily living. Attempts at nonoperative management, including physical therapy, non-steroidal anti-inflammatory medication, and cessation of activity had failed. As part of the diagnostic work-up, acetabular overcoverage was assessed with the lateral center edge angle (LCEA) on AP radiographs. Femoral asphericity was assessed with the alpha angle measured on frog-leg lateral radiographs. All patients reported pain during the impingement and FABER exams and exhibited grossly restricted range of motion. All three patients were treated with arthroscopic femoral osteochondroplasty, acetabuloplasty, and labral repair.

Patient 1 (male, 25 years, 180 cm, 85.3 kg, BMI 26.2 kg/m2) presented with a pistol-grip cam deformity and low hanging anterior inferior iliac spine. Radiographic findings included an LCEA of 20° and alpha angle of 80° (Figure 5.1). Intraoperative findings included a labral tear at the chondrolabral junction from 12-2 o'clock (Figure 5.1).

Patient 2 (female, 23 years, 168 cm, 63.5 kg, BMI 22.6 kg/m2) presented with protrusio, a downward sloping sourcil, a large pincer groove, and a large bony prominence located on the anterolateral femoral neck (Figure 5.2). LCEA was 42° and alpha angle was 71°. Upon intraoperative inspection, the labrum was separated from cartilage in the anterosuperior region of the acetabulum (Figure 5.2). Surface changes to cartilage were present on the posterosuperior femoral head and posterior acetabulum.

Patient 3 (female, 26 years, 173 cm, 56.7 kg, BMI 19.0 kg/m2) presented with mixed FAI, including acetabular overcoverage (LCEA 45°), and femoral head asphericity (alpha angle 70°), and a pincer groove on the anterolateral femoral neck (Figure 5.3). Intraoperatively, surface changes were observed at anterosuperior chondrolabral junction and posterior acetabulum. Mechanical wear was present at the pincer groove (Figure 5.3).

5.3.2 CT Arthrogram Image Acquisition and Segmentation

CT arthrogram images were acquired of each subject with a Siemens SOMATOM Definition CT Scanner.[21] Images of the pelvis and proximal femurs were acquired at 1 mm slice thickness, 342 ± 19.7 mm FOV, 512 x 512 matrix. To establish the femoral anatomical coordinate system, CT images of the knees were also acquired with the same FOV and matrix but with a 3 mm slices thickness. Images of the hip were upsampled to 3x resolution to reduce staircase artifact[21] and then segmented semi-automatically in Amira (5.4.1, Visage Imaging, San Diego, CA) to delineate the bones of interest and the acetabular labrum. 3D surface reconstructions of each bone were generated from the segmentations to define the anatomical coordinate systems, to visualize bone motion, and to calculate bone-to-bone distance. Individual image stacks were created for the affected

hemipelvis and femur for model-based tracking (left side on all subjects). These stacks contained all pixels and associated intensities representing each bone. Finally, 3D reconstructions of the labrum were created to visualize motion and to calculate overlap with the femur.

5.3.3 Dual Fluoroscopy

The dual fluoroscopy protocol validated in Chapter 4 was used in the present study. Briefly, dual fluoroscopy video was acquired at 100 Hz during the three physical exams. Each subject was positioned supine on a radiolucent table such that the left hip was centered in the combined field of view of both fluoroscopes. A wide seatbelt-like strap was secured over the anterior superior iliac spines to ensure that the pelvis remained in the FOV during each exam. An orthopaedic surgeon manipulated the subject's hip through three exams: impingement exam, FABER exam, and rotational profile in neutral flexion. Two trials were completed for each exam. The total fluoroscopy time required for each subject, including initial positioning and all exam trials, averaged 28.4 ± 3.88 s. The fluoroscopy energy settings were manually adjusted for each subject. Average tube voltage and current were 79 ± 7.0 kVp, 3.0 ± 0.37 mA, respectively.

5.3.4 Model-Based Tracking

Model-based tracking was used to determine the position and orientation of the pelvis and femur.[22] This previously validated technique can quantify hip joint kinematics with a positional error less than 0.48 mm and rotational error less than 0.58° (Chapter 4). Briefly, images of a calibration cube established the relative position and perspective of the two fluoroscopes. Knowing this geometry, digitally reconstructed radiographs

(DRRs) of the bone of interest relative to the two imaging planes were created via ray trace projection through the isolated bone image stacks. The user then manually moved the bone in six degrees of freedom (3 translations, 3 rotations) to roughly match the DRRs to the fluoroscope images for the first time point. The model-based tracking software then determined the optimal pose and orientation of the bone for each video frame by iteratively changing the six degrees of freedom to maximize the normalized cross-correlation between pixel intensities in the DRRs and the fluoroscope images.

5.3.5 Anatomical Coordinate Systems

Anatomical coordinate systems representing the pelvis and femur were established following the International Society of Biomechanics (ISB) recommendations.[23] The femoral and pelvic joint centers, mediolateral axis of the femur, and midpoint of the knee were calculated automatically. Specifically, principal curvature of the 3D bone reconstructions, calculated in PostView,[24] isolated the lunate surface of the acetabulum, femoral head, articulating surface of the femoral condyles and ridges on the medial and lateral femoral epicondyles. The center of the best fit sphere to the femoral head and lunate surface of the acetabulum, calculated in PreView,[25] defined the femoral and pelvic joint centers, respectively. In Matlab (R2009a, The MathWorks, Inc., Natick, MA), a plane was fit to the medial and lateral epicondyle ridges to isolate the posterior region of the femoral condyles, which was subsequently fit to a cylinder. The cylinder's axis and midpoint represented the mediolateral axis of the femur and midpoint of the knee, respectively.

The posterior superior iliac spine (PSIS) and anterior superior iliac spine (ASIS) were found semiautomatically. Principal curvature isolated the iliac crest and superior border of the sacroiliac joint. The PSIS was represented by the intersection of the superior border of the sacroiliac joint and medial border of the iliac crest, while the ASIS was represented as the intersection of the medial and lateral borders of the iliac crest. From the small region of nodes at each intersection, one observer selected a single node to represent each landmark. Node selection for the ASIS and PSIS has been shown to have minimal effect on the axes of the pelvic coordinate system (average variation was $0.07 \pm 0.10°$, Chapter 4).

5.3.6 Joint Angles and Translations

Joint angles were calculated using the Grood-Suntay convention.[26] Rotation about the mediolateral axis of the pelvis represented flexion and extension. Internal and external rotation was defined about the inferosuperior axis of the femur. Finally, rotation about the floating anteroposterior axis represented adduction and abduction.

For each trial, the position and orientation of the pelvic anatomical coordinate system in the first and last frames were averaged to define neutral. The transformation between this neutral coordinate system and the pelvic anatomical coordinate system in each frame was calculated to study relative pelvic angles. Angles were derived from the transformation matrix following the Grood-Suntay convention, with the proximal segment represented by the neutral coordinate system and the distal segment represented by the pelvic anatomical coordinate system of each frame.[26] Rotation about the

mediolateral axis represented pelvic tilt, rotation about the inferosuperior axis represented pelvic rotation, and rotation about the anteroposterior axis represented pelvic obliquity.

To facilitate comparisons between subjects, joint and pelvic angles were linearly interpolated between time points of interest. For the impingement exam, these time points included the first peak in flexion and the point of maximum internal rotation in flexion (terminal position). For the FABER exam, the first peak of flexion and the saddle point in flexion (representing the terminal figure-four position) were used. The terminal positions at maximum internal and maximum external rotation were selected for the rotational profile.

Angular repeatability between the two trials of each subject was calculated at the terminal points of each exam. Specifically, the difference in the three joint angles between the two trials was found for each individual and the differences were averaged for each terminal position across all nine subjects.

Joint translation was defined as the vector from the pelvic joint center to the femoral joint center. This vector was projected onto each of the pelvic coordinate axes (recalculated for the current frame) to obtain medial/lateral, anterior/posterior, superior/inferior translations. The minimum and maximum values along each axis were quantified to calculate the range of translation for each subject.

For all kinematic outcome measures, results were averaged between the two trials of each exam for each patient or normal subject. Data were presented as the average and standard deviation of the six normal subjects, while patient data were presented individually.

5.3.7 Evaluating Probable Regions of Impingement

A custom tool in PostView[24] was used to visualize bone motion and calculate the distance between surfaces. For the terminal point of the impingement exam (maximum internal rotation in flexion), the minimum bone-to-bone distance was found between the acetabular rim and femoral neck. The results were averaged between the two trials for each subject and then reported as the average and standard deviation of all subjects. Any nodes falling between the minimum distance and the minimum distance plus 0.5 mm were highlighted as the probable location of impingement. During each exam, the labrum surface was assumed to transform rigidly with the pelvis. At the same time point used to plot bone-to-bone distance, any overlap between the femoral neck and rigid labrum surface was highlighted and considered to be the actual region of contact. Finally, for each trial of the impingement exam, the frame of initial contact between the labrum and anterosuperior femoral head or neck was identified on the joint angles plot.

5.3.8 Measures of Anatomy and Regression Analysis

The association between radiographic measurements of anatomy and maximum range of motion at the terminal position of each exam was assessed. Measurements included the lateral center edge angle (anteroposterior view) and alpha angle (anteroposterior and frog-leg lateral views). Anteroposterior radiographs were available for both groups. However, frog-leg radiographs were only available for patients. Therefore, digitally reconstructed radiographs (DRRs) representing the frog-leg lateral radiographs were created for the normal subjects using their CT data and a previously reported methodology.[27] Alpha angles were then measured from the DRRs in the same

manner as patients. Finally, alpha angles and the lateral center edge angle were correlated to maximum range of motion at the terminal position of each exam using linear regression.

5.4 Results

The normal subjects achieved 19.1 ± 4.4° of internal rotation at the terminal position of the impingement exam. All patients exhibited decreased adduction and internal rotation in flexion when compared to the normal subjects (Figure 5.4, Table 5.1). As the hip was flexed, the pelvis tilted posteriorly. However, pelvic rotation and obliquity did not change substantially until initial contact was made between the labrum and anterosuperior femoral head-neck junction (Figure 5.4). For one normal subject, the femur did not contact the labrum during either trial of the impingement exam, and for a different normal subject, it there was no contact in one of the two trials. Patient 2 had the largest range of motion deficits, and exhibited less pelvic motion and increased flexion compared to the other subjects during the impingement exam.

The normal subjects experienced greater internal rotation during the rotational profile than the impingement exam (Table 5.1). For the rotational profile, Patients 1 and 3 demonstrated little difference in internal rotation when compared to the normal subjects (Figure 5.5). In contrast, patient 2 achieved 21° less internal rotation than the mean of the normal subjects (Table 5.1). In all subjects, maximum internal rotation did not appear to be limited by contact between the labrum/acetabulum and femur (Figure 5.6). In general, less pelvic motion was observed during the rotational profile compared to the impingement and FABER test.

Greater external rotation was achieved in the terminal, figure-four position of the FABER test compared to the rotational profile with minimal abduction and neutral flexion (Table 5.1). In the figure-four position, patients were in greater flexion, and less adducted and externally rotated compared to the average of the normal subjects (Figure 5.7).

Exam repeatability was very good between the two trials of each subject at the terminal position of each exam (Table 5.2). Internal/external rotation and abduction/adduction were noted to be slightly more repeatable than flexion/extension.

For all exams and subjects, the range of translation of the femoral joint center along any given anatomical direction was between 0.69-4.1 mm. Translations were greater during the FABER test and impingement exam than the rotational profile (Figure 5.8). Patient 1 exhibited greater translation in the anterior-posterior and inferior-superior directions than the other subjects during the FABER test. Patient 3 exhibited less translation than the average of the normal subjects for all exams.

In the terminal position of the impingement exam, minimum bone-to-bone distance between the acetabular rim and femoral head or neck was 3.0 ± 0.53 mm for all subjects. The region of minimum bone-to-bone distance was generally observed at the head-neck junction and at 1-2 o'clock of the acetabulum (3 o'clock representing anterior as a left hip) (Figures 5.9 and 5.10). However, for patient 2, the location of impingement was more distal on the femoral neck than the other subjects.

The location of minimum bone-to-bone distance coincided with the region of actual labral contact in only approximately half of all subjects. One normal subject did not contact the labrum during either trial. In the cases of disagreement, the region of

labral contact was observed more superior to that of minimum bone-to-bone distance on both the femur and acetabulum. With respect to the femur, the location of contact with the labrum varied between the three patients (Figure 5.11): on the cam lesion of patient 1, on the bony prominence lateral to the pincer groove on patient 2, and directly along the pincer groove on patient 3.

The alpha angle measured on both frog-leg lateral and anteroposterior radiographs was significantly correlated to maximum external rotation in the terminal positions of the FABER test and rotational profile (Table 5.3). The alpha angle measured on the anteroposterior radiographs was also significantly correlated to internal rotation during the impingement exam (Table 5.3). No significant correlations were observed for maximum internal rotation during the rotational profile or the lateral center edge angle.

5.5 Discussion

In this study, dual fluoroscopy and model-based tracking were employed to accurately quantify and visualize the 3D in vivo hip kinematics of a cohort of normal subjects and three FAI patients during clinical hip exams. As the first application of this methodology to study the hip joint in a cohort of live subjects, our data collectively demonstrate hip joint articulation and impingement to be highly complex processes, not only in FAI patients, but also in asymptomatic control subjects. Key findings were that the femur translates substantially, the labrum is contacted by the femur (often early during the impingement exam), and the pelvis moves. The location of impingement, as estimated by the region of minimum distance between bone surfaces, was coincident with the true location of contact between the femur and labrum in only half of the subjects

analyzed. Finally, statistically significant correlations were observed between hip anatomy and range of motion.

Results for the normal subjects provide an essential database for studying motion conflict and abnormal hip articulation in a larger cohort of FAI patients. Joint kinematics were found to be largely similar within the normal group (Table 5.1). However, the pattern of labrum contact and minimum bone-to-bone distance during the impingement exam varied substantially (Figures 5.9 and 5.10). This conclusion is analogous to that made in a recent subject-specific finite element (FE) study where cartilage contact stresses varied substantially between normal subjects of similar age and stature to the present study.[21] The authors of the FE study concluded that subtle differences in hip anatomy were responsible for the variation in cartilage stresses at the articulating surface.

Overall, the patients demonstrated decreased range of motion when individually compared to the normal group results. Patient 2 had an extremely deep acetabulum and the greatest limitations of motion during all exams, including obvious restrictions in internal rotation during the rotational profile. The effects of protrusio in Patient 2 were especially apparent when the location of minimum bone-to-bone distance and labral contact were visualized; both were well lateral to the femoral head and head-neck junction compared to all other subjects. Patient 1 had a relatively shallow socket, but still exhibited decreased range of motion. This finding suggests that cam-type deformities cause motion restrictions that may be independent from the morphology of the acetabulum. Out of the three patients, Patient 3 demonstrated the least deficits in each terminal position except for the impingement exam, which could be the result of less severe FAI-related deformities.

As this is the first study to use dual fluoroscopy and model-based-tracking to measure in vivo hip joint angles, it is difficult to directly compare the findings of this study with prior work. During a simulated impingement exam, maximum internal rotation was estimated at 27.9 ± 7.4° in normal subjects and 12.3 ± 6.5° in cam FAI patients.[28] These estimates are greater than the rotation measured in the present study (Table 5.1), possibly due to different flexion and adduction angles (not reported in[28]) and the absence of soft tissue restraints. In another simulation of 18 patients with cam FAI, maximum internal rotation in 85° flexion and 20° adduction was 5.7 ±15.7°. Despite less flexion and more adduction, this estimate of internal rotation is similar to the restrictions identified in the three patients in the present study.[29] However, in the same study, maximum external rotation in neutral flexion was 52.7 ± 15.9°, almost 20° greater than that reported in the present study for not only the FAI patients but also the normal subjects.[29] In the simulation, maximum range of motion was estimated from bone on bone collision; in external rotation, this resulted in direct collision between greater trochanter and ischium, which we believe is unrealistic. Finally, one previous study evaluated maximum rotation in neutral flexion with an electromagnetic tracking system. For normal subjects, mean internal and external rotation in a cohort of normal subjects were 34.1° and 38.4°, respectively, similar to that reported in the present study.[10]

In our study, the femoral head translated 0.7-0.4 mm relative to the acetabulum along each anatomical direction in all subjects. Compared to the rotational profile, translations were greater during the FABER test and impingement exam. This difference was possibly due to subtle hinging or subluxation observed at the terminal position of the FABER and impingement exams. This was not apparent in the rotational profile, where

the labrum was not contacted (Figure 5.6). Coupled with the finding that the femoral head of the patients generally translated more than normal subjects, our translation data support the hypothesis that subluxation occurs in FAI patients during the impingement and FABER exams as a result of contact to the labrum.

In skin marker motion analysis[13-16] and existing simulations of impingement,[17,20,28] the center of rotation (COR) is assumed to be fixed. However, using our technique, it was not necessary to assume a static COR when calculating joint angles. Given the magnitude of femoral head translations in normal subjects and patients observed in our study, it is possible that use of a static COR leads to erroneous measurements of hip joint angles and unrealistic visualization of hip joint articulation.

Except for one normal subject, internal rotation during the impingement exam was limited by contact between the femur and labrum. While contact was observed as overlap between the rigid femur and the rigid labrum (assumed to undergo the same motion of the pelvis), in reality the labrum would be compressed, stretched or pushed aside. Nonetheless, the region of overlap likely coincides with the region of labrum that would be strained. Our results corroborate those of a cadaver experiment, where strain in the anterosuperior labrum was significantly increased during the impingement exam compared to neutral.[30] In this study, maximum internal rotation in neutral flexion occurred without contact to the labrum, even in FAI patients, suggesting that other soft tissue restraints (i.e. capsular ligaments, surrounding musculature) may dictate the limits of this motion. For example, the ischiofemoral ligament has been reported to restrict internal rotation.[31,32]

During the impingement exam, contact generally occurred between the anterolateral femoral head-neck junction and anterosuperior labrum. Both the labral tear and cartilage delamination observed in Patients 1 and 2, respectively, occurred in the anterosuperior region. Indeed, this region has previously been reported to be a common location of chondrolabral damage observed in FAI patients.[33] On the femoral side, the morphology of the anterolateral femoral head and neck in contact with the labrum varied between patients. In patient 1, contact occurred in the middle of the cam deformity, possibly explaining the restricted motion observed in this patient. For patient 3, labral contact occurred directly within the pincer groove. While this finding is only for a single patient, it suggests that the groove may have formed during activities that incorporate similar motions to the impingement exam. In contrast, for patient 2, labrum contact occurred at the bony prominence immediately lateral to the pincer groove. For this patient, it is possible that the impingement exam did not replicate the same activities that were responsible for forming the pincer groove.

In this study, no direct bone-to-bone contact was observed. In fact, the minimum distance between the femoral neck and acetabular rim averaged three millimeters. Still, we choose to highlight the area of minimum bone to bone distance in the anterior femoral head and acetabulum as a means to compare that to the location of labrum contact in the same region. The minimum bone-to-bone distance only matched the location of contact with the labrum in approximately half of the subjects imaged (Figures 5.9 and 5.10). As such, we can confidently conclude that minimum bone-to-bone distance is not recommended as the only outcome measure to evaluate impingement. In fact, simulations that rely on direct bone-to-bone contact between the femur and acetabulum likely

overestimate range of motion and do not provide an accurate description of how the hip actually articulates in-vivo.

In this study, the pelvis was secured to the exam table to ensure that the hip joint remained in the field of view of both fluoroscopes. However, the pelvis moved during all clinical exams. As the hip was flexed during the impingement exam, the pelvis tilted posteriorly, while pelvic motion in the other planes remained relatively unchanged. It was not until the femoral head-neck junction made direct contact with the labrum that pelvic obliquity and rotation changed substantially. This observation provides evidence that the impingement exam indeed places the hip into terminal range of motion. In contrast, there was no contact between the labrum and femur during internal rotation in neutral flexion. Accordingly, pelvic motion was minimal in this particular terminal position (Figure 5.5).

Even with a limited sample size, significant correlations were observed between maximum external rotation and measures of cam morphology. Maximum internal rotation during the impingement exam (but not the rotational profile) was correlated to the alpha angle measured on the AP radiograph, but not the frog-leg lateral radiograph. This result was surprising as the morphology of the anterosuperior femoral head and neck, better visualized on lateral films,[34,35] has previously been correlated to internal rotation measured with a goniometer.[36,37] With nine subjects, a $p < 0.05$ can only occur with an $r > 0.67$, as the p value for simple linear regression is a direct function of r and the sample size.[38] Thus, it is possible that our correlations could change with a larger sample size. A larger sample size could be used to develop predictive models of impingement via multivariate regression. Such a model could be used to study the effects of femoral head and acetabular morphology, as well as extra-articular morphology such

as femoral version. However, multivariate analysis was not possible with nine subjects due to over-fitting (~10 subjects required per covariate).[39]

This study has limitations that warrant discussion. Only three FAI patients were included, prohibiting statistical comparisons between groups. The primary objective of this study was to establish a database of hip kinematics for normal subjects. Even with three patients, our study provides new information on how different presentations of FAI alter hip motion during clinical exams. Next, no specific radiographic cutoff values were employed to screen the normal subjects. Normal subjects were enrolled based on an absence of grossly abnormal deformities and osteoarthritic changes and no history of hip pain. As there is little consensus regarding which cutoffs should be used, we believe our selection criterion were reasonable. Finally, while the thickness of cartilage on the femur would certainly contribute the location of contact between the femur and labrum, cartilage was not included in this study. Cartilage is thin or nonexistent in the femoral neck region and therefore, it is expected that the region of contact would not change substantially by the inclusion of the cartilage.

In summary, our technique to measure hip motion provides the most accurate data collected on hip articulation to date. Data for the normal subjects provide the necessary baseline results for future studies, and the patient data show promise for using this technique to improve our understanding of FAI. Collectively, our results demonstrate that hip articulation is a highly complex process including translation, pelvic motion, no bone contact, and labrum involvement in large ranges of motion. Our data call into question the validity of prior simulations used to predict impingement that rely on the assumption of direct bone contact, a stationary pelvis, and a constant COR.[17-20] Data collected in this

study could validate computer simulations of impingement, guide pre-operative planning, and serve as boundary conditions in finite element models investigating labrum and cartilage mechanics.

5.6 Acknowledgements

I would like to thank my co-authors on this work, Stephen K. Aoki, Christopher L. Peters, and Andrew E. Anderson. I would also like to acknowledge Blake Zimmerman, Justine Goebel, and Mikey Kutschke for assistance with data processing. I also thank Steve Mass and David Rawlins for help with PreView and PostView.

5.7 References

1. Ganz R, Parvizi J, Beck M, et al. 2003. Femoroacetabular impingement: a cause for osteoarthritis of the hip. Clin Orthop Relat Res: 112-120.

2. Zebala LP, Schoenecker PL, Clohisy JC. 2007. Anterior femoroacetabular impingement: a diverse disease with evolving treatment options. Iowa Orthop J 27: 71-81.

3. Beck M, Kalhor M, Leunig M, et al. 2005. Hip morphology influences the pattern of damage to the acetabular cartilage: femoroacetabular impingement as a cause of early osteoarthritis of the hip. J Bone Joint Surg Br 87: 1012-1018.

4. Bedi A, Dolan M, Leunig M, et al. 2011. Static and dynamic mechanical causes of hip pain. Arthroscopy 27: 235-251.

5. Beaule PE, Hynes K, Parker G, et al. 2012. Can the alpha angle assessment of cam impingement predict acetabular cartilage delamination? Clin Orthop Relat Res 470: 3361-3367.

6. Beaule PE, O'Neill M, Rakhra K. 2009. Acetabular labral tears. J Bone Joint Surg Am 91: 701-710.

7. Pfirrmann CW, Mengiardi B, Dora C, et al. 2006. Cam and pincer femoroacetabular impingement: characteristic MR arthrographic findings in 50 patients. Radiology 240: 778-785.

8. Philippon M, Schenker M, Briggs K, et al. 2007. Femoroacetabular impingement in 45 professional athletes: associated pathologies and return to sport following arthroscopic decompression. Knee Surg Sports Traumatol Arthrosc 15: 908-914.

9. Philippon MJ, Maxwell RB, Johnston TL, et al. 2007. Clinical presentation of femoroacetabular impingement. Knee Surg Sports Traumatol Arthrosc 15: 1041-1047.

10. Audenaert E, Van Houcke J, Maes B, et al. 2012. Range of motion in femoroacetabular impingement. Acta Orthop Belg 78: 327-332.

11. Nussbaumer S, Leunig M, Glatthorn JF, et al. 2010. Validity and test-retest reliability of manual goniometers for measuring passive hip range of motion in femoroacetabular impingement patients. BMC Musculoskelet Disord 11: 194.

12. Chevillotte CJ, Ali MH, Trousdale RT, et al. 2009. Variability in hip range of motion on clinical examination. J Arthroplasty 24: 693-697.

13. Kennedy MJ, Lamontagne M, Beaule PE. 2009. Femoroacetabular impingement alters hip and pelvic biomechanics during gait Walking biomechanics of FAI. Gait & Posture 30: 41-44.

14. Rylander J, Shu B, Favre J, et al. 2013. Functional testing provides unique insights into the pathomechanics of femoroacetabular impingement and an objective basis for evaluating treatment outcome. J Orthop Res 31: 1461-1468.

15. Hunt MA, Gunether JR, Gilbart MK. 2013. Kinematic and kinetic differences during walking in patients with and without symptomatic femoroacetabular impingement. Clin Biomech 28: 519-523.

16. Lamontagne M, Kennedy MJ, Beaule PE. 2009. The effect of cam FAI on hip and pelvic motion during maximum squat. Clin Orthop Relat Res 467: 645-650.

17. Chang TC, Kang H, Arata L, et al. 2011. A pre-operative approach of range of motion simulation and verification for femoroacetabular impingement. Int J Med Robot 7: 318–326.

18. Audenaert EA, Mahieu P, Pattyn C. 2011. Three-dimensional assessment of cam engagement in femoroacetabular impingement. Arthroscopy 27: 167-171.

19. Bedi A, Dolan M, Magennis E, et al. 2012. Computer-assisted modeling of osseous impingement and resection in femoroacetabular impingement. Arthroscopy 28: 204-210.

20. Tannast M, Kubiak-Langer M, Langlotz F, et al. 2007. Noninvasive three-dimensional assessment of femoroacetabular impingement. J Orthop Res 25: 122-131.

21. Harris MD, Anderson AE, Henak CR, et al. 2012. Finite element prediction of cartilage contact stresses in normal human hips. J Orthop Res 30: 1133-1139.

22. Bey MJ, Zauel R, Brock SK, et al. 2006. Validation of a new model-based tracking technique for measuring three-dimensional, in vivo glenohumeral joint kinematics. J Biomech Eng 128: 604-609.

23. Wu G, Siegler S, Allard P, et al. 2002. ISB recommendation on definitions of joint coordinate system of various joints for the reporting of human joint motion--part I: ankle, hip, and spine. International Society of Biomechanics. J Biomech 35: 543-548.

24. Mass S, Rawlins D, Weiss JA. "PostView" Finite Element Post-Processing. http://www.febio.org/postview. Accessed July 25, 2013.

25. Mass S, Rawlins D, Weiss JA. "PreView" Finite Element Pre-Processing. http://www.febio.org/preview. Accessed July 25, 2013.

26. Grood ES, Suntay WJ. 1983. A joint coordinate system for the clinical description of three-dimensional motions: application to the knee. J Biomech Eng 105: 136-144.

27. Harris MD, Reese SP, Peters CL, et al. 2013. Three-dimensional Quantification of Femoral Head Shape in Controls and Patients with Cam-type Femoroacetabular Impingement. Ann Biomed Eng 41: 1162-1171.

28. Audenaert EA, Peeters I, Vigneron L, et al. 2012. Hip morphological characteristics and range of internal rotation in femoroacetabular impingement. Am J Sports Med 40: 1329-1336.

29. Bedi A, Thompson M, Uliana C, et al. 2013. Assessment of range of motion and contact zones with commonly performed physical exam manoeuvers for femoroacetabular impingement (FAI): what do these tests mean? Hip Int [Epub ahead of print].

30. Safran MR, Giordano G, Lindsey DP, et al. 2011. Strains across the acetabular labrum during hip motion: a cadaveric model. Am J Sports Med 39 Suppl: 92S-102S.

31. Martin HD, Savage A, Braly BA, et al. 2008. The function of the hip capsular ligaments: a quantitative report. Arthroscopy 24: 188-195.

32. Fuss FK, Bacher A. 1991. New aspects of the morphology and function of the human hip joint ligaments. Am J Anat 192: 1-13.

33. Tannast M, Goricki D, Beck M, et al. 2008. Hip damage occurs at the zone of femoroacetabular impingement. Clin Orthop Relat Res 466: 273-280.

34. Clohisy JC, Nunley RM, Otto RJ, et al. 2007. The frog-leg lateral radiograph accurately visualized hip cam impingement abnormalities. Clin Orthop Relat Res 462: 115-121.

35. Barton C, Salineros MJ, Rakhra KS, et al. 2011. Validity of the alpha angle measurement on plain radiographs in the evaluation of cam-type femoroacetabular impingement. Clin Orthop Relat Res 469: 464-469.

36. Kapron AL, Anderson AE, Peters CL, et al. 2012. Hip internal rotation is correlated to radiographic findings of cam femoroacetabular impingement in collegiate football players. Arthroscopy 28: 1661-1670.

37. Johnston TL, Schenker ML, Briggs KK, et al. 2008. Relationship between offset angle alpha and hip chondral injury in femoroacetabular impingement. Arthroscopy 24: 669-675.

38. Rosner B. 1995. Fundamentals of Biostatistics, 4th ed. Belmont, CA: Duxbury Press; 868 p.

39. Harrel Jr. F. 2001. Regression Modeling Strategies With Applications to Linear Models, Logistic Regression, and Survival Analysis. New York: Springer; 571 p.

Table 5.1

Joint Angles of Normal Subjects and FAI Patients at the Terminal Position of Each Exam

Exam	Angle	Normal	Patient 1	Patient 2	Patient 3
Impingement Exam	Flexion (+)	93.0 ± 6.4	94.7	107.0	97.1
	Adduction (+)	10.5 ± 3.7	5.7	2.2	3.2
	Internal Rotation (+)	19.1 ± 4.4	11.6	7.8	9.7
Internal Rotation	Flexion (+)	14.0 ± 8.4	22.1	17.4	18.2
	Adduction (+)	2.0 ± 3.3	5.1	4.2	-2.2
	Internal Rotation (+)	34.7 ± 6.4	38.3	13.4	38.4
External Rotation	Flexion (+)	14.4 ± 10.2	18.2	19.2	16.3
	Adduction (+)	-7.2 ± 2.3	-10.2	-3.1	-7.0
	Internal Rotation (+)	-36.4 ± 8.2	-27.6	-7.9	-29.4
FABER Test	Flexion (+)	38.6 ± 8.5	48.1	74.5	58.0
	Adduction (+)	-36.6 ± 4.0	-34.7	-26.7	-27.3
	Internal Rotation (+)	-48.3 ± 7.4	-36.5	-23.2	-41.6

All values in degrees.

Table 5.2

Repeatability of the Clinical Exams: Difference in Joint Angles

at the Terminal Exam Position between the Two Trials

Exam	Flexion/Extension	Abduction/Adduction	Internal/External Rotation
Impingement Exam	2.2 ± 2.2°	2.0 ± 1.6°	2.4 ± 1.7°
Internal Rotation	1.6 ± 1.6°	1.4 ± 1.5°	0.6 ± 0.48°
External Rotation	1.4 ± 1.7°	1.0 ± 0.89°	1.3 ± 0.85°
FABER	3.9 ± 1.9°	3.2 ± 3.8°	0.96 ± 1.1°

Table 5.3

Correlation between Maximum Hip Rotation during Clinical Exams

and Radiographic Measures of Femoroacetabular Impingement

Independent Variable	Dependent Variable	Regression Coefficient (Slope)	Correlation Coefficient (r)	Significance (p)
Frog-leg Lateral Alpha Angle	IR (Impingement)	-0.226	-0.45	0.224
	IR (Rotational Profile)	-0.412	-0.53	0.139
	ER (Rotational Profile)	-0.689	-0.71	0.033*
	ER (FABER)	-0.718	-0.81	0.008*
Anteroposterior Alpha Angle	IR (Impingement)	-0.256	-0.75	0.019*
	IR (Rotational Profile)	-0.228	-0.44	0.239
	ER (Rotational Profile)	-0.451	-0.69	0.041*
	ER (FABER)	-0.407	-0.68	0.044*
Lateral Center Edge Angle	IR (Impingement)	-0.299	-0.42	0.262
	IR (Rotational Profile)	-0.185	-0.17	0.665
	ER (Rotational Profile)	-0.232	-0.17	0.667
	ER (FABER)	0.033	0.03	0.947

IR = Internal Rotation, ER = External Rotation, * denotes significance at $p < 0.05$

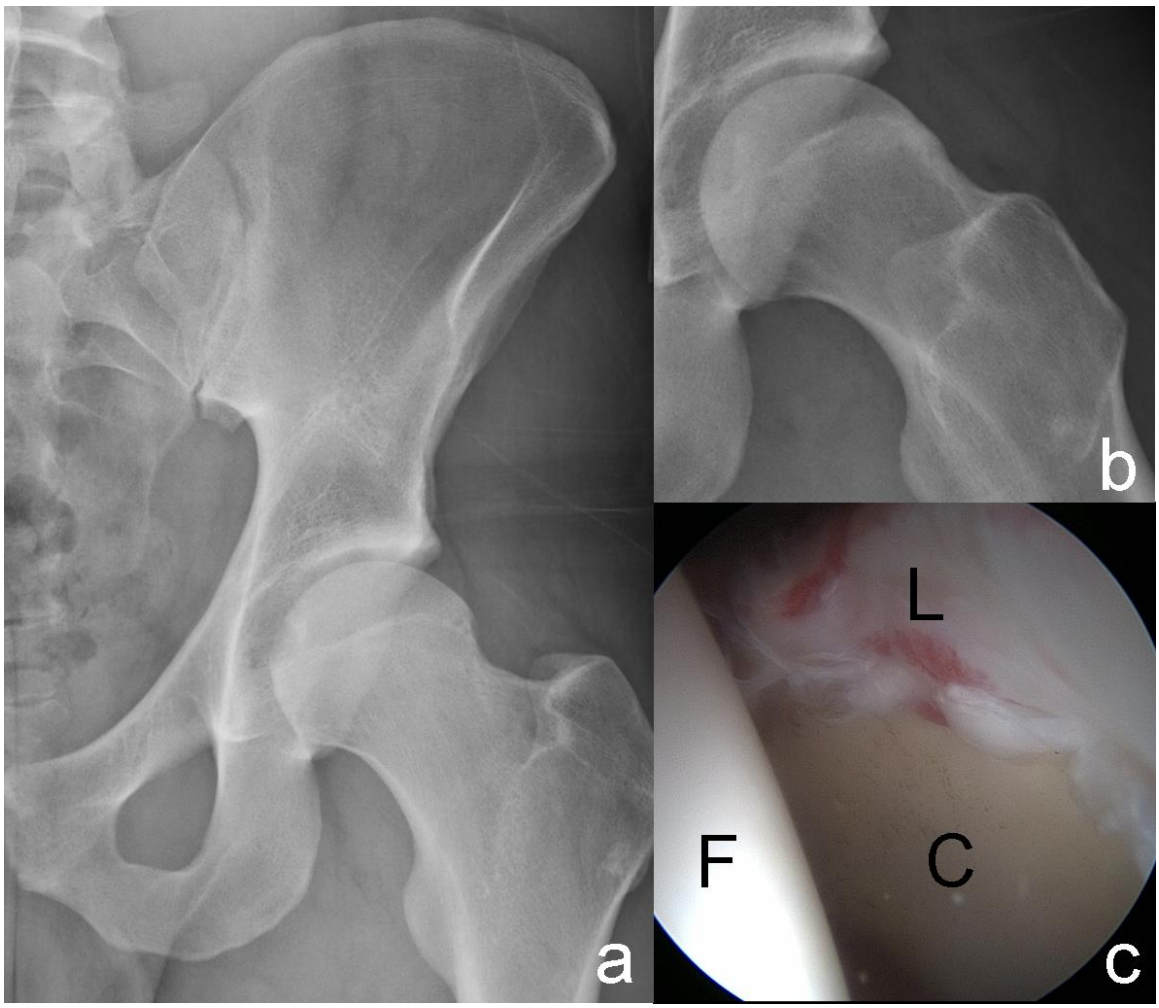

Figure 5.1. Radiographic and intraoperative imaging of the left hip of Patient 1. a) Anteroposterior radiograph showing a slightly shallow acetabulum and low-hanging AIIS. b) Frog-leg lateral radiograph highlighting decreased offset between the femoral head and neck. c) Arthroscopic view through the anterolateral portal (70 degree scope) showing a labral tear and bruising at the anterosuperior chondrolabral junction. F=Femoral head, L=Labral tear and bruising (red), C=Acetabular Cartilage.

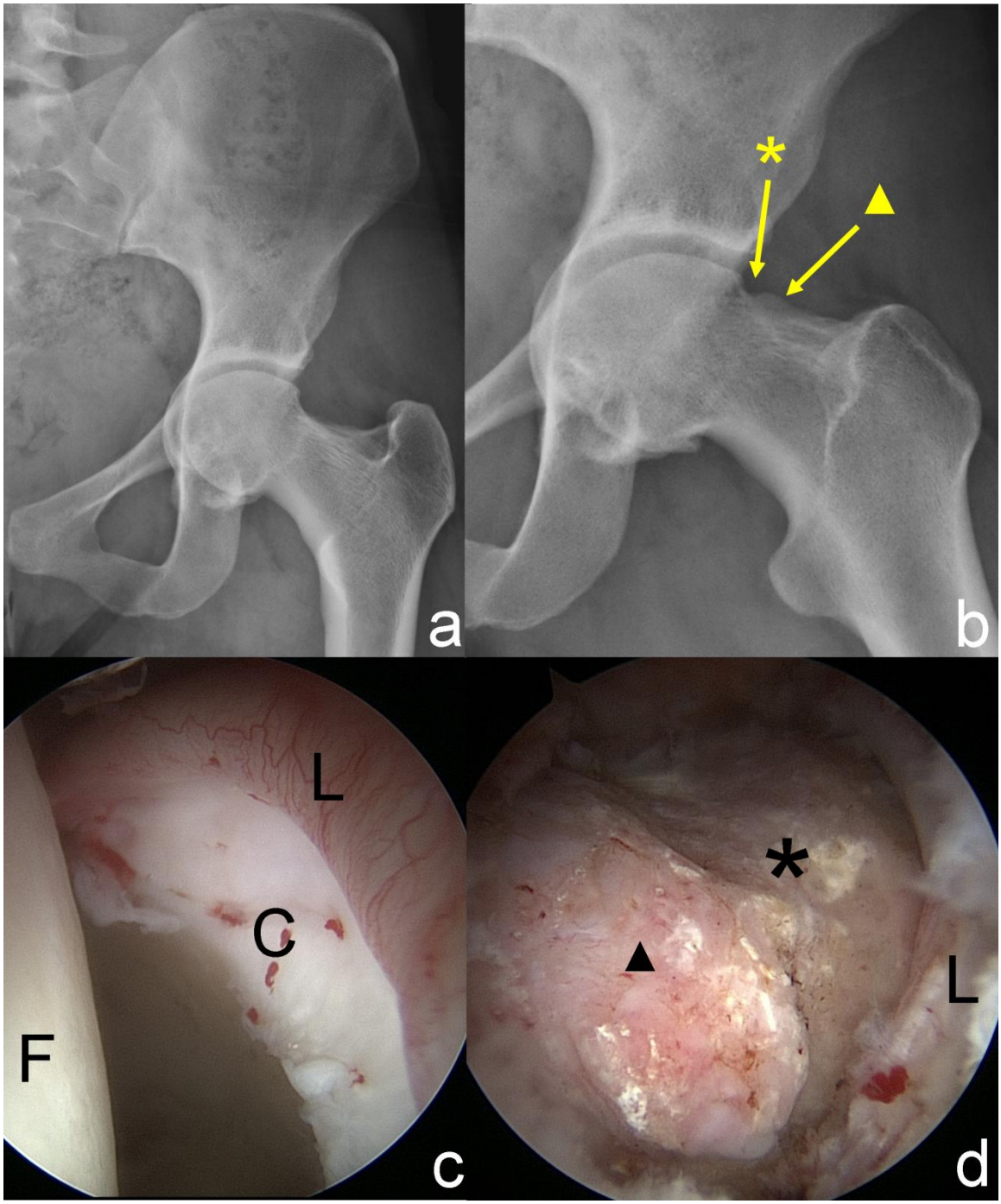

Figure 5.2 Radiographic and intraoperative imaging of the left hip of Patient 2. a) Anteroposterior radiograph showing protrusio. b) Frog-leg lateral radiograph showing pincer groove (*) and femoral neck prominence (▲). c) Arthroscopic view through the anterolateral portal (70 degree scope) of anterosuperior chondrolabral junction showing cartilage delamination. L=Labrum, F=Femoral Head, C=Cartilage Delamination d) Arthroscopic view of bony anatomy after soft tissue removal demonstrating large pincer groove and bony prominence on anterolateral femoral neck.

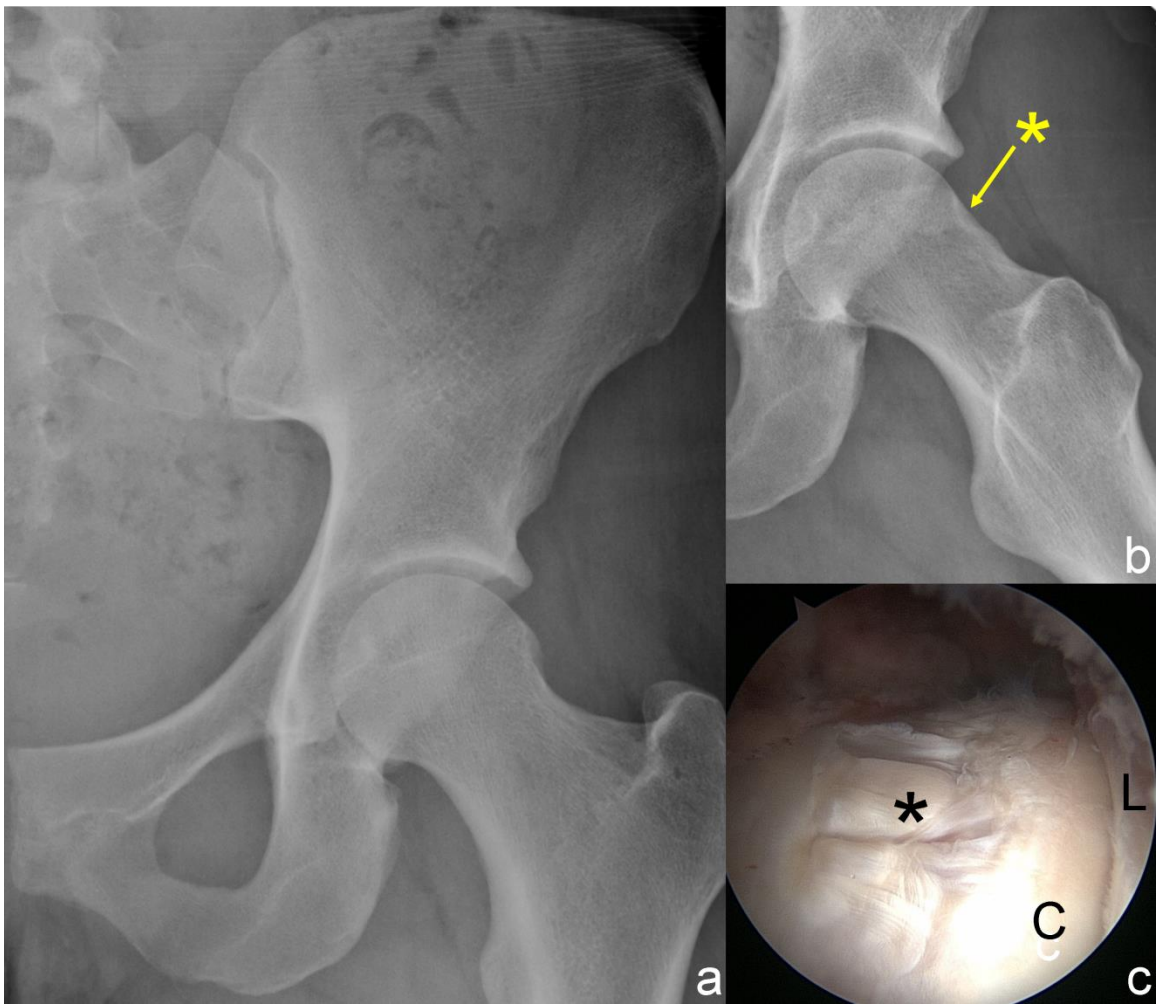

Figure 5.3. Radiographic and intraoperative imaging of the left hip of Patient 3. a) Anteroposterior radiograph showing acetabular overcoverage b) Frog-leg lateral radiograph showing pincer groove (*). c) Arthroscopic view through the anterolateral portal (70 degree scope) of mechanical wear at the location of the pincer groove on the anterolateral femoral neck. L= Labrum, C= Femoral Cartilage.

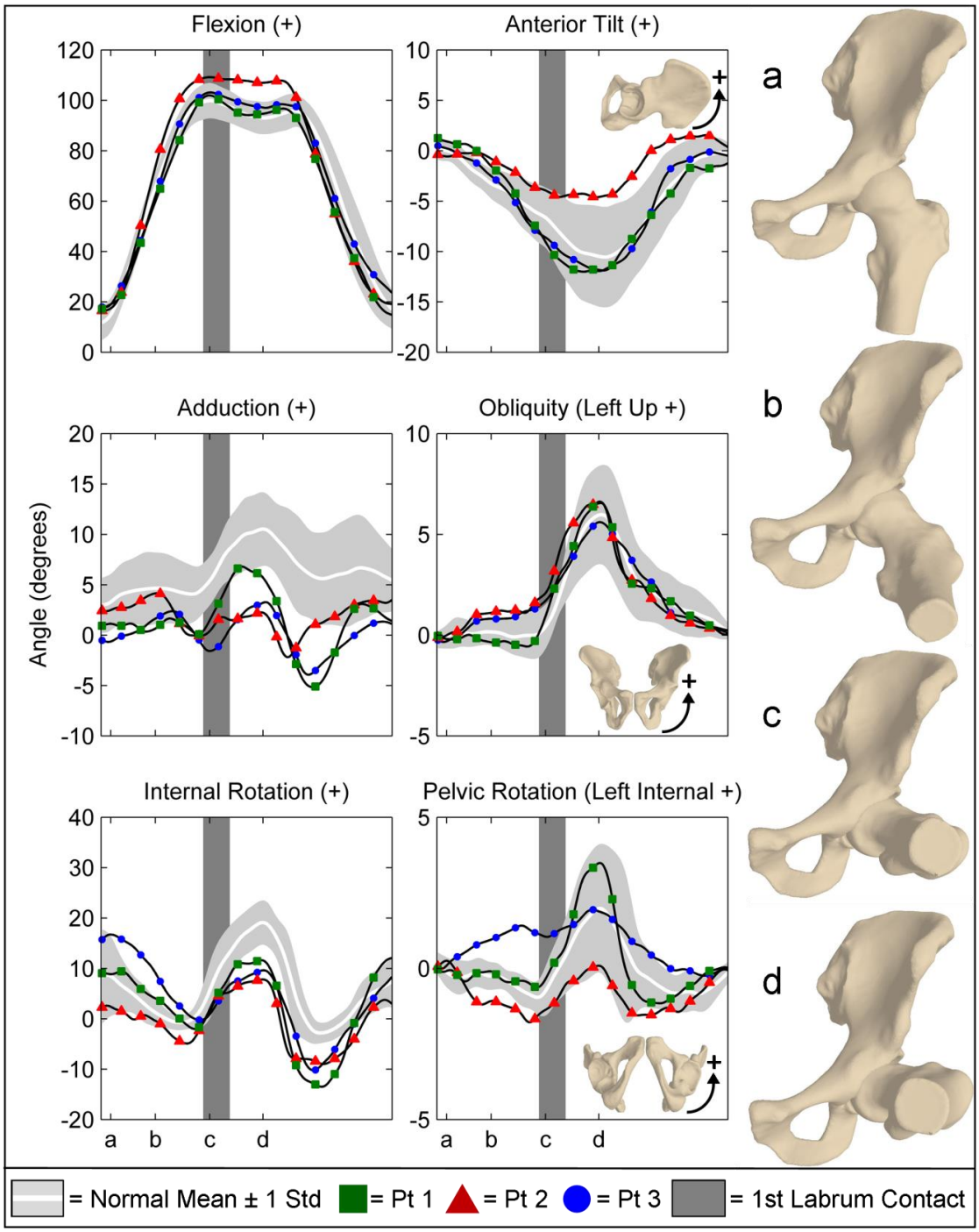

Figure 5.4. Joint angles (left column) and pelvic angles (middle column) of normal subjects and FAI patients during the impingement exam. Angles presented as mean ± one standard deviation for normal subjects. Vertical grey bar represents frame of initial contact between labrum and femoral head or neck, average ± 1 standard deviation for all subjects. Right column: schematic of normal subject at time points of interest: a) neutral; start of the exam, b) approximate midpoint of flexion, c) maximum flexion, d) maximum internal rotation in flexion (terminal position).

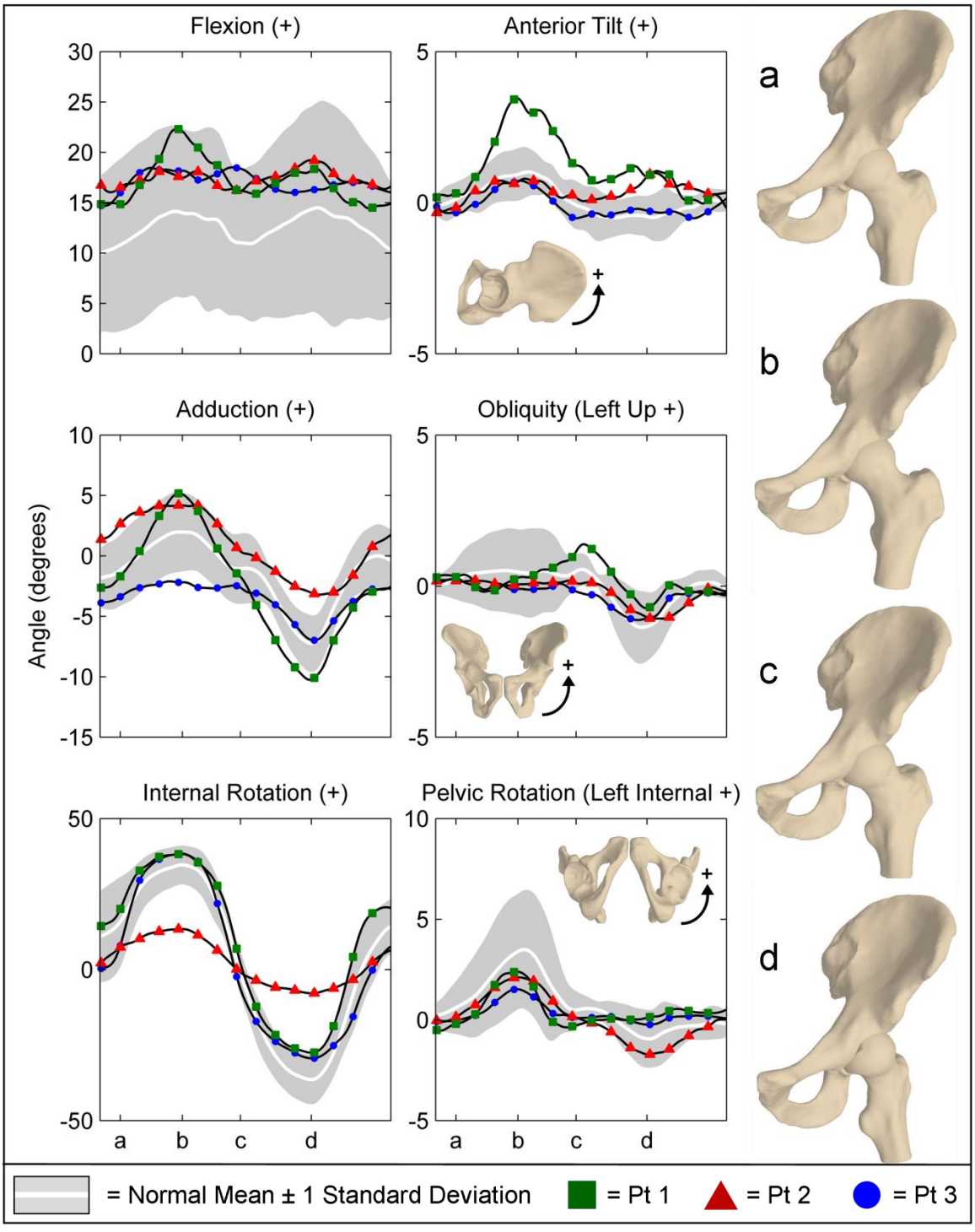

Figure 5.5. Joint angles (left column) and pelvic angles (middle column) of normal subjects and FAI patients during the rotational profile. Angles presented as mean ± one standard deviation for normal subjects. Right column: schematic of normal subject at time points of interest: a) neutral; start of the exam, b) maximum internal rotation (terminal position), c) neutral, d) maximum external rotation (terminal position).

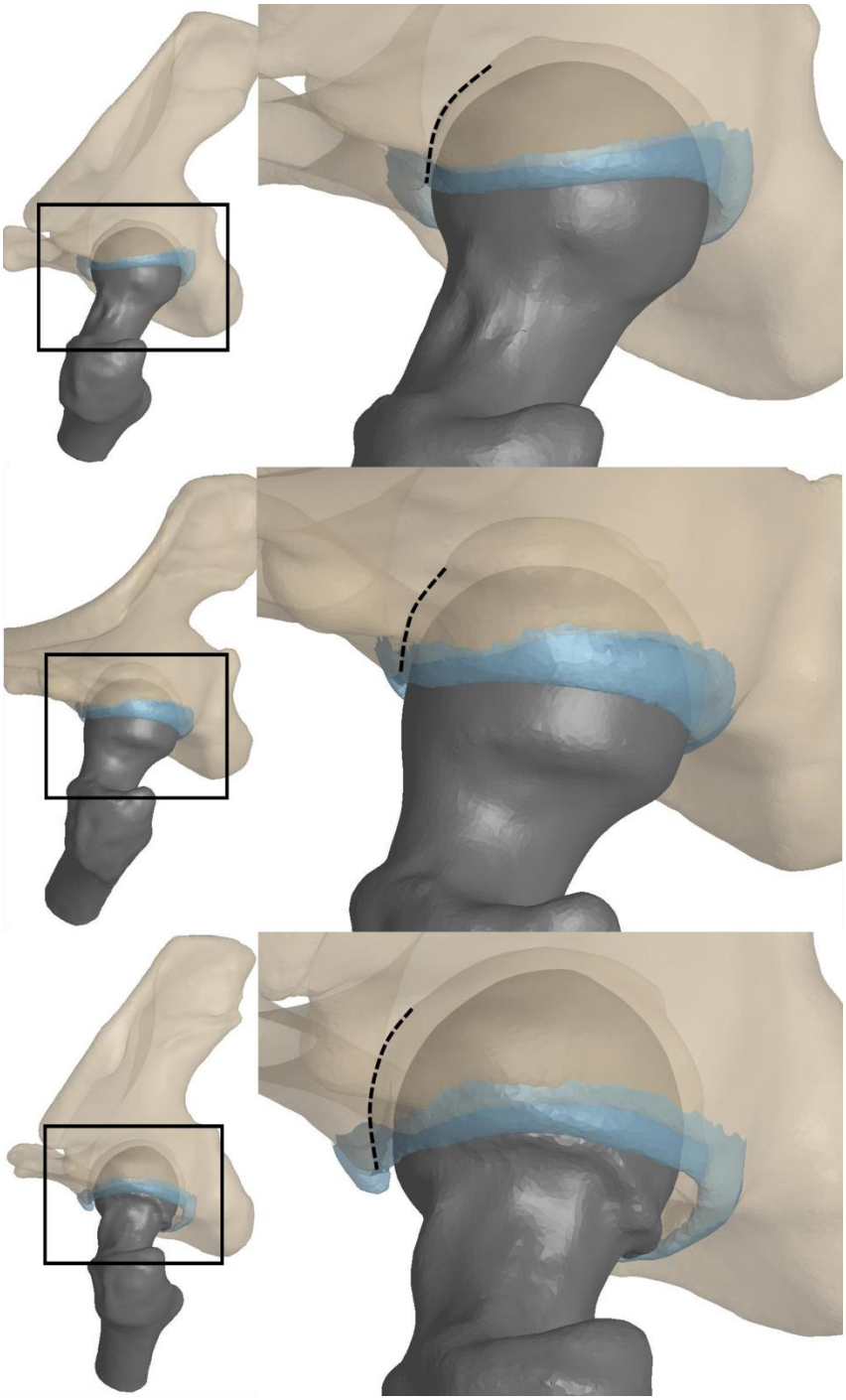

Figure 5.6. Maximum internal rotation in neutral flexion did not appear to be limited by contact to bone or the labrum. Similar internal rotation, without contact was achieved by normal male subject (top, 37.7°) and Patient 1 with cam FAI (middle, 38.3°). Even Patient 2, with severe restriction in internal rotation (bottom, 13.4°) was not limited by contact between bone or the labrum.

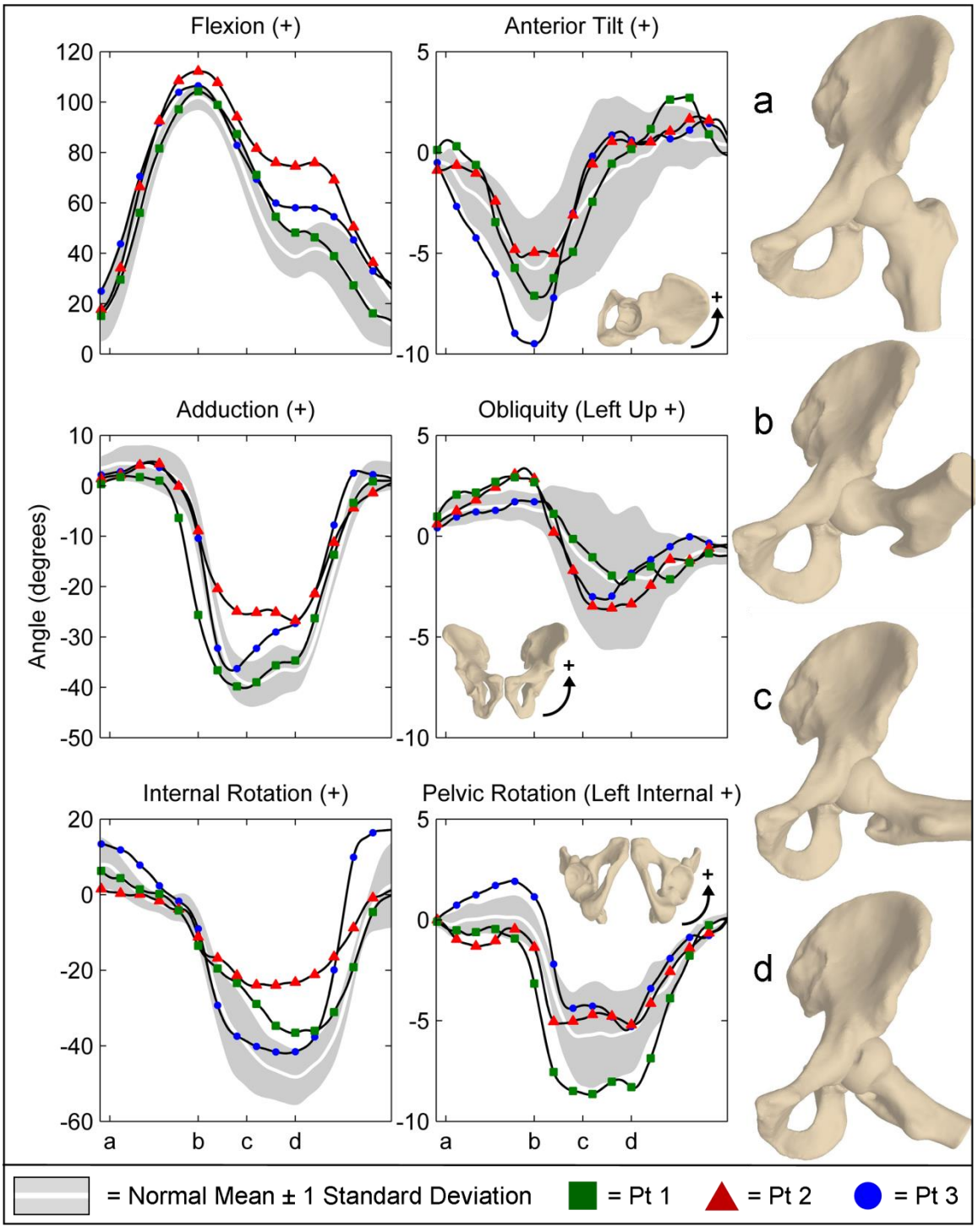

Figure 5.7. Joint angles (left column) and pelvic angles (middle column) of normal subjects and FAI patients during the FABER test. Angles presented as mean ± one standard deviation for normal subjects. Right column: schematic of normal subject at time points of interest: a) neutral (start of the exam), b) maximum flexion, c) approximate maximum adduction, d) terminal figure-four position.

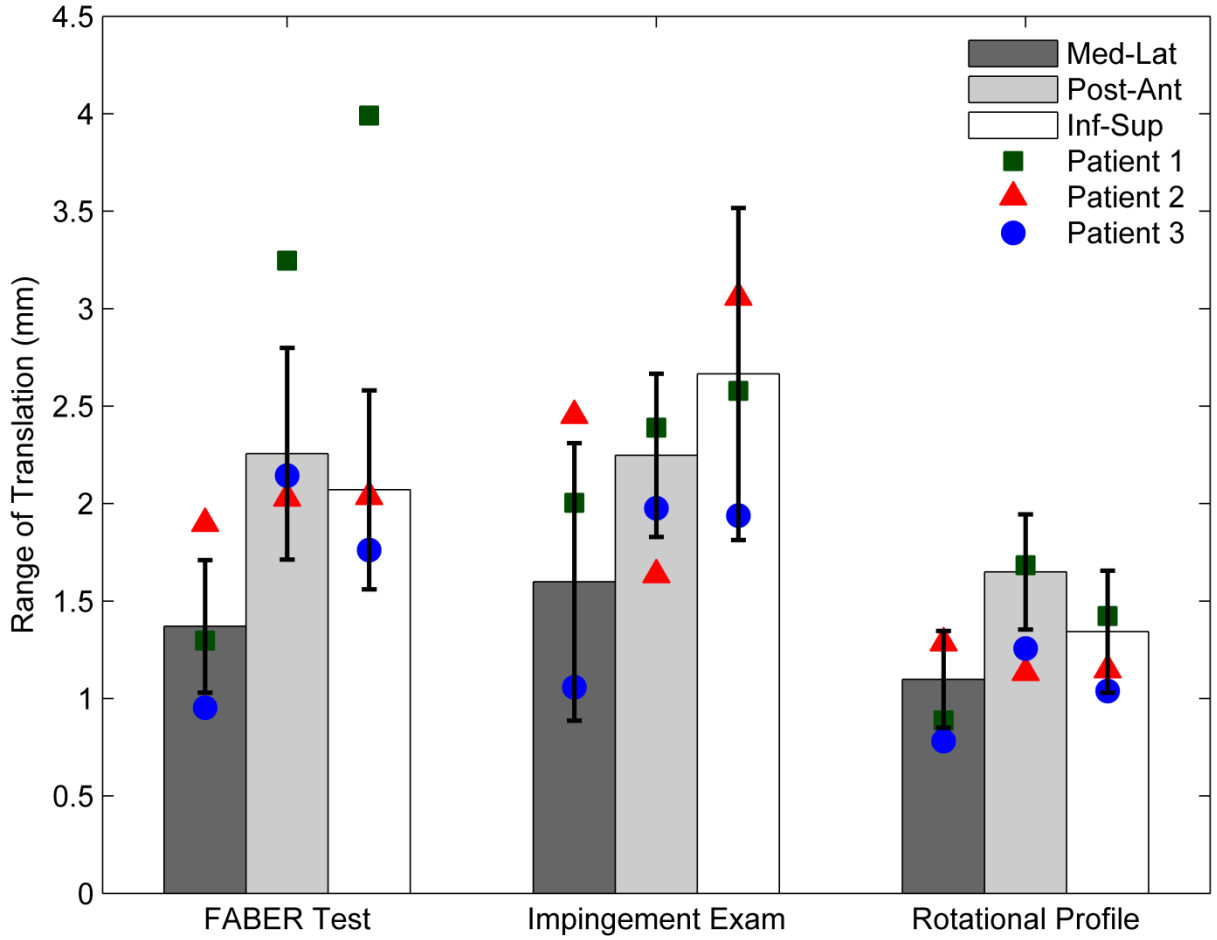

Figure 5.8. Range of femoral head translation in the three anatomical directions for each clinical exam. Bars represent mean plus and minus one standard deviation for normal subjects. Patient results plotted individually. Med-Lat: Medial-Lateral. Post-Ant=Posterior-Anterior. Inf-Sup=Inferior-Superior.

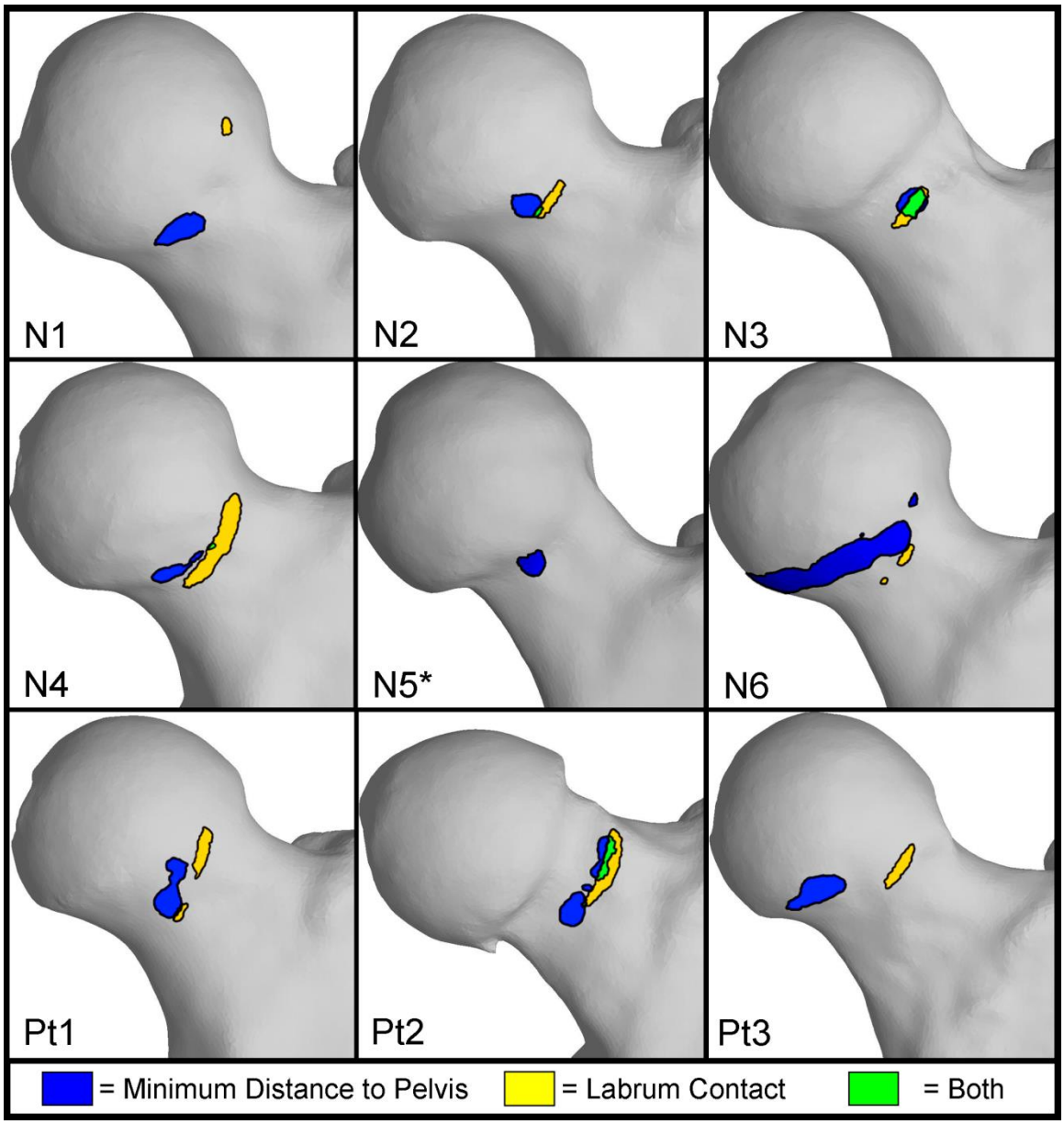

Figure 5.9. Location of minimum bone-to-bone distance and labral contact at the terminal position of the impingement exam (maximum internal rotation in flexion), displayed on the femur. The region of minimum bone-to-bone distance represents the region of the anterosuperior femoral head and neck closest to the acetabular rim. The region of labrum contact was defined as the region of overlap between the anterior/superior femoral head or neck and rigid labrum surface. Top and middle rows: normal subjects. Bottom row: Patients 1-3. *Note: No contact between the labrum and anterosuperior femoral head or neck was detected for normal subject 5.

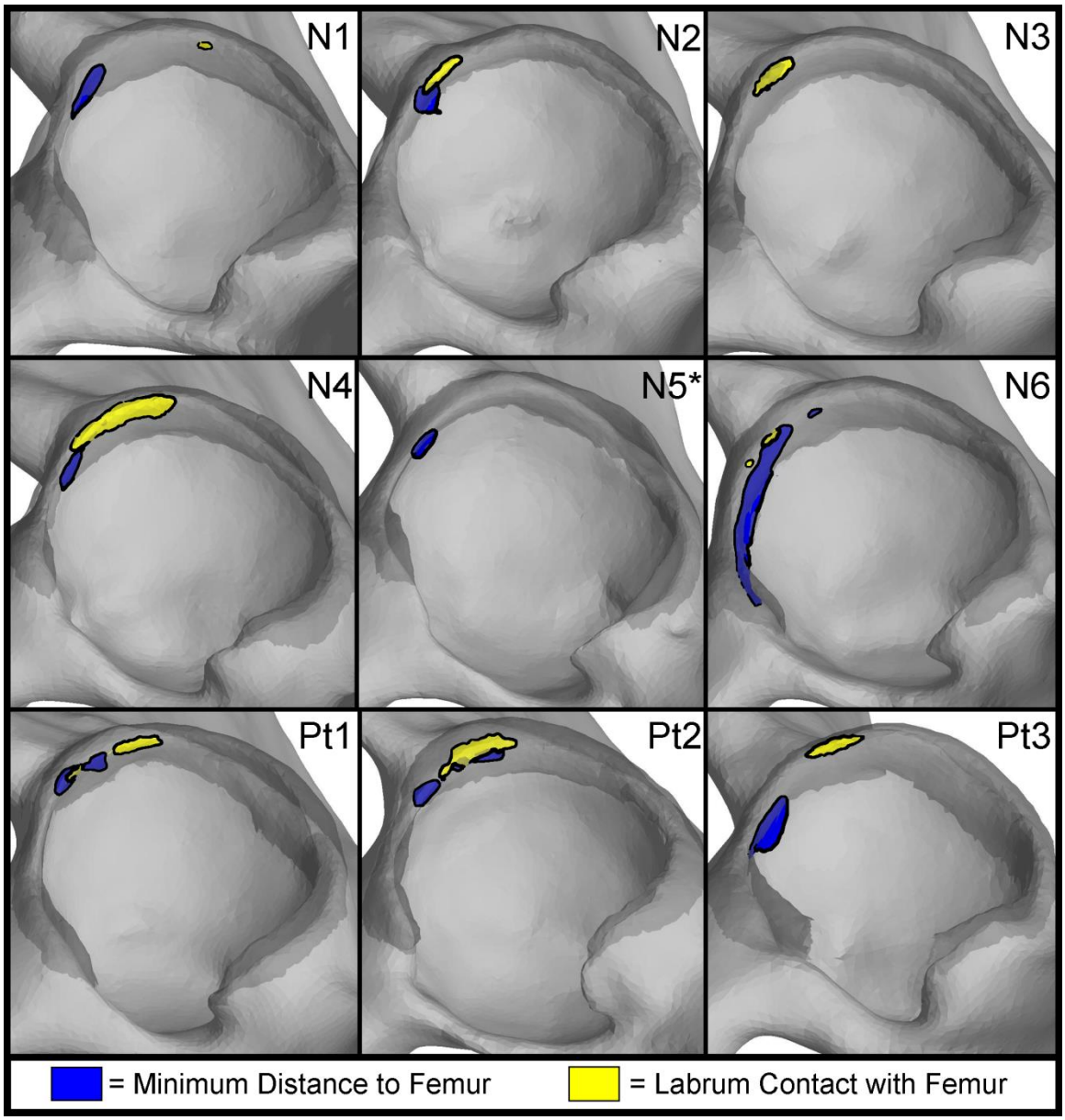

Figure 5.10 Location of minimum bone-to-bone distance and labral contact at the terminal position of the impingement exam (maximum internal rotation in flexion), displayed on the pelvis and labrum. The region of minimum bone-to-bone distance represents the region of the acetabular rim closest to the anterior/superior femoral head or neck. The region of labrum contact was defined as the region of overlap between the anterosuperior femoral head or neck and rigid labrum surface. Top and middle rows: normal subjects. Bottom row: Patients 1-3. *Note: No contact between the labrum and anterosuperior femoral head or neck was detected for normal subject 5. For normal subject 3, the location of labral contact was directly above the region of minimum bone-to-bone distance.

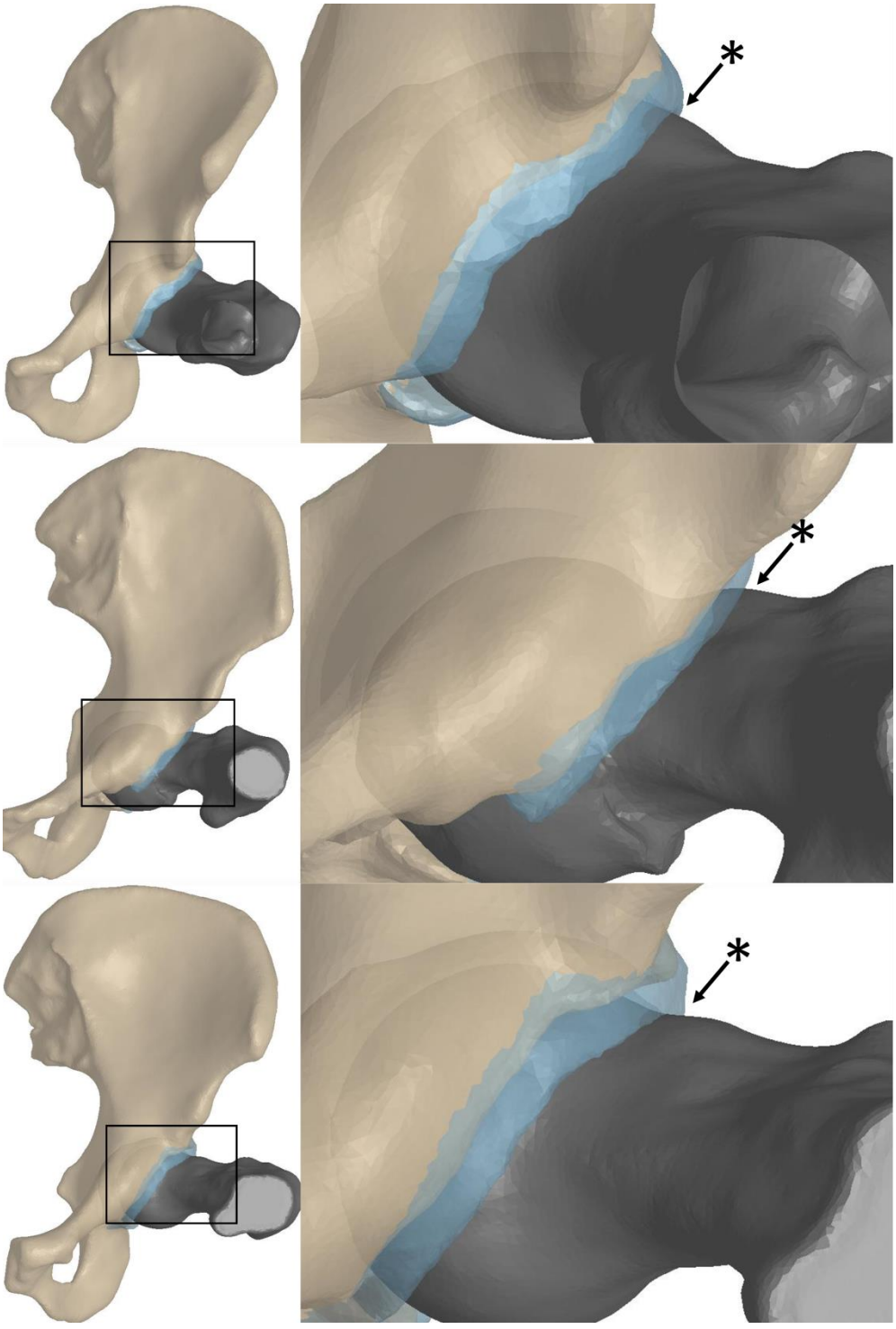

Figure 5.11. Position of the pelvis, femur, and labrum for the patients at the terminal position of the impingement exam, maximum internal rotation in flexion (left column). Black box highlights enlarged region shown in right column. Contact between femur and labrum (*) occurs on cam lesion (patient 1, top row), on bony prominence (patient 2, middle row), and on pincer groove (patient 3, Bottom row).

CHAPTER 6

CONCLUSIONS AND FUTURE DIRECTIONS

6.1 Summary

This dissertation applied clinical and basic science methodology to improve our understanding of femoroacetabular impingement. The research presented in Chapter 2 elucidated the association between athleticism and FAI. More specifically, it investigated the hypothesis that, compared to the incidence in the general population, athletes are at higher risk for symptomatic FAI because of an increased incidence of underlying structural deformities. Indeed, using current radiographic parameters and associated cutoff values, 95% of the male football players evaluated in the study had at least one abnormality consistent with those seen in FAI patients. Thus, it is likely that some of the players with radiographic findings of FAI will develop symptomatic FAI. In fact, at the time of the study, one subject reported limitations in activities of daily living and sports due to his hips, as quantified by the Hip Outcome Score. Nevertheless, it is unlikely that all or even the majority of players with radiographic FAI in this study will develop hip pain, chondrolabral damage, and/or early onset osteoarthritis. As such, this study highlights the fact that the current radiographic cutoff criterion may be too liberal to diagnose FAI.

The same football players were evaluated in Chapter 3 to determine if physical exams could be used to screen for radiographic FAI deformities in an asymptomatic population. The impingement exam, which has a high sensitivity in symptomatic FAI patients, was positive in only three of the 67 players. Regression analysis was completed between radiographic measures of FAI and range of motion (measured using a goniometer) to identify possible relationships between form and function. It was found that supine and sitting internal rotation was significantly but only mildly correlated to the degree of cam-type morphology, quantified by the alpha angle and head-neck offset. As such, it is possible that anatomy is not strongly associated with range of motion, especially in asymptomatic subjects with radiographic signs of FAI. However, goniometers have obvious limitations in their ability to accurately measure range of motion. Thus, a more accurate methodology to quantify hip range of motion could identify stronger correlations between anatomy and range of motion.

The need to implement a more accurate methodology to measure hip range of motion motivated the body of work performed in Chapter 4: validation of dual fluoroscopy and model-based tracking of the hip joint during supine clinical exams. In this chapter, model-based tracking results were compared to a reference standard (dynamic radiostereometric analysis) using two cadavers as a means to quantify the bias and precision of outcome measures derived from this technique. The bias of joint angles and joint translations were less than 0.58° and 0.48 mm, respectively, using dual fluoroscopy and model-based tracking. The average RMS error of bone-to-bone distance measurements was 0.52 mm. Chapter 4 also demonstrated the feasibility of using dual fluoroscopy and model-based tracking on live subjects. Specifically, one subject, with

normal hip geometry and no history of hip pain was imaged. Overall, the work completed for this chapter established the foundation not only for future comparisons between FAI patients and normal controls, as implemented in Chapter 5, but also other applications of dual fluoroscopy and model-based tracking.

In Chapter 5, the dual fluoroscopy and model-based tracking methodology validated in Chapter 4 was applied to study the hip kinematics of asymptomatic subjects with normal hip morphology and three FAI patients. The study represents the first application of dual fluoroscopy to evaluate hip articulation in a cohort of live subjects. This chapter established the baseline joint angles, translations, and bone-to-bone distances during clinical exams for a normal population. The patient results were compared to the normal results to identify range of motion limitations and understand how hip joint articulation differs in pathologic hips. The chapter demonstrated that hip joint articulation is a complex process, not only in FAI patients. In all subjects, the pelvis moved, the femur translated relative to the pelvis, and there was no contact between bone surfaces. Contact between the labrum and femoral head or neck was observed during the impingement exam and the location of contact was similar to the region of minimum distance between bone surfaces in half the cases. Results presented in this chapter can be used for future comparisons to additional patients with FAI or other hip pathologies.

6.2 FAI and Athletes: Recent Developments, Conclusions and Future Directions

Chapter 2 was the first report of FAI morphology in a cohort of asymptomatic athletes following modern radiographic parameters. Of the 67 collegiate football players

(134 hips) evaluated in the study, 78% had at least one finding of cam FAI and 66% had at least one finding of pincer FAI. In the discussion, it was noted that this prevalence was much higher than that reported in previous studies of asymptomatic members of the general population, suggesting that athleticism increases the risk of these deformities. While athleticism certainly is one explanation for the increased incidence of FAI in football players, these subjects do have additional possible risk factors for FAI, including male gender and an increased BMI. Further, football is arguably one of the most intense sports in terms of impact and loading. It is not possible, with this cohort alone, to differentiate the possible contributions of each risk factor. The results of the study must therefore be extended with caution to female athletes, male athletes from lower impact sports (swimming/cycling), or male athletes with smaller BMI (basketball, soccer).

Since the publication of the work in 2011 in *The Journal of Bone and Joint Surgery*, additional research has been completed by other groups investigating the relationship between athletic activity and FAI. The majority of these studies have focused on cam FAI, evaluating other sports including hockey, soccer, basketball, and skiing (Table 6.1).[1-8] Direct comparisons between studies are difficult due to varying imaging modalities (i.e. MRI vs. radiograph) and cutoff values (i.e., alpha angle cutoffs 50 to 60 degrees). This will continue to be a problem until diagnostic criterion are standardized and accepted by all. Nonetheless, comparing prevalence and mean alpha angles, male soccer and hockey player appear to have a greater prevalence of cam FAI deformities than the football players evaluated herein (Table 6.1).

Four of these athlete prevalence studies have included a control group of age-matched nonathletes for comparison (Table 6.2).[2,4,7,8] For the most part, athletes had a

higher prevalence of cam morphology than their nonathlete counterparts, supporting the relationship between athleticism and FAI. However, Johnson *et al*. reported no significant difference in alpha angle measured on frog-lateral radiographs in young adults who played high level soccer during adolescence and age-matched nonathletes.[4] In this study, the distinction between the athlete and control groups may not have been stringent enough. Specifically, the athlete group was comprised of individuals currently involved in "high-level soccer" (including high-level recreational), who participated in youth soccer at least three times a week, 36 weeks per year. The control group was limited to individuals who participated in youth sports (including soccer) less than two times week and less than 26 weeks a year. The difference between sports involvement two or three times a week during development may be insufficient in terms of its impact on the development of cam deformities.

To investigate when cam deformities may develop, Siebenrock *et al*. evaluated 37 male basketball players aged 9-25 from an elite club and 38 age matched nonathletes.[7] The distinction between athletes and nonathletes in this study was more stringent, with the athletes participating in 3-8 training sessions or games per week since the age of 8, and the controls' past or present athletic involvement limited to 2 hours a week. Alpha angles, measured in the anterosuperior quadrant of the femur on MR images, were significantly higher in the athletic group than the controls ($61 \pm 9.1°$ vs. $47 \pm 4.3°$, $p = 0.001$). The two subject groups were then subdivided based on an open or closed physis. Interesting, the athletes with a closed physis had a significantly higher alpha angle than the athletes with an open physis, but there was no significant difference between the control subgroups. A similar methodology was applied in a second study of 77 elite-level

hockey players, with comparable results (open physis alpha angle 58° vs closed physis 49°, p < 0 .001).[6] These studies support the hypothesis that FAI deformities may develop during adolescence due to increased or altered loading associated with athletic activity. However, they did not compare the anatomy of the same individuals before and after phyeal closure. A longitudinal study following children through adolescence could lend more specific insights into when cam-like deformities develop and to what degree sports activity influences the process.

There are relatively few studies that have quantified and compared prevalence of FAI in female athletes. Two studies on soccer players have reported prevalence by gender, with females demonstrating decreased alpha angles compared to their male counterparts (Table 6.1).[3,4] Of these two studies, only one compared the alpha angles of the athletes to nonathlete control females.[4] They found no significant difference between groups, but this was the same study discussed above that may not have had stringent enough distinctions between the athlete and control groups. Accordingly, there is a need for additional prevalence studies on females. The authors of Chapters 2 are currently applying the methodology presented in this chapter to study female collegiate athletes from volleyball, soccer, and track and field.

Pincer FAI has also been overlooked in the prevalence studies. Besides the work presented in Chapter 2, only one study has investigated pincer FAI. In this recent study, only the crossover sign was used to diagnose pincer FAI. They found a positive crossover sign in 27% of male and 10% of female soccer players and prevalence studies.[3] Unfortunately, the crossover sign is not the only indicator of pincer FAI. Specifically, the crossover sign is used to diagnose acetabular retroversion, which is considered only a

subtype of pincer FAI. Also, the ability to diagnose a crossover sign is highly subject to pelvic tilt; even in well-positioned radiographs, the crossover sign has been shown to overestimate the presence of pincer FAI due to acetabular retroversion.[9,10] Further, as the crossover sign only is a binary outcome, it may miss global overcoverage. Acetabular overcoverage, which is the general definition of pincer FAI, could be quantified with other measures such as the center edge angle. Therefore, use of the crossover sign alone may not provide a reliable estimate of the prevalence of pincer FAI. It is possible that there are not a large number of reports on pincer FAI because the incidence is too low. Overall, if radiographic or 3D data are collected in athletic populations, attempts should be made to use the available measures of pincer FAI to quantify the prevalence of this subtype of FAI, even if the incidence is low.

Ultimately, while prevalence studies provide better insights into which groups are more at risk for underlying FAI deformities, they do not answer the question of who is at risk for developing symptomatic FAI. A prospective, longitudinal study following athletes and controls over decades of life that encompass prepubescent, puberty, and adulthood is needed to fully understand who is at risk for development of symptomatic FAI. Such data could then be used to redefine morphologic criterion to make them more sensitive and specific for delineating normal from abnormal. Another approach to quantify morphologic criterion could be to use statistical shape modeling to objectively quantify three-dimensional differences in morphology between populations. Shape data could then relate the modes of variation to clinical images as a means to objectively define diagnostic criterion for each radiographic measurement currently in use. Shape

modeling could also be used to develop novel measurements that are perhaps even more sensitive and specific than those currently in use.

6.3 FAI, Physical Exams, and Screening: Recent Developments, Conclusions, and Future Directions

If a higher risk of FAI morphology is definitively identified for athletes or other populations, the next logical step is to establish the relevance of such findings. As suggested in Chapter 3, a method to identify those individuals at-risk for underlying deformities could improve the timeliness of diagnosis and treatment of FAI. While CT, MR, and clinical x-ray provide direct visualization of anatomy, the associated costs and/or radiation exposure preclude the use of medical imaging as a screening tool. In Chapter 3, clinical exams were evaluated as a tool to indirectly identify those with underlying FAI morphology. Symptomatic FAI patients often present with range of motion deficits and report pain during specific manipulations. It was therefore hypothesized that similar findings may be present in athletes who have FAI morphology, but no history of prolonged hip pain.

In Chapter 3, a significant, mild correlation was identified between measures of cam FAI and internal rotation. This relationship has been confirmed in a few studies since Chapter 3 was published in 2012 in *Arthroscopy: The Journal of Arthroscopic and Related Surgery*. For example, in a study by Siebenrock *et al*., supine internal rotation in a population of elite hockey players was significantly correlated to the alpha angle ($r = -0.274$, $p=0.008$).[6] In a related study of 89 elite adolescent soccer players, hips with an alpha angle greater than 60° exhibited significantly decreased internal rotation compared

to hips without (19.7° vs. 26.2°, p=0.002).[8] Finally, elite basketball players aged 9-25 demonstrated decreased range of motion compared to nonathlete controls (18.9 ± 11° vs, 30.1 ± 6.9°, p = 0.001).[7] However, a regression analysis was not completed to determine if the relationship between alpha angle and range of motion was significant.[7]

In Chapter 3, the impingement exam, which is almost always positive in symptomatic FAI patients,[11] had poor sensitivity in football players who had morphological findings consistent with FAI but no hip pain. In fact, while 95% had radiographic evidence of FAI, the impingement exam was positive in only three of the 67 players (4%). Recent findings by Laborie *et al*. corroborate those reported in Chapter 3. Specifically, in their study only 7.3% male and 4.8 % female subjects of a cohort of 1,170 asymptomatic young adults reported pain during the exam. Similarly, Yuan at al. found positive exam findings in only 3% of 226 asymptomatic adolescent athletes from a variety of sports.[12]

Though the impingement exam may have poor sensitivity, evidence suggests that it has high specificity for detecting FAI or associated damage. The high sensitivity of the impingement exam is likely the result of mechanical conflict between the femur and injured and/or irritated chondrolabral tissue. Though the players presented in Chapter 3 were not screened for damage using advanced imaging, each of the 3 players from this study who reported pain during the impingement exam had at least one radiographic abnormality consistent with FAI. Similarly, Yuan *et al*. found that 77% of the adolescent athletes with a positive impingement exam had an alpha angle greater than 50° and/or chondrolabral damage on MRI.[12]

In light of the research presented in Chapter 3 and recent findings, the future of physical exams in screening largely depends on the objective. If the goal is simply to spread awareness amongst individuals within an at-risk population, then an exam with a relatively high sensitivity and low specificity, such as internal rotation and associated cutoffs presented in Chapter 3 (Table 3.4), may be appropriate. In this case, the cutoffs were selected to identify at least 80% of the subjects with underlying cam-like anatomy. While false positives would occur (in ~49-66%, depending on the exam, Table 3.4), there would be minimal consequences to simply informing the individual that FAI is common amongst athletes (or other identified groups) and to be aware that persistent hip pain may be the result of abnormal hip morphology associated with this disease. In such a case, it is not unreasonable to assume that a screening protocol could reduce the time between onset of symptoms and treatment. Nevertheless, internal range of motion cutoff values would first need to be defined for a general population of athletes (or other groups) in addition to football players for this screening protocol to be a versatile tool.

If the goal is to identify those who may benefit from further evaluation or proactive monitoring, the impingement exam, which has a high specificity to detect labral tears and FAI morphology, may be more suitable. While the exam has a relatively low sensitivity, and may miss individuals with deformities, those that do test positive may have existing chondrolabral damage and/or be more likely to develop symptoms in daily or athletic activities. More work is still needed to elucidate those mechanisms responsible for a positive exam finding, to confirm the sensitivity to detect chondrolabral damage in a large cohort, and to follow individuals with positive exam findings to quantify the prevalence of who becomes symptomatic in daily life.

Biomarkers represent another area of future research that could be used to identify individuals with possible degenerative changes to chondrolabral tissue. Recently, blood screening of symptomatic FAI patients and controls have identified two biomarkers that occur at elevated levels in FAI patients, cartilage oligomeric matrix protein (COMP) and C-reactive protein (CRP).[13] COMP and CRP are associated with cartilage turnover and joint inflammation, respectively, and both are associated with OA.[14-17] More research is necessary to determine if these and other biomarkers associated with degenerative joint disease are elevated in individuals with underlying but asymptomatic FAI deformities. It is also important to understand if specific biomarkers decrease after surgical intervention and recovery. If such associations were found, blood biomarker screening could provide a more definitive approach to identify who could benefit from surgical intervention for FAI. Still, a substantial limitation of biomarkers extracted from blood is that they are not specific to a single joint such as the hip; false positives can result from tissue degeneration in any of the other diarthrodial joints.

6.4 Dual Fluoroscopy and Model-Based Tracking

6.4.1 The Foundation for Future Work

A great deal of time was spent developing, troubleshooting, modifying, and optimizing the dual fluoroscopy system to give it the functionality required to complete the research presented in Chapters 4 and 5. The final dual fluoroscopy system is very versatile. Specifically, with separate bases supporting the image intensifiers and emitters, it can be positioned around a radiolucent table, instrument treadmill, chair, or in-ground

force plates. Recently, the dual fluoroscopy system successfully imaged the shoulder, ankle, and the hip during weight-bearing activities; all with minimal modifications.

Standard Operating Procedures (SOPs) were developed for each step of data collection and processing. These include separate SOPs to align the image intensifier and emitter, calibrate the field of view, acquire images, preprocess CT data, perform marker and model-based tracking, and postprocess the data. The model-based tracking software only provides the position of the bones relative to the laboratory coordinate system. Thus, additional postprocessing was necessary to derive clinically relevant outcome measures, such as joint angles. To this end, custom code was written to calculate joint angles and translations and create transformation matrix input files. These transformations were then input into the PostView software[18] for the purpose of animating hip joint motion.

A large effort was also required to obtain institutional review board (IRB) approval to use the dual fluoroscopy system on live human subjects. First, it was necessary to document each modification made to the dual fluoroscopy system and submit a general proposal to the University and State of Utah to consider the device for research purposes only (the required modifications voided the system's status as an FDA approved device). Next, with the assistance of a radiation physicist, it was necessary to calibrate the device. These calibration data suggested additional modifications were necessary to limit the output from the system. Finally, pilot studies were conducted using cadaveric tissue to determine the energy settings and imaging configuration necessary to obtain images of sufficient quality to track the hip joint with the model-based tracking software. Collectively, this information was included in the proposal to the University, State of Utah, and first IRB application. Approval was obtained by each with minimal

revisions. The approved IRB application has already served as the template for future research studies (i.e. ankle) that propose to use the dual fluoroscopy system.

Owing to the large amount of soft-tissue surrounding the joint, the hip is arguably the most difficult diarthrodial joint to image with the dual fluoroscopy system. While surrounded by less soft tissue than the hip, imaging the other joints with dual fluoroscopy will certainly pose unique challenges. Still, the work completed in this dissertation provides confidence to execute future studies that aim to quantify joint kinematics. In fact, following the methodology outlined in Chapter 4, validation studies of ankle and shoulder motion, which began less than one year ago, are already near completion.

6.4.2 Suggested Directions for Software Development

As the first applications of model-based tracking to the native hip joint in a cohort of subjects, several challenges were encountered; each deserves discussion as they are likely to be present in future studies that utilize the equipment. The main challenge was noise in the fluoroscopic images. A short camera exposure of 3000 μs was selected to prevent motion blur in the images. With such a short exposure, a limited number of x-ray photons hit the image intensifier. This is the primary reason why fluoroscopic images acquired at a high frame rate are noisy compared to standard fluoroscope images, which are acquired at a much longer exposure. This noise is emphasized when Sobel edge detection is applied in the preprocessing steps of model-based tracking. The user has the option to apply a simple 3x3 smoothing kernel to the images prior to this step, but doing so provides little improvement. A number of advanced denoising algorithms have been developed for medical imaging and other applications.[19-21] It is possible that these

algorithms could substantially improve the correlation between digitally reconstructed radiographs and fluoroscopic images of the hip. Unfortunately, denoising is computationally expensive. As such, working with the large datasets inherent in high-speed dual fluoroscopy makes it difficult to envision widespread use of denoising for this particular application.

Another area where model-based tracking software could be improved would be to add an option for the user to emphasize specific regions of the image to guide the optimization. With the hip joint, there are times when the optimization algorithm fails to match the bone to the true boundary, which is likely due to noise in the image as described above. While the correct alignment can be manually obtained in these situations, it may be more accurate and repeatable if the user were given the ability to highlight or trace boundaries of confidence. Specifically, a weighting factor could be applied to these regions so that the optimization algorithm is biased to align or "snap" the bone to these borders. Currently, the user can only select regions in the fluoroscope image to be excluded from the optimization (e.g., metal objects, such as a button on the pants).

Postprocessing could also benefit from software development. In Chapter 5, regions of contact between the labrum and femur were manually identified by selecting those faces that protruded through the opposing surface. The magnitude of overlap could then be calculated with the same tool used to calculate the distance between bones. However, the tool reports an absolute distance, and currently does not distinguish between, for example, 1 mm of overlap or 1 mm of space between bones. An automatic

way to measure overlap could streamline the process and facilitate visualization of the magnitude of overlap during a video.

It is challenging to present and compare subject-specific results relative to anatomy. In Chapter 5, each subject's location of minimum bone-to-bone distance and labrum contact was displayed on their femur and acetabulum. With nine subjects, this resulted in two large figures. If additional patients and/or controls are collected in the future, a more efficient method is needed to compare regions of interest and spatially average results so as to be space-conserving. Ideally, results from each group could be averaged on a representative bone for that group. At present, the bone and labrum surfaces cannot be compared node to node as there is no guarantee that a node represents the same feature on each subject. As a precursor to statistical shape modeling, researchers have developed a method to automatically define equivalent points, or correspondence particles, on surfaces from multiple subjects.[22-24] This objective method could be used to create equivalently meshed surfaces between subjects. This was actually explored as an option for Chapter 5, but a method was not in place to create a geometrically realistic tessellation from the correspondence points. If a solution was found, the method could be used not only to average results from dual fluoroscopy but also fringe plot results from subject-specific finite element models.

6.4.3 Future Directions

The research completed in this dissertation has opened the door to a wealth of possible future research directions on the hip. As Chapter 5 included a limited number of normal subjects and FAI patients, more research is needed to identify significant

differences in motion between FAI and normal hips. Data from additional cam, pincer, and mixed FAI patients could elucidate the mechanisms behind different patterns of damage observed in each subtype and identify stronger correlations between 3D morphology and kinematics.

While the study of hip kinematics during clinical exams has and will continue to provide valuable insights, hip articulation may vary between passive and active motions. Future research should also incorporate weight bearing exercises, such as squatting, pivoting, walking, or stair-climbing. Chapter 4 has established that the hip can be imaged during a large range of motion. Accordingly, it should be relatively straightforward to image the hip during walking on a treadmill. Squatting and stair-climbing may be more challenging as they require a larger range of motion, but the fluoroscopes have a small field of view that cannot capture the entire activity. In these cases, it may be beneficial to have a larger image intensifier to effectively increase the combined field of view of the fluoroscopes.

When imaging the hip with dual fluoroscopy, especially during activities where the hip remains relatively stationary with respect to the combined field of view (i.e. treadmill gait), it will be possible to collect other sources of data simultaneously. For example, ground reaction forces could be measured with an instrumented treadmill or ground force plates. Also, the motion of the remainder of the body could be captured with skin marker motion analysis. Additionally, electromyography data could identify any differences in muscle activation at very specific time points. Overall, collecting multiple sources of data during a single session or activity could provide important inputs for finite element and muscle models. For example, research is underway to determine if the

subject-specific kinematics, kinetics, and muscle forces are needed to predict cartilage contact stress in the hip joint .

In Chapter 5, the femoral head contacted the labrum during motion. This was observed as overlap between the rigid femur and the rigid labrum (which was assumed to undergo the same motion of the pelvis). In reality, the labrum would be compressed, stretched or pushed aside. Finite element models, driven using joint kinematics quantified by the dual fluoroscopy system, could possibly be used to predict strains in the labrum in-vivo. However, even small displacements of the femur can lead to substantial changes in force transmission across the hip joint. For example, a displacement of the femur into the acetabulum of only 2-4 mm is sufficient to create a physiological joint reaction force of 2-3 times bodyweight.[25,26] To this end, a cadaveric validation study could be completed in which small radiopaque beads are implanted into the labrum and tracked in the dual fluoroscopy system. The measured interbead strains could be compared to the finite element predictions for validation. Once validated, patient- and subject-specific FE models could provide valuable insight into the origins of labral tears and the variety of tears observed. Pre- and postoperative models could be used to predict the success of surgery based on the reduction in labral strains and/or load transfer. Overall, the incorporation of accurate joint kinematics into FE and musculoskeletal models is quite compelling as they could offer estimates of parameters that cannot be directly measured in vivo.

To fully understand the relationship between form and function in hip pathology, accurate measurements of both kinematics and anatomy are needed. 3D statistical shape analysis could classify the true variation between normal and FAI hips, as was done

recently in the laboratory.[24] Correlating modes of variation with accurate kinematic measures from dual fluoroscopy could objectively identify the morphologic abnormalities that have the largest effect on motion. Taking this one step further, recent developments in statistical shape modeling have enabled "4D" analyses of the lungs and wrist in which principal component analysis was used to simultaneously describe variation of morphology and motion. [19,20] Applying a similar methodology to the hip may be the optimal approach to classify the variation of normal and pathological hips and the expected motion of each group. This approach could be enable predictions of an individual's motion based on their anatomy.

Finally, impingement between the acetabular rim and femoral head or neck may not be the only impingement occurring between the femur and pelvis. The concept of extra-articular impingement is gaining traction. Specifically, impingement may occur between low-hanging anterior inferior iliac spines and the femoral neck, the trochanter and the pelvis, and the ischium and the femur.[27] The dual fluoroscopy methodology described herein could provide 3D information in support or refute of these possible mechanisms of pain and restricted motion. The same could apply to other joints where impingement may be occurring, such as the shoulder[28,29] and ankle.[30,31]

6.5 References

1. Silvis ML, Mosher TJ, Smetana BS, et al. 2011. High prevalence of pelvic and hip magnetic resonance imaging findings in asymptomatic collegiate and professional hockey players. Am J Sports Med 39: 715-721.

2. Ayeni OR, Banga K, Bhandari M, et al. 2013. Femoroacetabular impingement in elite ice hockey players. Knee Surg Sports Traumatol Arthrosc [Epub ahead of print].

3. Gerhardt MB, Romero AA, Silvers HJ, et al. 2012. The prevalence of radiographic hip abnormalities in elite soccer players. Am J Sports Med 40: 584-588.

4. Johnson AC, Shaman MA, Ryan TG. 2012. Femoroacetabular impingement in former high-level youth soccer players. Am J Sports Med 40: 1342-1346.

5. Philippon MJ, Ho CP, Briggs KK, et al. 2013. Prevalence of increased alpha angles as a measure of cam-type femoroacetabular impingement in youth ice hockey players. Am J Sports Med 41: 1357-1362.

6. Siebenrock KA, Kaschka I, Frauchiger L, et al. 2013. Prevalence of Cam-Type Deformity and Hip Pain in Elite Ice Hockey Players Before and After the End of Growth. Am J Sports Med [Epub ahead of print].

7. Siebenrock KA, Ferner F, Noble PC, et al. 2011. The cam-type deformity of the proximal femur arises in childhood in response to vigorous sporting activity. Clin Orthop Relat Res 469: 3229-3240.

8. Agricola R, Bessems JH, Ginai AZ, et al. 2012. The development of Cam-type deformity in adolescent and young male soccer players. Am J Sports Med 40: 1099-1106.

9. Zaltz I, Kelly BT, Hetsroni I, et al. 2013. The crossover sign overestimates acetabular retroversion. Clin Orthop Relat Res 471: 2463-2470.

10. Henebry A, Gaskill T. 2013. The Effect of Pelvic Tilt on Radiographic Markers of Acetabular Coverage. Am J Sports Med 41: 2599-2603.

11. Philippon MJ, Maxwell RB, Johnston TL, et al. 2007. Clinical presentation of femoroacetabular impingement. Knee Surg Sports Traumatol Arthrosc 15: 1041-1047.

12. Yuan BJ, Bartelt RB, Levy BA, et al. 2013. Decreased range of motion is associated with structural hip deformity in asymptomatic adolescent athletes. Am J Sports Med 41: 1519-1525.

13. Bedi A, Lynch EB, Sibilsky Enselman ER, et al. 2013. Elevation in Circulating Biomarkers of Cartilage Damage and Inflammation in Athletes With Femoroacetabular Impingement. Am J Sports Med 41: 2585-2590.

14. Garvican ER, Vaughan-Thomas A, Clegg PD, et al. 2010. Biomarkers of cartilage turnover. Part 2: Non-collagenous markers. Vet J 185: 43-49.

15. Posey KL, Hecht JT. 2008. The role of cartilage oligomeric matrix protein (COMP) in skeletal disease. Curr Drug Targets 9: 869-877.

16. Black S, Kushner I, Samols D. 2004. C-reactive Protein. J Biol Chem 279: 48487-48490.

17. Punzi L, Oliviero F, Plebani M. 2005. New biochemical insights into the pathogenesis of osteoarthritis and the role of laboratory investigations in clinical assessment. Crit Rev Clin Lab Sci 42: 279-309.

18. Mass S, Rawlins D, Weiss JA. "PostView" Finite Element Post-Processing. http://www.febio.org/postview. Accessed July 25, 2013.

19. Awate S, Whitaker R. 2006. Unsupervised, Information-Theoretic, Adaptive Image Filtering for Image Restoration. IEEE Trans Pattern Anal Mach Intell 28: 364-376.

20. Hensel M, Pralow T, Grigat R-R. 2006. Real-Time Denoising of Medical X-Ray Image Sequences: Three Entirely Different Approaches. In: Campilho A, Kamel M editors. Image Analysis and Recognition: Springer Berlin Heidelberg; pp. 479-490.

21. Preston JS, Rottman C, Cheryauka A, et al. 2013. Multi-layer Deformation Estimation for Fluoroscopic Imaging. In: Gee J, Joshi S, Pohl K, et al. editors. Information Processing in Medical Imaging: Springer Berlin Heidelberg; pp. 123-134.

22. Datar M, Cates J, Fletcher PT, et al. 2009. Particle based shape regression of open surfaces with applications to developmental neuroimaging. Med Image Comput Comput Assist Interv 12: 167-174.

23. Cates J, Fletcher PT, Styner M, et al. 2007. Shape modeling and analysis with entropy-based particle systems. Inf Process Med Imaging 20: 333-345.

24. Harris MD, Datar M, Whitaker RT, et al. 2013. Statistical shape modeling of cam femoroacetabular impingement. J Orthop Res 31: 1620-1626.

25. Harris MD, Anderson AE, Henak CR, et al. 2012. Finite element prediction of cartilage contact stresses in normal human hips. J Orthop Res 30: 1133-1139.

26. Anderson AE, Ellis BJ, Maas SA, et al. 2008. Validation of finite element predictions of cartilage contact pressure in the human hip joint. J Biomech Eng 130: 051008.

27. Larson CM, Stone RM. 2013. Current concepts and trends for operative treatment of FAI: hip arthroscopy. Curr Rev Musculoskelet Med 6: 242-249.

28. Guanche CA. 1994. Shoulder impingement syndrome: diagnosis, radiographic evaluation, and treatment with a modified Neer acromioplasty. J Bone Joint Surg Am 76: 473-474.

29. Papadonikolakis A, McKenna M, Warme W, et al. 2011. Published evidence relevant to the diagnosis of impingement syndrome of the shoulder. J Bone Joint Surg Am 93: 1827-1832.

30. Hess GW. 2011. Ankle impingement syndromes: a review of etiology and related implications. Foot Ankle Spec 4: 290-297.

31. Messerli B, Harrast M. 2011. Evaluation and treatment of anterolateral ankle impingement syndrome. Pm R 3: 776-780.

Table 6.1

Prevalence of Cam Femoroacetabular Impingement in Athletes from Different Sports

Author	Year	Gender	N	Sport	Age	Imaging Modality	Alpha Angle Cutoff (°)	Prevalence Cam FAI (%)	Mean Alpha Angle (°)
Kapron	**2011**	**Male**	**78**	**Football**	**17 - 26**	**Frog-lateral**	**50**	**54**	**52 ± 10**
Silvis	2011	Male	39	Hockey	-	MRI	50	38	-
Ayeni	2013	Both	20	Hockey	16-30	MRI	50	55	54 ± 12
Kapron	**2011**	**Male**	**78**	**Football**	**17 - 26**	**Frog-lateral**	**55**	**36**	**52 ± 10**
Gerhardt	2012	Male	75	Soccer	25.8 ± 4.4	Frog-lateral	55	68*	66
Gerhardt	2012	Female	20	Soccer	23.8 ± 2.3	Frog-lateral	55	50*	53
Johnson	2012	Male	25	Soccer	18-30	Frog-lateral	55	60	56 **
Johnson	2012	Female	27	Soccer	18-30	Frog-lateral	55	36	50 **
Philippon	2013	Male	61	Hockey	10-18	MRI	55	75	60 ± 7
Philippon	2013	Male	27	Skiing	10-18	MRI	55	42	55 ± 7
Siebenrock	2013	Male	77	Hockey	9-36	MRI	55	56†	54 ± 10
Siebenrock	2011	Male	37	Basketball	9-25	MRI	55	89†	61 ± 9
Kapron	**2011**	**Male**	**78**	**Football**	**17 - 26**	**Frog-lateral**	**60**	**20**	**52 ± 10**
Agricola	2012	Male	89	Soccer	12-19	Frog-lateral	60	26	-

*Gerhardt *et al*. reported a positive finding of cam FAI if any of the following criterion were met: excessive bone at the head-neck junction, loss of head asphericity, flattening of offset between the femoral head and neck, or alpha angle > 55°. **Average values reported separately for Right and Left Hips. Values averaged for this table. †A positive finding of cam FAI included an alpha angle > 55° in any MRI slice.

Table 6.2

Prevalence of Cam Femoroacetabular Impingement in Athletes Compared to Nonathlete Controls

Author	Year	Age Range	Imaging Modality	Alpha Angle Cutoff (°)	N	Gender	Group	Prevalence (%)	Mean Alpha Angle (°)
Ayeni	2013	16-30	MRI	50	20	Both	Hockey	55	54 ± 12
					20	Both	Control	25	43 ± 10
Johnson	2012	18-30	Frog-lateral	55	25	Male	Soccer	60	56*
					25	Male	Control	56	55*
					27	Female	Soccer	36	50*
					25	Female	Control	32	49*
Siebenrock	2011	9-25	MRI	55	37	Male	Basketball	89**	61 ± 9
					38	Male	Control	9**	47 ± 4
Agricola	2012	12-19	Frog-lateral	60	89	Male	Soccer	26	-
					92	Male	Control	17	-

*Average values reported separately for Right and Left Hips. Values averaged for this table. **A positive finding of cam FAI included an alpha angle > 55° in any MRI slice.